



Interannual variability of the rainfall regime and strong ENSO events along the Peruvian Pacific Basin : large-scale control mechanisms

Janeet Margarita Sanabria Quispe Sanabria

► To cite this version:

Janeet Margarita Sanabria Quispe Sanabria. Interannual variability of the rainfall regime and strong ENSO events along the Peruvian Pacific Basin : large-scale control mechanisms. Meteorology. Université Paul Sabatier - Toulouse III, 2018. English. NNT : 2018TOU30143 . tel-02301101

HAL Id: tel-02301101

<https://theses.hal.science/tel-02301101>

Submitted on 30 Sep 2019

HAL is a multi-disciplinary open access archive for the deposit and dissemination of scientific research documents, whether they are published or not. The documents may come from teaching and research institutions in France or abroad, or from public or private research centers.

L'archive ouverte pluridisciplinaire **HAL**, est destinée au dépôt et à la diffusion de documents scientifiques de niveau recherche, publiés ou non, émanant des établissements d'enseignement et de recherche français ou étrangers, des laboratoires publics ou privés.



THÈSE

En vue de l'obtention du

DOCTORAT DE L'UNIVERSITÉ DE TOULOUSE

Délivré par :

Université Toulouse 3 Paul Sabatier (UT3 Paul Sabatier)

Présentée et soutenue par :
Janeet Margarita SANABRIA QUISPE

le 16 avril 2018

Titre :

"Variabilité interannuelle du régime des pluies et des événements extrêmes
ENSO le long du Versant Pacifique Péruvien
: mécanismes de contrôle à grande échelle"

École doctorale et discipline ou spécialité :
ED SDU2E : Océan, Atmosphère, Climat

Unité de recherche :
Géosciences Environnement Toulouse (GET) UMR 5563, UPS- CNRS-IRD-OMP-CNES

Directeur/trice(s) de Thèse :
David LABAT - Professeur des Universités UPS (GET) - Directeur
Luc BOURREL - Chargé de Recherche IRD (GET) - Co-directeur

Jury :

Marie-Paule BONNET – Directrice de Recherche IRD (UMR 228) – Rapporteur
Thomas CONDOM – Chargé de Recherche IRD (UMR 5001) – Rapporteur
Waldo LAVADO – Chargé de Recherche (SENAMHI, Lima, Pérou) – Invité

I dedicate this thesis to my father who generates in my inspiration, motivation, strength and conclusion. Also, to my mother who transmits dedication and perseverance.

ACKNOWLEDGEMENTS

I must thank my thesis advisors, Dr. David Labat and Dr. Luc Bourrel who have welcomed me into the GET (Geosciences Environnement Toulouse) Laboratory, UMR 5563, UPS-CNRS-IRD-OMP-CNES, also for their direction and contributions in the development and culmination of the thesis, besides by the constant encouragement transmitted. Also, to Dr. Boris Dewitte for his brilliant shared ideas and to have learned the rigor and precision of science, increasing my motivation for scientific research. Likewise, to Dr. Mauricio Carrillo for all our discussions and advice that have accompanied me throughout the course of the fourth year of the thesis.

I extend my thanks to Dr. Thomas Condom, researcher of Institut des Géosciences de environment (IGE-Grenoble)-IRD and Dra. Marie Paul Bonnet, researcher of UMR ESPACE-DEV, Montpellier pour le développement-IRD, for the honor they have given me in accepting to be reviewers of this thesis and for their constructive comments.

How not to thank many friends for their disposition (Fausto Lopez, Dr. Jean-Paul Lhomme, Dr. Jerome Ramillien, etc.) also to the doctoral colleagues who share the encouragement for the development and culmination of our theses.

This work would not have been possible without the scholarship "Republic President" of the PRONABEC (National scholarship and educational credit program) of the Peruvian Government; who has also allowed an assignment of research and several financial aids, serenely devoting myself to the development of my thesis. My thanks to SENAMHI (National Service of Meteorology and Hydrology of Peru) for providing the raw data set.

Title: "Interannual variability of the rainfall regime and strong ENSO events along the Peruvian Pacific Basin: large-scale control mechanisms"

ABSTRACT

Four strong El Niño events took place within the last five decades (1972/1973, 1982/1983, 1997/1998 and 2015/2016) recorded as strong in the Niño 3.4 region. They can exhibit significant differences in their evolution associated with a distinct rainfall anomaly evolution along the PPB (Peruvian Pacific Basin), which illustrates the strong nonlinearity of the ENSO teleconnection on the rainfall in this area. These extreme rainfalls have harmful impacts on the population and productive sectors due to floods and landslides which are triggered by them. Yet the key climatic circulation pattern for their different evolution and magnitude are still unknown. Here we show that different rainfall patterns during these events are associated with moisture transport originated from different large-scale moisture sources. For example, in the 1983 - 1998 (2016) events appear as related with strong (weak to moderate) moisture coming from the Pacific warming (also coming from Atlantic Ocean through the Amazon basin). Characteristic of these moisture transports is due to an atmospheric response opposite between the 1983-1998 events (that are similar) and 2016 event experiencing out-of-phase moisture transport patterns. Although these rainfalls are linked to the moisture arrival from those sources, the moisture amount entering the PPB can be also influenced by regional atmospheric circulation of upper level winds (100 to 300 hPa) leading to different enhanced moisture transport associated with different rainfall anomalies in the North-Centre PPB. The interplay of large-scale and regional circulation and Pacific moisture transport explains the Ep mode associated with rainfall in the north-Centre PPB. The high dispersion of rainfall in highlands (Cp mode) during the moderate (extremes) El Niño appears as linked to low-middle (high level) moisture transport from the Amazon (Pacific) reaching highlands.

KEYWORDS: **strong El Niño events; rainfall variability; rainfall modes; moisture transport; large-scale and regional circulation; Peruvian Pacific Basin; highlands; coast.**

**Titre : " Variabilité interannuelle du régime des pluies et des événements extrêmes
ENSO le long du Versant Pacifique Péruvien
: mécanismes de contrôle à grande échelle"**

RÉSUMÉ

Quatre événements El Niño extrêmes ont eu lieu durant les cinq dernières décennies (1972/1973, 1982/1983, 1997/1998 et 2015/2016) et étaient caractérisés comme forts dans la région Niño 3.4. Ils présentent des différences significatives dans leur évolution qui induisent des anomalies distinctes de précipitations le long du versant Pacifique Péruvien illustrant la non-linéarité de la téléconnexion ENSO sur les précipitations dans cette région. Les pluies extrêmes ont un impact néfaste sur la population et les secteurs productifs en raison des inondations et des glissements de terrain qui s'ensuivent. Néanmoins, à ce jour, les patrons de circulation climatique clé de leurs évolutions et magnitudes différentes sont encore très peu connus. Dans cette thèse, nous montrons que les différentes configurations de précipitations lors de ces événements sont associées au transport de l'humidité provenant de différentes sources d'humidité à grande échelle. Lors des événements 1983-1998 (2016), ils sont respectivement liés à une forte (faible à modérée) humidité provenant du réchauffement du Pacifique (également mais aussi provenant de L'Atlantique via l'Amazonie). La caractéristique de ces transports d'humidité est due à une réponse atmosphérique opposée entre les événements de 1983-1998 (qui sont similaires) et l'événement de 2016 qui présente des patterns de transport d'humidité déphasés. Ces précipitations sont liées à l'humidité provenant de ces sources et la circulation atmosphérique régionale des vents de niveau supérieur (100 à 300 hPa) influe sur la quantité d'humidité qui pénètre dans la région Nord-Centre du versant Pacifique Péruvien. L'interaction de la circulation à grande échelle et régionale et le transport de l'humidité du Pacifique est expliquée par le mode Ep qui est associé à des précipitations dans la région Centre-Nord. La forte dispersion des précipitations dans les régions montagneuses est expliquée par le mode Cp pendant les phénomènes El Niño modérés (extrêmes) et est liée au transport d'humidité de niveau moyen-bas (haut) de l'Amazonie (Pacifique) atteignant les hautes terres.

MOTS-CLÉS : événements extrêmes El Niño ; variabilité des précipitations ; modes de précipitations ; transport d'humidité ; circulation à grande échelle et régionale ; versant Pacifique Péruvien ; Côte ; Andes.

Table of contents

Chapter 1

Introduction

1 Introduction	19
1.1 Mean seasonal climate conditions in the Peruvian Pacific Basin	20
1.2 Hydrology in the Peruvian Pacific basin.	23
1.3 El Niño and its diversity.	24
1.3.1 ENSO	24
1.3.1.1 El Niño.	24
1.3.1.1.1 El Niño events	26
1.3.1.1.2 Type of El Niño events	26
1.3.1.2 La Niña	27
1.3.1.3 Neutral	28
1.3.2 ENSO Indices	28
1.3.3 Teleconnections	30
1.3.4 El Niño diversity: Eastern (EP) and Central Pacific (CP) El Niño	32
1.3.4.1 C and E indices	34
1.4 Mechanisms triggering rainfall events during extreme El Niño events	35
2 Motivations of the study.	37
2.1 Objectif	38
2.2.1 Specific Objectives	38

Introduction (Version française)

1 Introduction	41
2 Motivations d'Etude	44
2.1 Objectif	45
2.2.1 Objectives spécifiques	45

Chapter 2

Rainfall along the Pacific slope and coast of Peru during Strong El Niño events

Preamble	48
Rainfall along the coast of Peru during Strong El Niño events (<i>Published Article in International Journal of Climatology</i>)	50

Chapter 3

Comparison of rainfall reanalysis data to develop atmospheric scenarios during extreme El Niño episodes (observations and evaluations).

3.1 Reanalysis	62
3.2 Atmospheric Reanalysis	63
3.2.1 Reanalysis system	64
3.2.1.1 ECMWF Reanalysis	64
3.2.1.2 JMA Reanalysis	65
3.2.1.3 NASA GMAO Reanalysis	65
3.2.1.4 NOAA/NCEP and related Reanalysis	65
3.3 Reanalysis rainfall over the Peruvian Pacific Basin (PPB)	69
Preamble	70
Rainfall during the strong El Niño events from Reanalysis: ERA-Interim, CFSR and JRA-55 in the Pacific Peruvian basin” (Research work. Manuscript to be submitted to <i>Atmospheric Research</i>)	71

Chapter 4

Large scale and local atmospheric factors that controls the rainfall variability along the Peruvian Pacific slope and coast during strong El Niño events.

4.1 Strong El Niño events with regard to the transport of moisture and atmospheric factors	90
4.2 Moisture transport and its convergence	94
4.2.1 Approaches of the moisture transport (Q) and its convergence ($-\nabla \cdot Q$)	95
4.3 Rainfall and moisture patterns associated with strong El Niño events in the eastern Pacific region	97
Preamble	98
Rainfall and moisture patterns associated with strong El Niño events in the eastern Pacific region (Research work. Manuscript to be submitted to <i>Geophysical Research Letters</i>)	99

Chapter 5

Conclusions and perspectives

5.1 Conclusions	123
5.2 Perspectives	126

Conclusions et perspectives (Version française)	
5.1 Conclusions	128
5.2 Perspectives	131
BIBLIOGRAPHY	
ANNEX 1	149

List of figures

Chapter 1

ocean water in the eastern Pacific, while warmer water prevails in the western Pacific. The trades are part of a circulation (called the *Walker circulation*) that typically lead convection and heavy rain over the western Pacific and air subsidence and generally dry weather over the eastern Pacific. When the trades are exceptionally strong, water along the equator in the eastern Pacific becomes quite cool. This cool event is called La Niña. (b) El Niño conditions: atmospheric pressure decreases over the eastern Pacific and subsidence over the western Pacific. This change in pressure causes the trade winds to weaken or reverse direction. This situation enhances the westerly winds that carry warm water from the west toward the central to eastern tropical Pacific that lead to convection and trigger heavy rainfalls over the eastern Pacific. The thermocline, which separates the warm water of the upper ocean from the cold waters below, in response to the equatorial winds, flattens during El Niño and becomes more tilted during La Niña.

Source: Meteorology today (Ahrens, D. 2009, pp 277).

Figure 1.6. Location of the Niño regions for measuring Sea Surface Temperature (SST) in the eastern and central tropical Pacific Ocean. The SST in the Niño3.4 region, spanning from 120°W to 170°W longitude, when averaged over a 3-month period, forms NOAA's official Oceanic Niño Index (the ONI). Source: NOAA Climate.gov.

25

Figure 1.7. Monthly values of the Oceanic Niño Index (the ONI) from ERSST.v5 SSTdata over the period 1955 through present. The signal of ONI is clearly observed during the strong El Niño events of 1982/1983, 1997/1998 and 2015/2016 with values higher than 2°C. Source: NOAA Climate.gov.

28

Figure 1.8. Monthly values of the Southern Oscillation Index (SOI) of the period 1955 to present. The signal of SOI is clearly observed during the strong El Niño events of 1982/1983 and 1997/1998 with values around 4 and 3, respectively. While 2015/2016 El Niño is less clear. Source. NOAA Climate.gov.

29

Figure 1.9 (a) Rainfall anomalies in Arequipa (16°4' S located to South of the Lima region) relative to its climatology (thin lines; based on 1920-1939) associated with (b) SST anomalies (with respect to 1920-1939) along the near-coastal track during El Niño 1925. (c) Report of 1925-1926 summer “exceptionally warm and early”. Source: *Takahashi and Martinez, 2017. The very strong El Niño in 1925 in the far-eastern Pacific. Journal: Climate Dynamics.*

30

Figure 1.10 Teleconnections in the tropical zone. (a) El Niño event associated with strong convection over the southeastern Pacific Ocean and subsidence over the Amazon (b) Neutral conditions associated with strong subsidence over the southeastern Pacific and convection over the Amazon. Source: Revision World. World-wide impacts of El Niño Southern Oscillation. Retrieved from <http://www.revisionworld.com/a2-level-level-revision/geography/synoptic-assessment-0/drought-and-its-teleconnection-enso> 31

31

Figure 1.11. El Niño Diversity (a) Neutral conditions (b) EP El Niño event (c) CP El Niño event. Neutral conditions associated with southerlies winds blow east to west across the surface of the tropical Pacific Ocean, bringing warm moist air and warmer surface water towards the western Pacific and keeping the central Pacific Ocean relatively cool. Whereas EP El Niño event the southerlies winds weaken or may even reverse allowing the area of warmer than normal water to move into the central and eastern tropical Pacific Ocean. It is associated with reversed atmospheric circulation linked to ascending motions and weakened low-level winds in the eastern equatorial Pacific (150°E and 85°W) triggered an eastern Pacific wetter and the western Pacific drier. Instead, CP El Niño anomalous warming in the central Pacific flanked by anomalous cooling in the eastern and western sides of the Pacific basin (Ashok and Yamagata, 2009) which is associated with a double Walker cell with the anomalous ascending branch in the central Pacific, and descending branches in the western and eastern equatorial Pacific leading to a western and eastern Pacific drier. Source: Ashok and Yamagata, 2009.

33

Chapter 2

Figures of “Rainfall along the coast of Peru during Strong El Niño events” (Published Article)

Figure 4. Climatological root mean square (RMS) of (a) the Ep mode and (b) Cp mode. 56

Figure 6. Evolution of the Ep and Cp modes during the four strong El Niño events and the composite of moderate events: Ep mode (left-hand side) and Cp mode (right-hand side). The composite for moderate events includes the same events than in Figure 1(b). The hatching in grey line represents the dispersion (standard deviation) among moderate El Niño events. [Colour figure can be viewed at wileyonlinelibrary.com]. 57

Figure 7. Evolution of the Ep and Cp indices and precipitation anomaly in the homogeneous regions during the four strong El Niño events 1972/1973, 1982/1983, 1997/1998 and 2015/2016. [Colour figure can be viewed at wileyonlinelibrary.com]. 57

Figure 8. Evolution of the SST in the Niño1+2 region during the fourth strong El Niño events. The horizontal line indicates the convection threshold temperature ($\sim 26^\circ\text{C}$). SST is obtained from the HadISST data set over the period 1950–2016. [Colour figure can be viewed at wileyonlinelibrary.com]. 59

Figure 9. Evolution of SST and precipitation anomalies during the fourth strong El Niño events. Monthly averaged anomalies for (top) D(0)JF(+1) and (bottom) MAM(+1). Unit is in $^\circ\text{C}$ for SST (in the bottom right-hand corner) and in mm for precipitation (in the top right-hand corner for precipitation. For precipitation, the thick black line indicates the zero contour. For SST the contour in white line indicates the 2°C isotherm. Anomalies are relative to the seasonal cycle calculated over the period 1964–1977 (1978–2008) for the 1972/1973 El Niño the 1982/1983 and 1997/1998 El Niño). [Colour figure can be viewed at wileyonlinelibrary.com]. 59

Chapter 3

Figure 3.1. Global climatic system components (atmosphere, land, Ocean, and cryosphere) and their main interactions. The climate system data are used for the production of global reanalysis. Reanalysis data covers the globe from the Earth's surface to beyond the stratosphere. Credit: European Reanalysis of the Global Climate System. <http://www.era-clim.eu/ERA-CLIM2/>. 63

Figures of Manuscript for submitting “ Rainfall during the strong El Niño events from Reanalysis: ERA-interim, CFSR and JRA-55 in the Pacific Peruvian basin”

Figure 1: Correlation between the observed and reanalysis (ERA-Interim, CFSR and JRA-55) rainfall. The average value and value for each point grid (scale of values) of the correlation are presented. Period 1979-2009.	77
Figure 2: (a) Mean square error (b) Bias of observed and reanalysis (ERA-Interim, CFSR and JRA-55) rainfall anomalies. Period 1979-2009. Bias CFSR *50000.	78
Figure 3: Climatology of observed and reanalysis (ERA-Interim, CFSR and JRA-55) rainfall over the period 1979-2009.	79
Figure 4: Associated patterns (Ep and Cp) of rainfall anomalies over the period 1979–2009. Ep mode (first mode) (left-hand side) and Cp mode (second mode) (right-hand side). The thick black line indicates the zero contour. (a) Observed (b) Era-interim (c) CFSR (d) JRA-55.	81
Figure 5: Phase space of the evolution of the Ep and Cp modes. The evolution of the four strong El Niño event is highlighted with lines connecting the dots for the months between January of the first year J(Y0) and December of the second year D(Y1). (Y0: developing El Niño, Y1: decaying El Niño). (a) Observed (b) ERA-Interim (c) CFSR (d) JRA-55.	82
Figure 6: The temporal evolution of the strong El Niño events on the Ep and Cp mode observed in the three reanalysis (ERA-Interim, CFSR and JRA-55). January of the first year J(Y0) and December of the second year D(Y1).	84

Chapter 4

Fig 4.1. Moisture transport (Q) patterns associated with Eastern (EP) and Central (CP) Pacific El Niño. Patterns obtained from EOF regression 1964–2016. Q obtained from ERA-Interim reanalysis of the period 1979–2016. Source: Own elaboration.	93
---	----

Fig 4.2. Moisture convergence ($-\nabla \cdot Q$) patterns associated with Eastern (EP) and

Central (CP) Pacific El Niño. Patterns obtained from EOF regression. $-\nabla \cdot Q$ obtained from ERA-Interim reanalysis of the period 1979–2016. Source: Own elaboration. 93

Figure 4.3. Schematic diagram of the atmospheric and terrestrial branches of the hydrological cycle: the importance of evaporation E , transport of water vapor in the atmosphere Q , precipitation P , river runoff R_o and underground runoff R_u . (Peixoto and Oort, 1992). 94

Figures of manuscript for submitting “Rainfall and moisture patterns associated with strong El Niño events in the eastern Pacific region”

Figure 1. Phase space of the evolution of the Ep and Cp modes: (a) Precipitation (b) vertically integrated water vapor transport convergence ($-\nabla \cdot Q$). The evolution of the 3 strong el Niño events is highlighted with lines connecting the dots for month between January of the first year and December of the second year. Mode patterns associated with Eastern (EP) and Central (CP) Pacific El Niño obtained from EOF regression of period 1979–2016: (c) Precipitation (d) $-\nabla \cdot Q$. Precipitation data used from the Climate Prediction Center (CPC) Merged Analysis of Precipitation (CMAP). $-\nabla \cdot Q$ data used from ERA-Interim reanalysis 106

Figure 2. (a) JFMA Composites of observed precipitation anomalies (mm/day) over Peruvian Pacific region (b) JFMA Composites of vertically integrated water vapor transport (Q) anomalies ($\text{kg m}^{-1} \text{s}^{-1}$) (vector) and Q convergence anomalies ($-\nabla \cdot Q$) y/o Q divergence anomalies ($\nabla \cdot Q$) (mm/day). Respective climatology over 1979–2016 period. The continuous shading encompasses positive and negative significant values at the 95% confidence level using the Student’s t-test. 108

Figure 3. JFMA composites of longitude vertical cross-section of (a) specific moisture anomalies (g kg^{-1}) and (b) vertical motion anomalies ω (kPa s^{-1}), averaged between 2°S and 7.5°S (northern region) for El Niño of 1983, 1998 and 2016. Respective climatology over 1979–2016 period. The continuous shading encompasses positive and negative significant values at the 95% confidence level using the Student’s t-test. 109

Figure 4. JFMA composites of longitude vertical cross-section of specific moisture anomalies (g kg^{-1}) associated with (a) meridional wind anomalies (m s^{-1}) and (b)

zonal wind anomalies (m s^{-1}) averaged between 2°S and 7.5°S (northern region) for El Niño of 1983, 1998 and 2016. Respective climatology over 1979-2016 period. The continuous shading encompasses positive and negative significant values at the 95% confidence level using the Student's t-test 111

Figure S1. JFMA composites of (a) the vertically integrated water vapor transport(Q) anomalies ($\text{kg m}^{-1} \text{s}^{-1}$) (vector) and Q convergence ($-\nabla \cdot Q$) y/o Q divergence ($-\nabla \cdot Q$) anomalies (mm/day) for El Niño of 1983, 1998 and 2016 along of the zone Lon: $120^{\circ}\text{W} - 30^{\circ}\text{W}$ Lat: 20°S to 10°N . The Q and $-\nabla \cdot Q$ integrated between 1000 and 300 hPa. The continuous shading encompasses positive and negative significant values at the 95% confidence level using the Student's t-test. 114

Figure S2. JFMA composites of (a) the vertically integrated water vapor transport (Q) anomalies ($\text{kg m}^{-1} \text{s}^{-1}$) (vector) and Q convergence ($-\nabla \cdot Q$) y/o Q divergence ($-\nabla \cdot Q$) anomalies (mm/day), integrated between 1000 and 800 hPa, for El Niño of 1983, 1998 and 2016 events along of the zone Lon: $120^{\circ}\text{W} - 30^{\circ}\text{W}$ Lat: 20°S to 10°N . (b) The same figure but Q and $-\nabla \cdot Q$ integrated between 600 and 400 hPa. The continuous shading encompasses positive and negative significant values at the 95% confidence level using the Student's t-test 115

Chapter 5

Figure S1. Evolution of the anomalous MJO activity for the 1982/1983, 1997/1998 and 2015/2016 El Niño events. The MJO activity is defined as 3-month running variance of the RMM index (daily) as defined by Wheeler and Hendon (2004). Anomalies of the MJO activity are relative to the average seasonal cycle over the period 1980-2015. The mean evolution for moderate El Niño events along with the dispersion among events is also shown. Data are from <https://iridl.ldeo.columbia.edu/SOURCES/.BoM/.MJO/.RMM/> 126

Figure S1. Evolution des anomalies de l'activité MJO pour les évènements El Niño forts de 1982/1983, 1997/1998 and 2015/2016. L'activité MJO est définie par variance glissante sur 3 mois de l'indice RMM (journalier) définie par Wheeler and Hendon (2004). Les anomalies de l'activité de la MJO sont relatives au cycle moyen saisonnier sur la période 1980-2015. L'évolution moyenne pour les El Niño modérés est aussi montrée en regard avec la dispersion entre les évènements.

Les données sont issues de https://iridl.ldeo.columbia.edu/SOURCES/.BoM/.MJO/.RMM/	132
--	-----

Table

Chapter 2

Table of “Rainfall along the coast of Peru during Strong El Niño events” (Published Article)

Table 1. Observed monthly rainfall with respect to mean climatology (M. C. over the 1964–2016 period) during the El Niño events of 1972/1973, 1982/1983, 1997/1998 and 2015/2016 [between January of the developing year J(Y0) and December of the decaying year D(Y1)]. The dark green colour represents rain values above 80% of the monthly mean climatology. [Colour table can be viewed at wileyonlinelibrary.com].	58
---	----

Chapter 3

Table 3.1 List of global atmospheric reanalysis systems. Approximate longitude grid spacing is reported in degrees for models with regular Gaussian grids (Fn) and in kilometers for models with reduced Gaussian grids (Nn). Wavenumber truncations for models with Gaussian grids are reported in parentheses. * Year in parentheses indicates the year for the version of the operational analysis system that was used for the reanalysis.	67
--	----

Table 3.2 Sources of SST used in reanalysis	68
---	----

Chapter 1: Introduction

1. INTRODUCTION

Temporal changes in atmospheric conditions, such as temperature, rainfall, and wind, over a given region exhibit irregular fluctuations across a broad range of scales superimposed on the mean diurnal and annual cycles. These fluctuations include synoptic-scale variability, broadly associated with weather, as well as intraseasonal, interannual, interdecadal, and longer-scale variations. These fluctuations arise from the internal variability of the atmosphere and are coupling with other components of the Earth system such as Oceans, land vegetation, and sea-ice (Garreaud and Aceituno, 2007).

Over South America (SA) the precipitation exhibits significant variability on interannual to interdecadal timescales (Garreaud et al., 2009). This variability is mainly caused by Ocean–atmosphere interactions (Vuille and Garreaud, 2012) that lead to a reorganization of the large-scale circulation over SA and the neighbouring oceans. The Ocean–atmosphere interactions, with often oscillatory behaviour affect the interannual to multidecadal climate variability in a region. The spatial influence of these interactions is assessed by documenting their role in driving interannual precipitation variability.

It is well documented that the warm phase of ENSO (El Niño Southern Oscillation) “El Niño” is the major driver of interannual variability of rainfall in the worldwide (McPhaden et al., 2006) and specially in South America (Marengo et al., 2013) where the mean of interannual variability is the ENSO (Garreaud et al., 2009). The El Niño Ocean-atmosphere interaction involves both variations of the large-scale (Walker circulation and the tropospheric Rossby-wave trains) atmospheric circulation patterns that respond to the SST anomalies in the Equatorial Pacific (Bjerknes 1969; Kug et al., 2009; Trenberth et al., 1998; Hoerling and Kumar, 2002) and variations of local (South American Low-Level Jet – LLJ) atmospheric circulation patterns which lead to distinct rainfall anomaly patterns over South America (Andreoli et al., 2016). The Ecuador and northern-central region of Peru are the regions where El Niño yields extreme rainfall anomalies (Rasmusson and Carpenter, 1982; Horel et al., 1986; Goldberg RA et al., 1987; Tapley T et al., 1990; Trenberth et al., 1998; Bendix E et al., 2006; McPhaden et al., 2006; Douglas M et al., 2009; Lavado et al., 2014; Capotondi et al., 2015) and where the

quantity of rainfall is different from one event to another (Rome and Ronchail, 1998) with an uncertainty on their magnitude and extent (Rau *et al.*, 2017). Specifically, the Peruvian Pacific basin of arid and semiarid climate is directly impacted by “El Niño” with devastating rainfall (Young *et al.*, 2007) more in the northern than the center (See Fig 1.1).

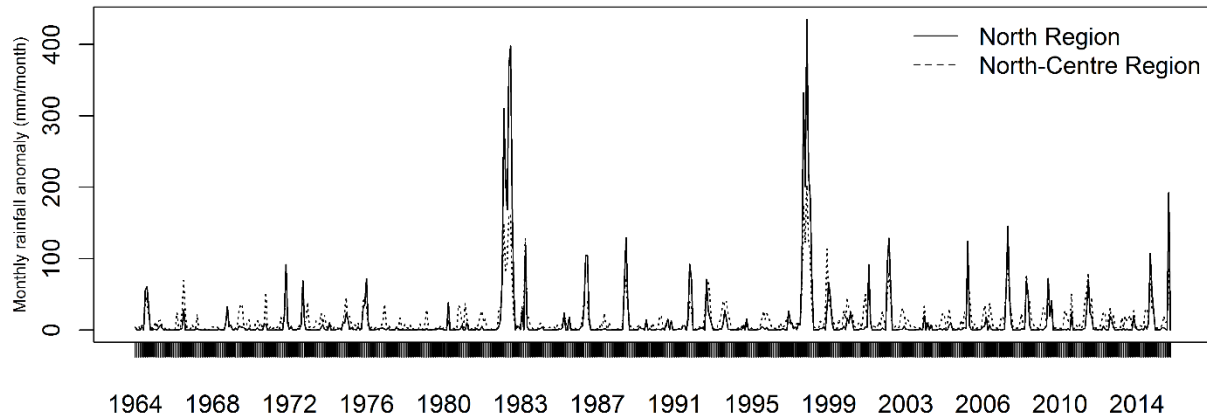


Figure 1.1. Rainfall anomalies (1964 to 2016) in the North of Peru, versus rainfall anomalies in the central Part of Peru where the impact of ENSO on the rainfalls is noted clearly during the strong El Niño events of 1982/1983 and 1997/1998 in the North than central Part of Peru. Data provided by the National Service of Meteorology and Hydrology of Peru (SENAMHI).

This has had strong implications for the Peruvian Economy, reflecting strong declines in the Gross Domestic Product (GDP) due to the effects on population and productive sectors (agriculture, energy, transport, miner and other). Therefore, there is a clear need to understand the conditions that favour these differences of extreme rainfall events as well as the mechanisms involved, allowing improvements in their forecasting.

1.1 MEAN SEASONAL CLIMATE CONDITIONS IN THE PERUVIAN PACIFIC BASIN

In our study, we call “The Peruvian Pacific Basin (PPB)” the region limited by the line of high peaks along the main ranges of the Andean Cordillera (the hydrological division between the Amazonian Basin -west side of the Andes- and the Peruvian Pacific slope and coast -east side-) and the coastal line of Peruvian territory (for details, see Fig 2, Chapter 2, section 2.1). This region, from North to South, is subdivided by 62 watersheds (see “The National Peruvian Water Authority-ANA, 2012). The PPB is characterized by arid and semiarid climate (Rundel *et al.*, 1991) (See Fig. 1.2) associated to the subsiding air that maintains the very persistent cells of surface high pressure and low-level anticyclonic circulation (South

Pacific anticyclone, SPA, that lead to trade winds) over the southeast Pacific (Takahashi *et al.*, 2007) and associated also to the effect of the Andes that block intrusion of moist air from the Atlantic region (South American summer monsoon (SASM) (Garreaud and Aceituno 2007; Vuille *et al.*, 2012). This aridity is also associated with upwelling coastal conditions that help stabilize the atmospheric boundary layer. The upwelling conditions are sustained by the South-East branch of the trade winds. Every two to seven years however these trade winds collapse in the central equatorial Pacific, and the El Niño Southern Oscillation (ENSO) develops.

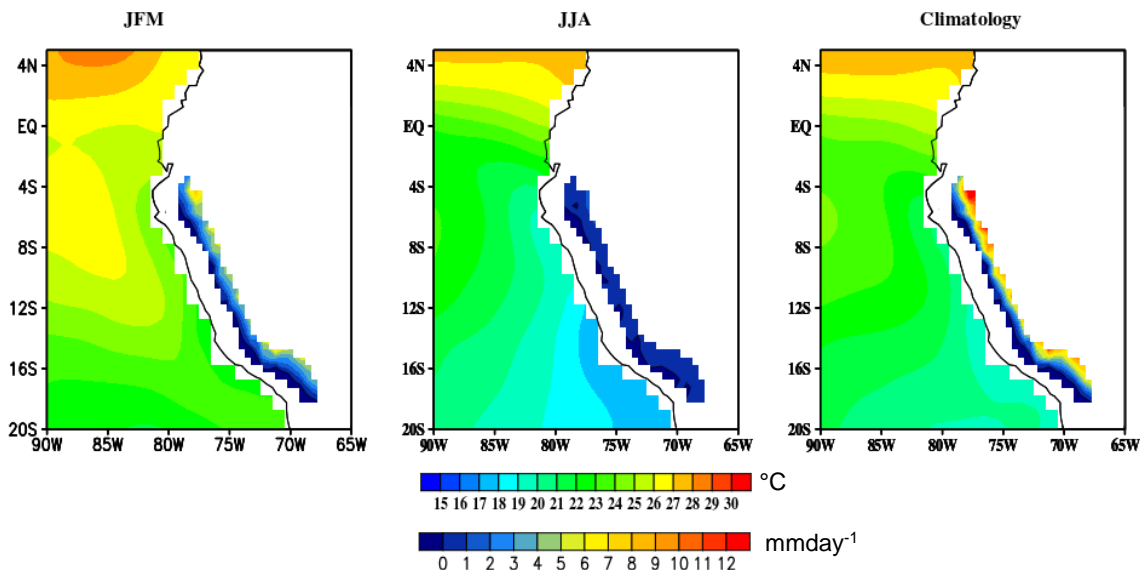


Figure 1.2 Sea surface temperature (SST) and mean precipitation for the rainy (January, February, March -JFM-), dry (June, July, August -JJA-) season and for annual cycle (1964 to 2016) in the Peruvian Pacific basin (PPB), computed as the simple average of corresponding monthly data from 1964 to 2016.

The climate of PPB is dominated by the seasonal migration of the Intertropical Convergence Zone (ITCZ) over the Pacific, as it is characterized by a fairly well-constrained narrow band of low-level wind convergence over the equatorial oceans (Flantua *et al.*, 2016; Vuille *et al.*, 2012). As well as the highlands of the PPB probably dominated by the extent of South American Summer Monsoon (SASM) (Vuille *et al.*, 2012; Eichler and Londono, 2013) (See Fig 1.3).

The SASM (see figure 1.4) reaches its maximum development during December to February (DJF) and is associated with the seasonal development of convective activity linked with heavy rainfall advancing southward from tropical to subtropical latitudes. To the east of the tropical Andes a strong low-level wind, the Andean Low-Level Jet (LLJ), transports moisture in a

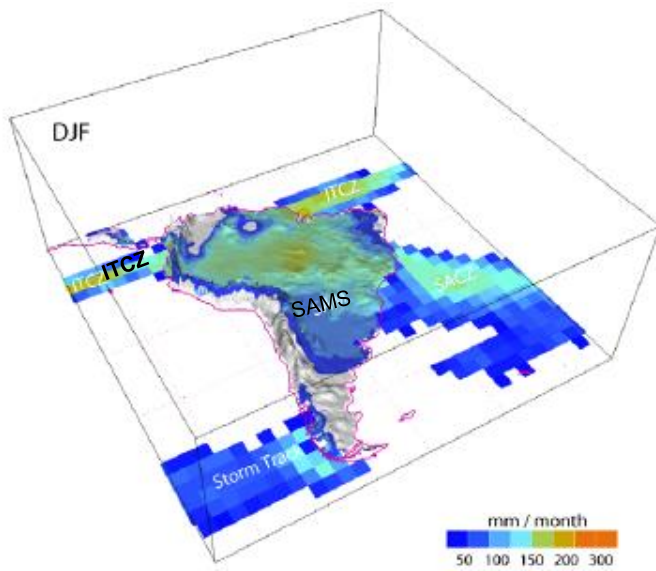


Figure 1.3 Precipitation mean over South America in the austral summer (December-January-February). The Intertropical Convergence Zone (ITCZ) and South American Summer Monsoon (SASM) are the main systems that dominate the climate in South America. Cold and arid conditions prevail along the Pacific coast extending well into the Andes western slopes, while moist and rainy conditions prevail over the eastern slopes. Rainfall data obtained from Delaware University (continental) and CMAP (Ocean) Source: Garreaud 2009 "The Andes climate and weather".

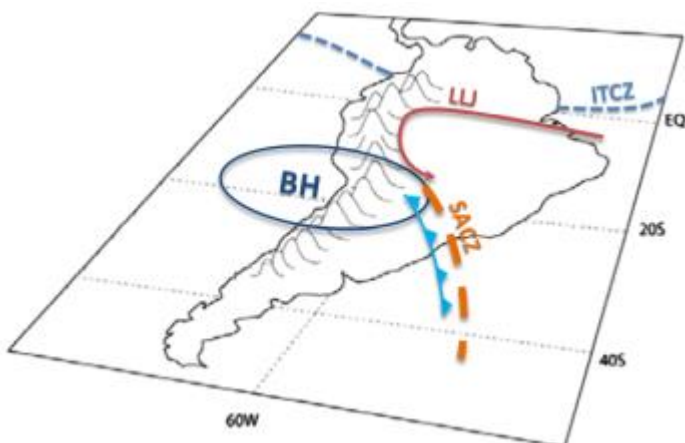


Figure 1.4. Major components of the SASM, including South Atlantic Convergence Zone (SACZ, orange dashed lines), Low-Level Jet (LLJ, red continue lines) and the Bolivian High (BH, blue continue lines) (Vera et al., 2006). The winds entering from the northeast are forced towards the south by the Andes, thus forming the South American Low-Level Jet (SALLJ). These low-level winds advect humid air. As a result, precipitation over Amazonia, central and southeastern Brazil and the South American Convergence Zone (SACZ) is increased. Moisture convergence at low levels and the latent heat release at mid-levels help sustain the upward movement and maintain a BH and relatively warm troposphere in the region.

southeasterly direction from the tropics to the subtropical plains (Cheng et al., 2013), feeding the South Atlantic Convergence Zone (SACZ), extending from the southeastern Amazon basin toward the southeast out over the South Atlantic. On the other hand, the Bolivian High (BH) (Upper circulation resulted of condensational heating over the Amazon basin (Lenters and Cook, 1997) favors the moist air influx from the Amazon basin onto the central Andes, feeding convective storms (Garreaud 1999, 2000; Vuille 1999; Vuille et al. 2000; Vuille and Keimig 2004; Garreaud et al. 2003) concurrently contributes to the intensification of the SACZ. This BH is accompanied by a convergence region along the coast of Peru and Ecuador (Virji 1981; Lenters and Cook, 1997; Garreaud and Aceituno, 2007).

1.2 HYDROLOGY IN THE PERUVIAN PACIFIC BASIN

In the Peruvian Pacific Basin (PPB) previous research has founded that the effects of strong El Niño events are linked with large positive anomalies of rainfall in the North-Centre region (Bourrel et al., 2015; Rau et al. 2017) leading to positive anomalies of continental discharge (until around 1800 mm/year) (Lavado et al., 2012, 2013; Rau et al., 2017), while in the south region the continental discharge anomalies are negatives (Lavado et al., 2012, 2013). These findings reveal that the rivers of northern Peru display the most direct reactions to El Niño in the form of massive floods during wet summers (Waylen and Caviedes, 1986). With elevation, the El Niño signal fades in the watercourses of the Peruvian Andes and even shifts to deficit discharges in rivers of the slopes of the Andes.

The variability of anomalies (floods and droughts) increase the existing vulnerability of a continental discharge of arid climate (49 to 541 mm/year). The PPB includes 54 main rivers that flow from the Andes toward the Pacific Ocean (from east to west). Their continental discharges represent 2% of the national total of available fresh water used as for an extensive agriculture under irrigation, for the consumption of 50% of the Peruvian population which is concentrated in the PPB, for the ten large reservoirs and hydraulic systems located in the upper and middle parts along the PPB and for other human activities (e. g. mining and industry). Identifying ENSO and hydrologic relationships can aid water management decision making by providing a lead-time of one month to mitigate floods or drought impacts.

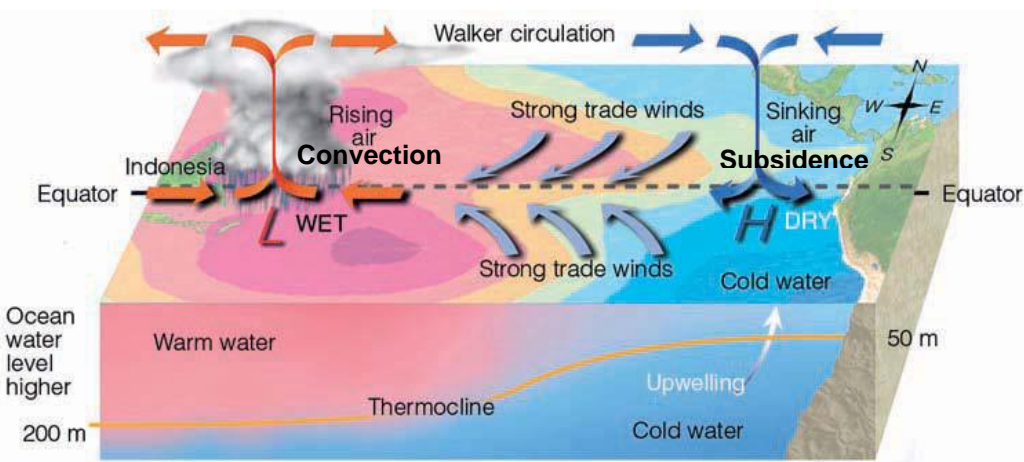
1.3 EL NIÑO AND ITS DIVERSITY

1.3.1 ENSO

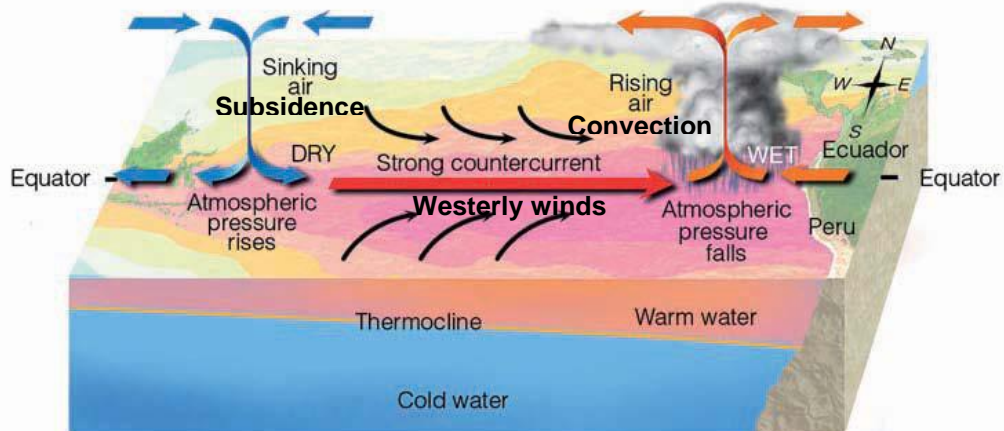
The ENSO, recognized as the El Niño-Southern Oscillation, presents an intimate linkage between El Niño events and the Southern Oscillation (AMS, 2013). ENSO refers to the Ocean and atmosphere coupled climate phenomenon, triggered by changes in sea temperatures in the Pacific Ocean and response in the global atmospheric circulation. These coupled interactions can amplify initial anomalies, resulting in unusually high Sea Surface Temperatures (SST) that cover much of the eastern and central tropical Pacific Ocean. The ENSO cycles are opposite phases El Niño and La Niña that require certain changes in both the ocean and the atmosphere. The ENSO neutral phase is in the middle of continuum.

1.3.1.1 EL NIÑO

El Niño refers to a warming of the Ocean surface, or above-average SST, in the central and eastern tropical Pacific Ocean. The tropical SST changes influence the atmosphere through surface fluxes of moisture, heat, and momentum and a readjustment of the tropical circulation in a thermally direct sense. The low-level surface winds which normally blow from east to west along equator (“easterly winds”), instead weaken or, in some cases, start blowing in the other direction (from west to east or “westerly winds”) which involve variations in the Hadley and Walker circulations (Ambrizzi et al., 2005; Shimizu et al., 2016) and atmospherics Rossby-wave (Andreoli et al., 2016) (see Fig 1.5). Anomalous rising motion over the eastern Pacific (Walker circulations) results in anomalous subsidence over the Amazon which are associated with the occurrence of excessive rainfall along the Northern Peruvian Coast (Rasmusson and Carpenter, 1982; Horel et al., 1986; Goldberg RA et al., 1987; Tapley T et al., 1990; Bendix E et al., 2006; McPhaden et al., 2006; Douglas M et al., 2009; Lavado et al., 2014; Capotondi et al., 2015) and dryness in the northern and Centre Amazon basin, respectively. The anomalous Rossby wave activity propagating into South America via midlatitudes, result in anticyclonic low-level anomalies over tropical South America and southeastern Brazil. These anomalies divert Atlantic moisture into northern South America and Southern Brazil, resulting in negative precipitation anomalies in north and central-east Brazil and positive anomalies in south Brazil (Grimm 2003).



(a) Neutral ENSO



(b) El Niño phase

Figure 1.5. El Niño-Southern Oscillation (ENSO). (a) Neutral ENSO: higher pressure over the eastern Pacific and lower pressure near Indonesia produce easterly trade winds along the equator. These winds promote upwelling and cooler ocean water in the eastern Pacific, while warmer water prevails in the western Pacific. The trades are part of a circulation (called the *Walker circulation*) that typically lead convection and heavy rain over the western Pacific and air subsidence and generally dry weather over the eastern Pacific. When the trades are exceptionally strong, water along the equator in the eastern Pacific becomes quite cool. This cool event is called La Niña. (b) El Niño conditions: atmospheric pressure decreases over the eastern Pacific and subsidence over the western Pacific. This change in pressure causes the trade winds to weaken or reverse direction. This situation enhances the westerly winds that carry warm water from the west toward the central to eastern tropical Pacific that lead to convection and trigger heavy rainfalls over the eastern Pacific. The thermocline, which separates the warm water of the upper ocean from the cold waters below, in response to the equatorial winds, flattens during El Niño and becomes more tilted during La Niña. Source: Meteorology today (Ahrens, D. 2009, pp 277).

1.3.1.1.1 EL NIÑO EVENTS

El Niño events are episodes El Niño that appear irregularly, every 2 to 7 years. These events usually begin in the middle of the year and last from 6 to 18 months later. They reach their maximum intensity around Christmas. The name El Niño subsequently became more commonly used in reference to the occasional very strong coastal warmings that are associated with intense rainfall in the otherwise dry and cold eastern equatorial Pacific Ocean (AMS, 2013). However, El Niño events differ in amplitude, temporal evolution, and spatial pattern. Significant research has been conducted to identify, describe, and understand the El Niño types.

1.3.1.1.2 TYPE OF EL NIÑO EVENTS.

Extreme ultimate El Niño events are recognized to be the events of 1982/1983 and 1997/1998 which were the most intense and peculiar in the modern observational registry. They exhibit unusual characteristics from any other observed El Niño events (Santoso et al., 2017). These include an eastward propagation of SST anomalies (McPhaden and Zhang, 2009; Santoso et al., 2013) which exceed a threshold of $\sim + 2^{\circ}\text{C}$ in the far eastern Pacific and involve an enhancement of the Bjerknes feedback (Takahashi et al. 2011, 2017; Takahashi and Dewitte, 2016). These events are associated with torrential rainfalls in the desert coastal regions of southern Ecuador– northern Peru (Cai, Borlace, et al., 2014) and subsequent high socioeconomic impacts (Philander, 1983; McPhaden, 1999).

However, the recent literature, confusingly refer to extreme El Niño events as “canonical”, even though the latter are rare compared to the moderate events to which the term originally applied.

“Canonical” El Niño events refer to the eastern Pacific SST decreasing very rapidly at the end of the event and falling below the climatological value (Cane, 1983). This type of canonical El Niño is described by the pre-1982 El Niño composites of Rasmusson and Carpenter (1982) and Harrison and Larkin (1998), which was built from moderate events and, in boreal winter, they share more characteristics with moderate Central Pacific El Niño events than to the extreme events (Takahashi et al., 2011, Dewitte and Takahashi., 2017).

El Niño “Modoki” events (a Japanese word that means similar but different: “pseudo” El Niño) has been defined by Ashok et al. (2007) and refer to a different type of El Niño with positive SST anomalies in the central equatorial Pacific, and peak near the date line (180°),

with no significant warming of the east Pacific (cold tongue region). This type of El Niño involves ocean-atmosphere coupled processes which include a unique tripolar sea level pressure pattern during the evolution. Being associated with remote impacts on surface air temperature and precipitation different from those related to “typical” El Niño conditions (Larkin and Harrison, 2005) and Ashok et al. (2007).

Events into Central Pacific, also termed the “dateline El Niño” or “warm pool El Niño”, present a location of maximum SST anomalies in the Central Pacific (Yeh et al., 2009) and include also “Modoki” (Ashok et al., 2007) and “Canonical” (Rasmusson and Carpenter, 1982) El Niño.

1.3.1.2 LA NIÑA

La Niña (opposite conditions to El Niño) presents sea surface temperatures colder than the average over most of the tropical Pacific Ocean. La Niña also involves oceanic processes (Frauen et al., 2010). The normal easterly winds along the equator become even stronger therefore the Pacific warm pool and equatorial convective rainfall are confined to the extreme western part of the basin (Indonesia). During La Niña events, anomalous heavy rainfalls take place during the rainy season in central-east Brazil and at the end of the rainy period: the anomalous rainfall is displaced to the Northeast Brazil and southeastern South America (Aceituno 1988; Ropelewski and Halpert 1989; Grimm et al. 2000; 2004; 2009), which is associated with the prevalence of regional processes over remote influences during part of the season (Grimm, 2004). In the Peruvian Andes during La Niña event, above than normal rainfall also take place (Lavado and Espinoza, 2014), which is due to convergence in the Amazon region in response to the compensation of surface divergence over the east tropical Pacific (Torralba et al., 2015). The convergence is linked to a develop close of the Intertropical Convergence Zone (ITCZ) to the Northeast (De Souza and Ambrizzi, 2002; Grimm, 2003) that diverts moisture influx toward the Amazon by the low-level cyclonic anomaly north of equator (Grimm, 2004), and also is linked to a prominent South Atlantic convergence zone (SACZ) that contributes to the tropical moisture flux divergence toward the Amazon basin (Ferreira et al., 2003).

El Niño and La Niña are extreme phases in the SST manifestation of the coupled Ocean–atmosphere ENSO phenomenon, which represents the single most prominent mode of climate variability at seasonal to interannual time scales.

1.3.1.3 NEUTRAL

Neutral ENSO refers to those periods when neither El Niño nor La Niña is present. Tropical Pacific SST is generally near the long-term average. During this period, surface trade winds blow westward across the equatorial Pacific Ocean. Blowing against the ocean surface, these winds result in a westward current. However, there are some instances when the Ocean can look like an El Niño or La Niña state, but the atmosphere is not playing its role in the continuity of the initial conditions (L'Heureux, 2014).

1.3.2 ENSO INDICES

The Oceanic Niño Index (ONI) is NOAA's primary indicator for monitoring El Niño and La Niña, which are opposite phases of the ENSO phenomenon. It is the running 3-month mean SST anomaly for the Niño 3.4 region (see Fig.1.6) from ERSST.v5 SST data (Huang *et al.*, 2017). Events are defined as 5 consecutive overlapping 3-month periods at or above the +0.5° anomaly for warm (El Niño) events and at or below the -0.5 anomalies for cold (La Niña) events (See figure 2.10). The threshold is further broken down into Weak (with a 0.5 to 0.9 SST anomaly), Moderate (1.0 to 1.4), Strong (1.5 to 1.9) and Very Strong (≥ 2.0) events. This report for an event to be categorized as weak, moderate, strong or very strong must have equaled or exceeded the threshold for at least 3 consecutive overlapping 3-month periods (see Fig. 1.7).

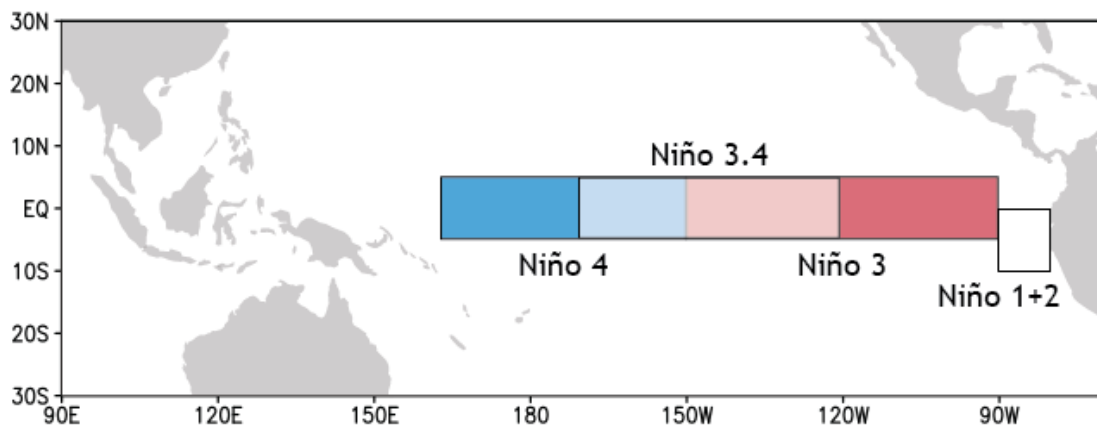


Figure 1.6. Location of the Niño regions for measuring Sea Surface Temperature (SST) in the eastern and central tropical Pacific Ocean. The SST in the Niño3.4 region, spanning from 120°W to 170°W longitude, when averaged over a 3-month period, forms NOAA's official Oceanic Niño Index (the ONI). Source: NOAA Climate.gov.

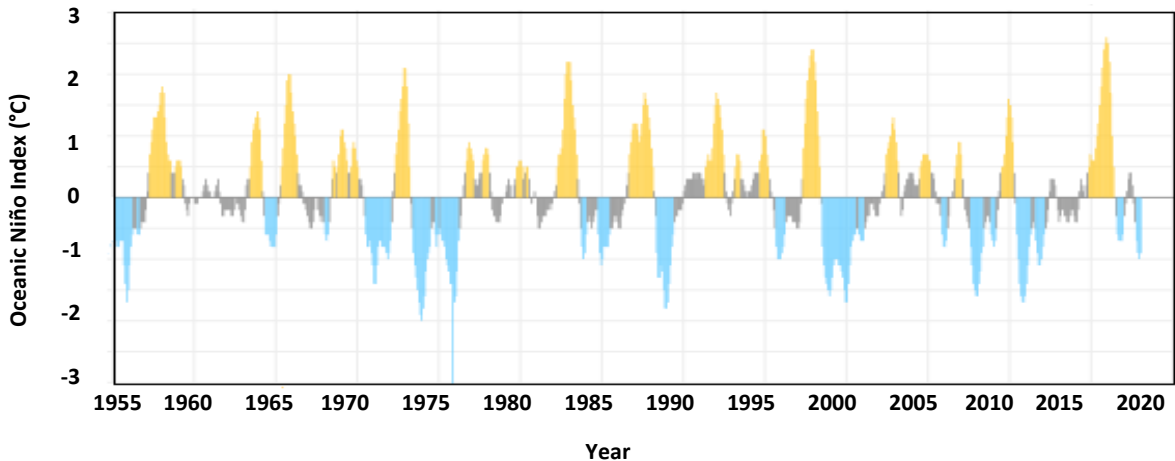


Figure 1.7. Monthly values of the Oceanic Niño Index (the ONI) from ERSST.v5 SSTdata over the period 1955 through present. The signal of ONI is clearly observed during the strong El Niño events of 1982/1983, 1997/1998 and 2015/2016 with values higher than 2°C. Source: NOAA Climate.gov.

In addition to the Ocean Niño index, atmospheric measurements can indicate the status of the El Niño - Southern Oscillation cycle. As El Niño conditions develop, sea surface temperatures in the eastern Pacific Ocean increase and air pressure over the region decreases. Simultaneously, higher air pressure develops over the cooler sea surface in the western Pacific, near Indonesia. Thus, the difference in air pressure between these two regions provides another way to monitor the ENSO cycle through the Southern Oscillation Index (SOI). The SOI is negative during El Niño years and positive during La Niña years. SOI measurements can reflect local variability and weather disturbance, usually it is an average value for a minimum period of 5-month consecutives (see Fig. 1.8).

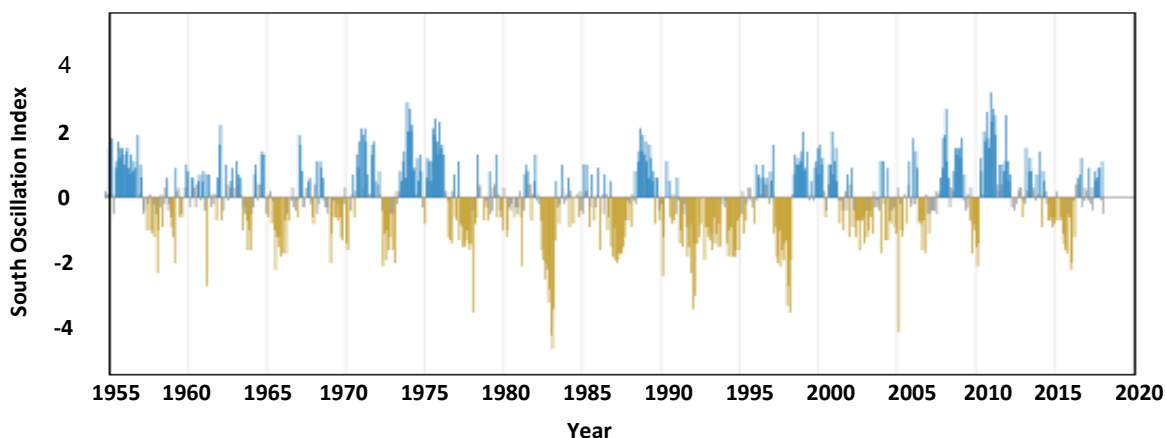


Figure 1.8. Monthly values of the Southern Oscillation Index (SOI) of the period 1955 to present. The signal of SOI is clearly observed during the strong El Niño events of 1982/1983 and 1997/1998 with values around 4 and 3, respectively. While 2015/2016 El Niño is less clear. Source. NOAA Climate.gov.

1.3.3 TELECONNECTIONS

The ENSO phenomenon influences the regional climate remotely through so-called teleconnections. First, ENSO is associated with the release of adiabatic heat to the troposphere, modifying main atmospheric pathways, leading to the so-called atmospheric teleconnections (Bjerknes, 1969; Horel and Wallace, 1981; Keshavamurty, 1982; Philander, 1985; Trenberth et al., 1998; Diaz et al., 2001). The atmospheric ENSO teleconnections have been extensively studied as they can provide a mechanism by which the main mode of interannual variability in the tropics can impact regional climate over the globe. For the coast of Peru where dry mean conditions usually prevail below south of 7°S, these teleconnections are particularly spectacular during strong El Niño events, because the coastal region experiences heavy rainfall from the North to South of the Lima region (around 12°S) (Takahashi and Martinez, 2017) (See Fig. 1.9). Also, ENSO is associated with planetary oceanic waves activity along the equator (i.e. Kelvin waves) which can propagate along the coasts of South America and alter the local oceanic circulation in regions that usually experience a persistent upwelling (Clarke, 1983).

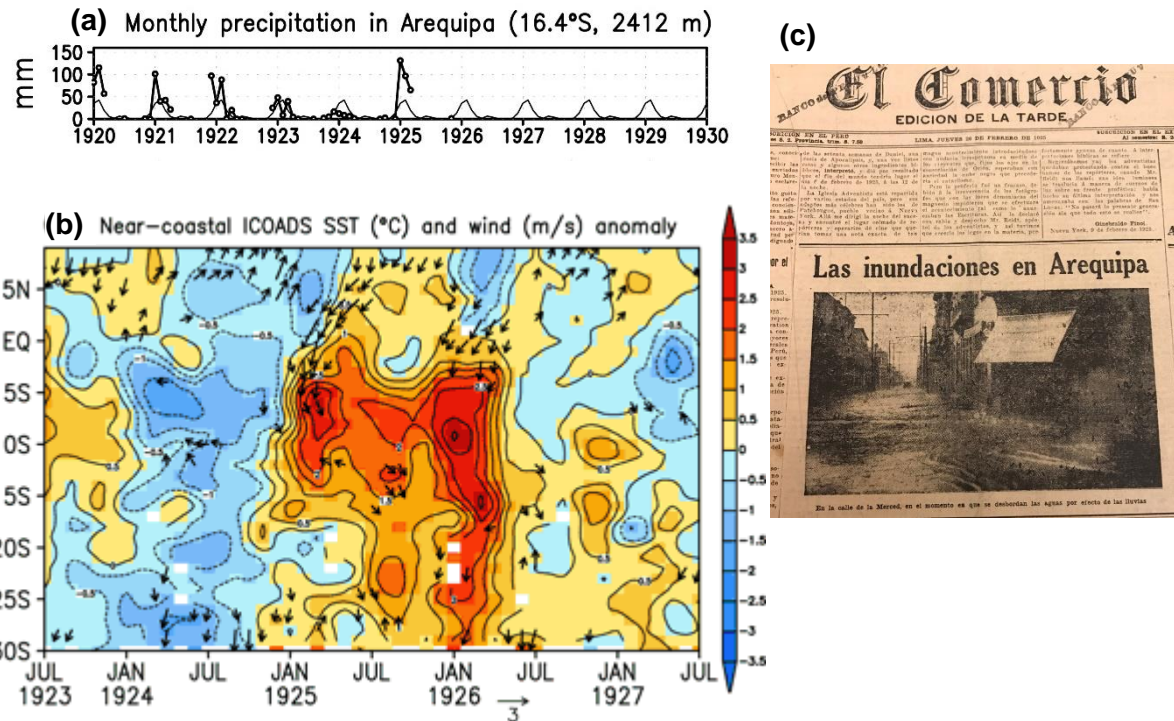


Figure 1.9 (a) Rainfall anomalies in Arequipa (16.4 °S located to South of the Lima region) relative to its climatology (thin lines; based on 1920-1939) associated with (b) SST anomalies (with respect to 1920-1939) along the near- coastal track during EL Niño 1925. (c) Report of 1925-1926 summer “exceptionally warm and early”. Source: *Takahashi and Martinez, 2017*. *The very strong El Niño in 1925 in the far-eastern Pacific. Journal: Climate Dynamics.*

Teleconnections are relationships between the temporal fluctuations of climatic variables separated by large distances. They are highlighted by statistical relationships between large scale modes of climate variability with regional rainfall patterns or other variables (Goddard *et al.*, 2001). ENSO has global influence through atmospheric teleconnections that affect patterns of weather variability worldwide. The worldwide signatures of ENSO in surface pressure and rainfall were first recognized by Walker and Bliss (1932), and the link between the atmospheric anomalies and tropical Pacific SST anomalies was discovered in the late 1950s and 1960s (e.g. Bjerknes, 1966). Major advances in ENSO research developed since 1980. ENSO teleconnections are directly forced by the anomalies in convection and vertical motion in response to tropical SST anomalies (see Fig 1.10), which force the stationary extra-tropical Rossby wave (e.g. Trenberth *et al.*, 1998) and equatorial waves patterns (Gill, 1980). In the Southern Hemisphere, where the climatological stationary wave pattern is not as noticeable, we could also expect a larger sensitivity to the specific pattern of the convective response to ENSO.

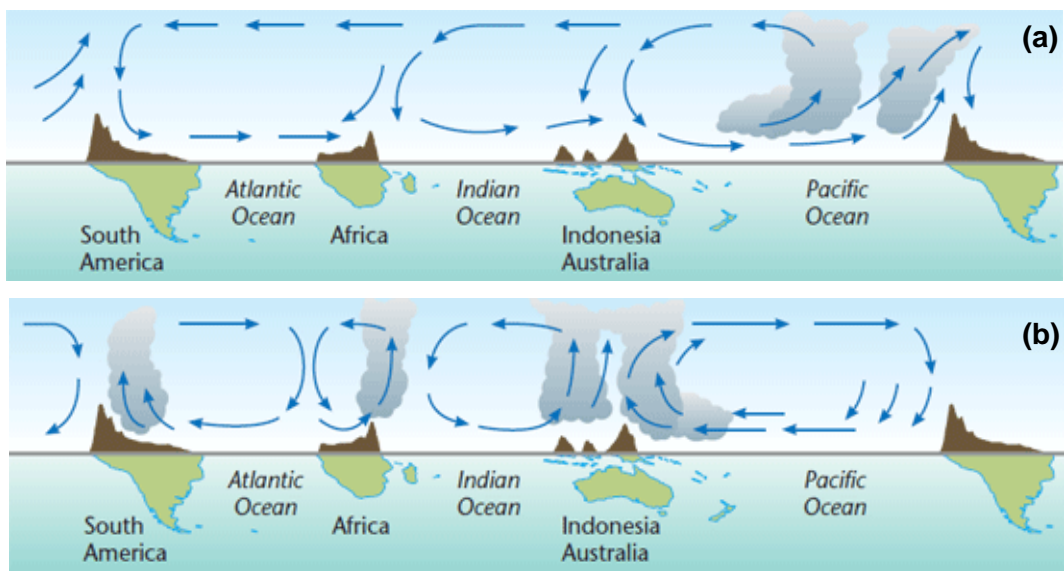


Figure 1.10 Teleconnections in the tropical zone. (a) El Niño event associated with strong convection over the southeastern Pacific Ocean and subsidence over the Amazon (b) Neutral conditions associated with strong subsidence over the southeastern Pacific and convection over the Amazon. Source: Revision World. World-wide impacts of El Niño Southern Oscillation. Retrieved from <http://www.revisionworld.com/a2-level-revision/geography/synoptic-assessment-0/drought-and-its-teleconnection-enso>

The amplitude to which ENSO events shift the range of climate outcomes locally depends on the region, season, and also the strength and spatial distribution of the ENSO-related SST anomalies. The conditioned probabilistic climate anomalies suggest relative robustness of regional teleconnections associated with ENSO (Mason and Goddard, 2001). Differences between events in tropical Pacific SST forcing and internal variability of the atmosphere, some studies suggest reciprocal interactions between equatorial and midlatitudinal weather systems (Stephens *et al.*, 2007). ENSO teleconnections are also affected by SST anomalies in the tropical Indian and Atlantic Oceans that produce their own regional climate variations (Bazo *et al.*, 2013).

1.3.4 EL NIÑO DIVERSITY: EASTERN (EP) AND CENTRAL PACIFIC (CP) EL NIÑO

In the recent decades, the concept of ENSO diversity has emerged. It refers to the existence of two different types of El Niño events: the Eastern Pacific (EP) and Central Pacific (CP) El Niño events differing in the locations of the maximum Sea Surface Temperature (SST) anomalies, in the EP and CP, respectively (Larkin and Harrison, 2005; Ashok *et al.*, 2007; Yu and Kao, 2007; Kao and Yu, 2009) (See Fig. 1.11). While much efforts had been done on understanding the mechanisms associated to the extreme EP El Niño events because of their tremendous societal impacts, the community has disregarded for many years the other type of event, the CP type, although the variability associated to this type of event can explain a large amount of variance of SST anomalies in the tropical Pacific (Takahashi *et al.*, 2011). Ashok *et al.* (2007) renewed the interest in this type of event because they noticed that they had a distinct ENSO teleconnection than the EP events. For the PPB, Bourrel *et al.*, (2015) and Rau *et al.*, (2017) showed in particular that CP El Niño events are associated with rainfall deficit in the Andes, and EP El Niño events with extreme rainfall in the north to central coastal region.

The concept of ENSO diversity is quite useful for addressing ENSO teleconnection (Hastenrath, 1978; Keshavamurty 1982; Ropelewski and Halpert, 1987; Navarra *et al.* 1999; Barsugli and Sardeshmukh, 2002; Larkin and Harrison 2005; Weng *et al.* 2007, 2009; Ashok *et al.*, 2007; Yeh *et al.* 2009; Trenberth and Smith 2009; Frauen *et al.*, 2014; Capotondi *et al.*, 2015) since it assumes that the ENSO variability can be decomposed into two independent (uncorrelated) regimes that are accounted for by some indices. Previous studies have used classical indices of ENSO as the NOAA (U.S. National Oceanographic and Atmospheric Administration) who has defined certain regions for measurements namely Niño1+2 region (10°S- 0°S and 90W- 80W) that may be the first to warm during an El Niño, the NINO3 region

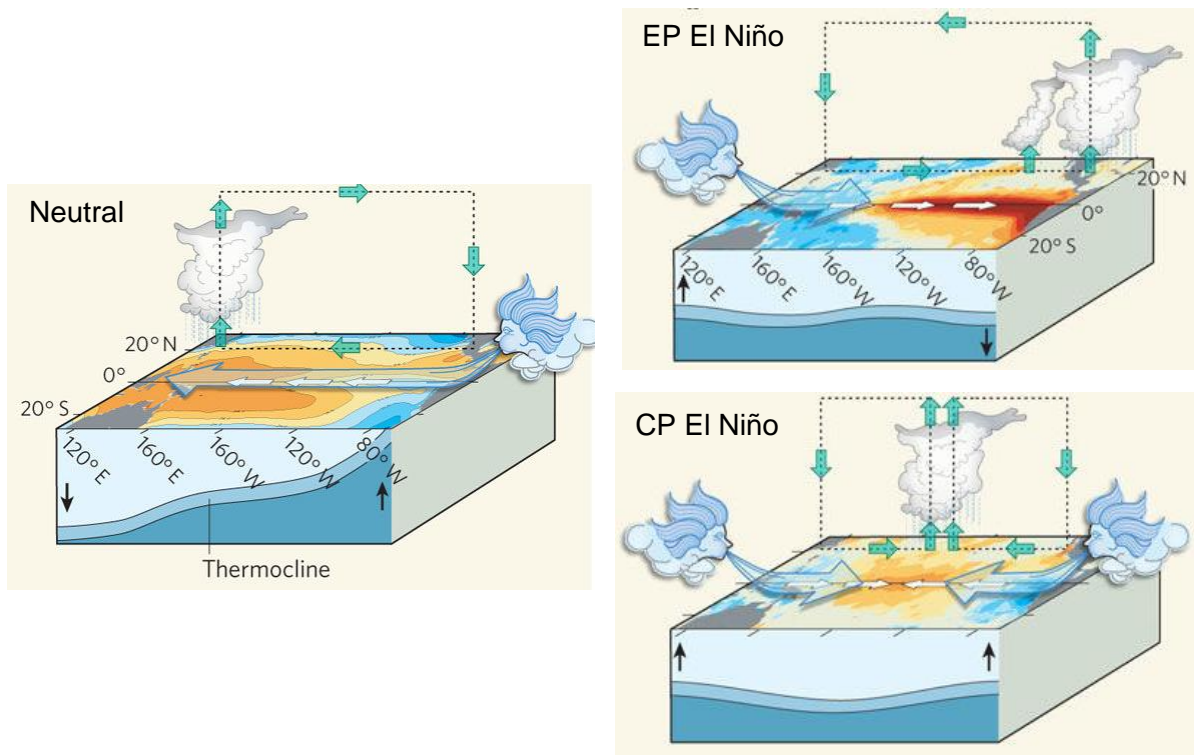


Figure 1.11. El Niño Diversity (a) Neutral conditions (b) EP El Niño event (c) CP El Niño event. Neutral conditions associated with southerlies winds blow east to west across the surface of the tropical Pacific Ocean, bringing warm moist air and warmer surface water towards the western Pacific and keeping the central Pacific Ocean relatively cool. Whereas EP El Niño event the southerlies winds weaken or may even reverse allowing the area of warmer than normal water to move into the central and eastern tropical Pacific Ocean. It is associated with reversed atmospheric circulation linked to ascending motions and weakened low-level winds in the eastern equatorial Pacific (150°E and 85°W) triggered an eastern Pacific wetter and the western Pacific drier. Instead, CP El Niño anomalous warming in the central Pacific flanked by anomalous cooling in the eastern and western sides of the Pacific basin (Ashok and Yamagata, 2009) which is associated with a double Walker cell with the anomalous ascending branch in the central Pacific, and descending branches in the western and eastern equatorial Pacific leading to a western and eastern Pacific drier. Source: Ashok and Yamagata, 2009. <http://www.nature.com/nature/journal/v461/n7263/full/461481a.html>

(5°S - 5°N and 90°W - 150°W) which experiences the most temperature variability, and the NINO4 region (5°S - 5°N and 150°W - 160°E) which represents a strong indicator for precipitation conditions over Indonesia. Later, the Niño3.4 region (5°S - 5°N and 170°W - 120°W) most notably (Barnston et al. 1997; Trenberth 1997) considered as the mean SST throughout the equatorial Pacific east of the date line (Trenberth and Stepaniak, 2001) (see Fig 1.6).

Unfortunately, these indices are strongly correlated with each others, which tends to obscure the teleconnection pattern and mixed different processes of teleconnection. Takahashi et al. (2011) proposed to use new indices, uncorrelated by construction, that account for the two El Niño regimes that respectively account for extreme warm events in the eastern equatorial Pacific and cold/moderate events in the central equatorial Pacific, corresponding to regimes with different evolution. This approach has been shown to be useful for addressing the teleconnection of ENSO in the PPB and its low-frequency modulation (Bourrel et al., 2015; Rau et al., 2017). We will build on a similar methodological approach in Chapter 2.

1.3.4.1 C AND E INDICES

The E and C indices (Takahashi et al., 2011) were constructed using two orthogonal axes that are rotated 45° relative to the principal components of SST anomalies of the Tropical Pacific Ocean. The associated projections of the SST anomalies onto these rotated axes provide the E-index (representing the eastern Pacific El Niño) and the C-index (representing both the central Pacific El Niño and La Niña events).

The corresponding indices are defined as:

The PC1 and PC2 are the first two principal components (PCs). The PCs were linearly combined to estimate the values of E and C indices. These C and E indices are well correlated with the central (Niño 4; $R = 0.98$) and eastern (Niño 1 + 2; $R = 0.94$) Pacific SST indices, respectively. The E pattern has its strongest amplitude and explained variance along the eastern equatorial Pacific (east of 120°W) and along the coast of Peru, whereas the C pattern has its amplitude and explained variance in the central equatorial Pacific (170°E – 100°W , maximum in the Niño 4 region) both on a domain limited by 10°N and 10°S .

Kao and Yu, 2009; Capotondi et al., 2015 pointed that El Niño can be understand as resulting from these two regimes and which encompass the two different types of events (Yeh et al., 2009; Takahashi et al., 2011).

1.4 MECHANISMS TRIGGERING RAINFALL EVENTS DURING EXTREME EL NIÑO EVENTS

The South Pacific anticyclone centered near Easter Island (27°S , 110°W), during the extreme El Niño events, this is weakened and loses intensity, concurrently the Trade Winds slacken and the thermocline thickens in the eastern tropical Pacific, give rise to westerly winds replacing the usual equatorial easterlies. Concomitantly, the positive SST anomalies over the Central - eastern Pacific lead to stronger than normal evaporation which supported by westerly winds inducing to a stronger moisture transport (Mayer *et al.*, 2013) to the east (Gimeno *et al.*, 2016) releasing torrential rains over the arid coasts of Ecuador and northern Peru (e.g. Rasmusson and Carpenter, 1982; Horel *et al.*, 1986; Goldberg RA *et al.*, 1987; Tapley T *et al.*, 1990; Trenberth *et al.*, 1998; Bendi E *et al.*, 2006; McPhaden *et al.*, 2006; Douglas M *et al.*, 2008; Lavado *et al.*, 2014; Capotondi *et al.*, 2015, Bourrel *et al.*, 2015; Rau *et al.*, 2017; Sulca *et al.*, 2017). It is clearly observed convection in Central Pacific and moisture eastward advected (Paixao Veiga *et al.*, 2005; Boers *et al.*, 2014; Xu *et al.*, 2015). The moisture transport follows the eastward shift of warm equatorial SST of two El Niño regimes observing for EP El Niño more moisture transport anomalies than CP El Niño (Gu *et al.*, 2016) which are associated with distinct atmospheric circulation patterns (Kug *et al.*, 2009; Tedeschi *et al.*, 2013; Zhelezova and Gushchina, 2015; Andreoli *et al.*, 2016) leading to different rainfall anomaly patterns (Gu *et al.*, 2016).

This dynamic atmospheric ocean during the EP (CP) Niño is linked with southward displacement about 5° (a dominate position in the central-eastern Pacific) of the Pacific ITCZ (Goldberg *et al.*, 1987; Vecchi, 2006; Takahashi and Battisti, 2007; Tedeschi *et al.*, 2013; Schneider *et al.*, 2014), and connected to ascent motion over the Pacific and subsidence over northern\northeastern South America (east of 60°W) resulted of a shift Walker circulation (Liebmann and Marengo, 2001; Ronchail *et al.*, 2002; Ambrizzi *et al.*, 2005; Shimizu *et al.*, 2016) associated with wet and dry conditions, respectively (See Fig 1.12) being stronger in EP than CP El Niño (Tedeschi *et al.*, 2013; Andreoli *et al.*, 2016; Sulca *et al.*, 2017).

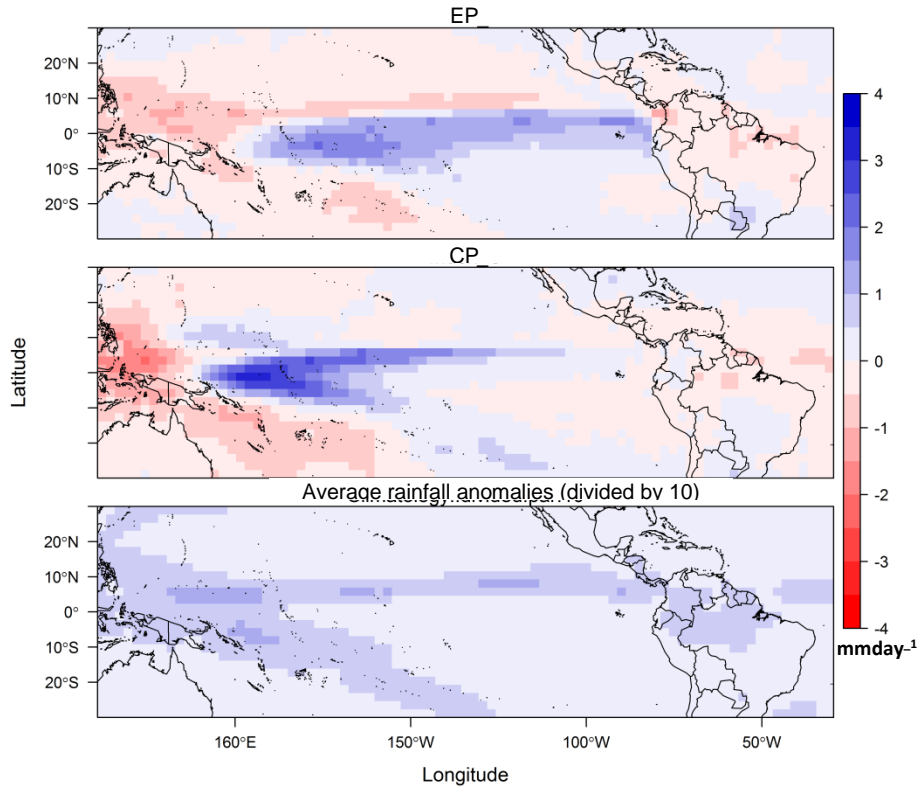


Figure 1.12. Rainfall anomalies patterns associated with the eastern Pacific (EP) and central Pacific (CP) El Niño. EP El Niño (top) exhibits rainfalls extended to the coast of South America while CP El Niño (bottom) shows rainfalls confined in the Central Pacific. Mean rainfall over 37 years (1979-2016 period) (bottom inferior) extended along tropical Pacific over north latitude. Monthly rainfall data are from CPC Merged Analysis Precipitation (CMAP) provided by the NOAA/OAR/ESRL PSD, Boulder, Colorado, USA, from their Web site at <https://www.esrl.noaa.gov/psd/>.

During the strong El Niño events the SASM is weakened while the South Atlantic Convergence Zone (SACZ) is enhanced a little more southward (Robertson and Mechoso, 2000; Zhou and Lau, 2001, Carvalho et al., 2004; Sulca et al., 2017) and the Low-Level Jet east of the Andes (LLJ) is intensified transferring humidity associated with anomalous moisture flux from tropical to southern regions (Marengo et al., 2004; Silva and Ambrizzi, 2006; Silva et al., 2009) linked with extreme precipitation. Also, BH is weakened by stronger-than-average subtropical westerlies over the Altiplano, inhibiting the advection of moisture from Atlantic towards the northern and central Andes of the Pacific basin. Precipitation impacts in tropical South American precipitation during extreme El Niño is related to anomalies in the Walker circulation. In extra-tropical South America, the precipitation impacts are due to differences in the Pacific wave trains (Rossby wave) and differences in moisture flux intensity over the continent (Grimm 2003; Tedeschi et al, 2013). In general terms, such variations observed during El Niño episodes may include the displacement of equatorial Pacific rainfall toward the eastern basin, the weakening of the major America south summer monsoon system.

2. MOTIVATIONS OF THE STUDY

Mechanisms of large scale moisture advection and local convection activation due to warm water conditions during strong El Niño events lead to different rainfall patterns in the PPB which are not well understood. There is evidence that large scale moisture advection associated with the strong 1982/1983 and 1997/1998 El Niño events include process of moisture transport that reaches the Northern Peruvian coast which is channelized by the mountains determining rainfall particularly over the Andes foothills (Goldberg and Tisnado 1987). These strong events seem to include also process of local convection producing rainfall which is triggered by anomalously warm waters along the coast of northern Peru (Horel and Cornejo-Garrido, 1986; Goldberg *et al.*, 1987; Bendix and Bendix 1998; Takahashi, 2004).

Other mechanisms of activation of local convection associated with “coastal El Niño” like the strong 1925 El Niño (Murphy, 1926) present a different dynamic characterized by warm conditions in the eastern Pacific, but cool conditions elsewhere in the central Pacific. This local warming involves a coupled meridional ocean–atmosphere feedback dynamics associated with the ITCZ, northerly winds, and the north–south SST asymmetry in the Eastern Pacific lead to the enhancement of the seasonal cycle that produced this costal event. The ocean warming probably involves a combination of the wind-evaporation-SST mechanism and oceanic southward warm advection. This El Niño of local meridional dynamic lead to very strong rainfall along the coast of PPB (Murphy, 1926; Takahashi *et al.*, 2017).

It is also noted a mechanism that have failed to evolve as a EP El Niño type like El Niño 2015/2016, although this event in the Niño3 and Niño4 regions reached a large magnitudes of SST anomalies exceeding 4°C as the previous extreme event of 1997/98 (Hu and Fedorov, 2017) but the Eastern Pacific was substantially weaker compared to 1982/1983 and 1997/1998 (L'Heureux *et al.* 2017), and hence weaker rainfall anomalies along the coast in the Northern Peru (Sanabria *et al.*, 2018).

Two mechanisms (the strong 1982/1983 and 1997/1998 El Niño events, and the very strong “coastal Niño” like 1925) apparently associated with nonlinear convective feedbacks but with very different dynamic of the El Niño event are some prominent features of interannual variability. As well, other events (2015/2016) associated to a dynamic that combine processes of the EP El Niño type and the CP El Niño type (Paek *et al.*, 2017) added the complexity of the characteristics of the interannual variability. Being a motivation for investigate the interannual rainfall variability in the PPB and how these mechanisms determine the different rainfall patterns associated with the strong El Niño events. Other motivation is the increase in

occurrences of extremes El Niño events in the future in response to greenhouse warming (Cai et al., 2014). But these future projections arise of SST increases which are not always related to the development of an EP El Niño type and impacts of heavy rainfalls in the PPB as 2015/2016 El Niño, also there are other key forcing to take into account.

Different mechanisms El Niño associated to different extreme rainfall patterns (extension and magnitude) in the PPB need to be elucidated. In all the mentioned context, the focus of the thesis is to provide an assessment of the strong El Niño impacts on precipitation that can be used for identifying key climatic circulation pattern responsible for their different evolution and magnitude. These key patterns are very important for the diagnosis and forecast of the strong El Niño events, in order to reduce impacts of ENSO on the Peruvian socio economics.

2.1 OBJECTIVES

The main objective is to document the interannual rainfall variability in the PPB and interpret it in light of recent progress in our understanding of ENSO, in particular the notion of ENSO diversity (see section 1.3.1). We also want evaluate the extent to which Reanalysis data can account for the details of the ENSO teleconnection patterns in the PPB and investigate the mechanism at work during the development of extreme El Niño events.

2.1.1 SPECIFIC OBJECTIVES

Specific objectives are:

- I. Analyze in situ observation over the period 1964-2016
- II. Document the seasonal evolution of strong El Niño events

We assess the relationship between ENSO and rainfall during strong El Niño events by observing that these events can be characterized by different evolutions. Such dispersion in evolution and magnitude is likely to reflect onto precipitation along the slope and coast of the PPB. In particular, we document the relationship between the temporal evolution of strong El Niño events and rainfall along the coast of Peru to gain knowledge in the local and large-scale factors that determine the extent and magnitude of rainfall. We took into account the four strong El Niño events which took place over the last five decades (1972/1973, 1982/1983, 1997/1998 and 2015/2016 El Niño events) and produced noticeable rainfall in Peru.

Three previous proposals are addressed to achieve this goal:

- Estimate the modes of rainfall variability of the PPB using the methodology of rotated EOF modes
- Evaluate the seasonality of rainfall modes and link with ENSO
- Analyze the differences between strong events

III. Evaluate atmospheric Reanalysis data in terms of their mean state and interannual variability

One of the main difficulties for addressing the atmospheric processes regarding the link of atmospheric water transport and precipitation are the significant differences between the different available reanalysis that leads to evaluate this reanalysis and to provide a reasonable choice for representing better this atmospheric process. If rainfall reanalysis is generated by its atmospheric water balance model (coherent with observed rainfall) then we suggested that reanalysis well simulates the moisture transport. Singularly, we analyze the comparison between the rainfall variability in the PPB region in three reanalysis products (ERA-Interim, CFSR and JRA-55) and observed rainfall variability, which will allow us to identify the reanalysis bias and ability to reproduce this in situ variability.

We focus on the skill of the reanalysis to reproduce the spatial patterns that characterize rainfall variability, and also to reproduce the evolution of the four-major strong El Niño events over the last five decades: the 1972/1973, 1982/1983, 1997/1998 and 2015/2016 El Niño events. We aim to address the following question:

- How rainfall variability is accounted for in the three reanalysis products ?

IV. Document the transport of humidity in the most skill full Reanalysis products during the last three strong El Nino events and provide a mechanistic understanding of the rainfall events in the PPB

The four chapter examines how preferential moisture transport contributes to different patterns of rainfall over the PPB during strong El Niño conditions (1983, 1998, and 2016). We investigate how patterns of rainfall, in the PPB region, associated to El Niño can lead to different responses, (i.e. opposite anomaly phases), and if these differences are based on local variability (e.g. Niño 1+2). We also examine how changes in the regional and large-scale atmospheric circulation

impact these rainfall patterns. We hypothesize that rainfall in PPB can experience out-of-phase patterns (inverted pattern with respect to other) in similar El Niño events as measured by the El Niño 3.4. However, these patterns must fulfill water balance over the tropical South America. Thus, we test this hypothesis by analyzing variations related to moisture transport following the changes in rainfall and atmospheric circulation. Our approaches consider that observed rainfall and atmospheric water balance (convergence of vertically integrated moisture flux) are comparable (Paixao Veiga *et al.*, 2005; Wei *et al.*, 2016).

Our methodological approach combines the use of classical statistical analysis such as EOF and the diagnostic analysis of Reanalysis outputs through estimate of moisture convergence and humidity transport.

Chapitre 1 : Introduction

(Version française)

1. INTRODUCTION

Le bassin du Pacifique péruvien (PPB) est caractérisé par un climat aride et semi-aride. Les fluctuations des précipitations entre les grandes inondations et les grandes années de sécheresse ne peuvent pas être facilement expliquées en termes de fluctuations aléatoires des divers types de précipitations. Le mécanisme ENSO (El Niño - Southern Oscillation) durant certaines années peut aussi agir pour augmenter ou supprimer les systèmes tropicaux et de latitude moyenne qui régissent la pluie.

Il est bien documenté que la phase chaude de ENSO "El Niño" est le principal facteur de la variabilité interannuelle des précipitations dans le monde (McPhaden et al., 2006) et surtout en Amérique du Sud (Marengo et al., 2013). El Niño, interaction océan-atmosphère implique à la fois des variations de la circulation atmosphérique à grande échelle (circulation de Walker et trains d'ondes troposphériques de Rossby) qui répondent aux anomalies de SST dans le Pacifique équatorial (Bjerknes 1969 ; Trenberth et al., 1998; Hoerling et Kumar, 2002; Kug et al., 2009) et des variations de la circulation atmosphérique locale (South American Low-Level Jet - LLJ) qui conduisent à des anomalies distinctes des précipitations sur l'Amérique du Sud (Andreoli et al., 2016). L'Equateur et la région centre-nord du Pérou sont les régions où El Niño affecte directement les anomalies extrêmes des précipitations (Rasmusson et Carpenter, 1982, Horel et al., 1986, Goldberg RA et al., 1987, Tapley T et al., 1990; Trenberth et al., 1998, Bendix E et al., 2006, McPhaden et al., 2006, Douglas M et al., 2009, Lavado et al., 2014, Capotondi et al., 2015) et où la quantité de pluie est différente d'un événement à l'autre (Rome et Ronchail, 1998) avec une incertitude sur leur amplitude et leur extension (Rau et al., 2017). Il a eu de fortes implications pour l'économie péruvienne, reflétant de fortes baisses du produit intérieur brut (PIB) dues aux effets sur la population et les secteurs productifs (agriculture, énergie, transports, mines et autres). Par conséquent, il est clairement nécessaire de comprendre les conditions qui favorisent ces différences d'événements de précipitations extrêmes ainsi que les mécanismes impliqués, permettant ainsi d'améliorer leurs prévisions.

Le phénomène ENSO influence le climat régional à distance à travers de ce qu'on appelle les téléconnexions. Tout d'abord, ENSO est associé à la libération de chaleur adiabatique de la troposphère, en modifiant principales voies atmosphériques, ce qui conduit à ce qu'on appelle les téléconnexions atmosphériques (Bjerknes, 1969 ; Horel et Wallace, 1981 ; Keshavamurty, 1982 ; Philander, 1985 ; Trenberth et al 1998, Diaz et al., 2001). Les téléconnexions atmosphériques ENSO ont été largement étudiées car elles peuvent fournir un mécanisme par lequel le principal mode de variabilité interannuelle dans les tropiques peut affecter le climat régional dans le monde. Pour la côte péruvienne où les conditions sèches prévalent généralement en dessous de 7 ° S, ces téléconnexions sont particulièrement spectaculaires pendant les épisodes El Niño, car la région côtière expérimente de fortes pluies du nord au sud de la région de Lima (autour de 12 ° S) (Takahashi et Martinez, 2017). En outre, ENSO est associé à l'activité océanique planétaire le long de l'équateur (ondes de Kelvin) qui peut se propager le long des côtes d'Amérique du Sud et altérer la circulation océanique locale dans les régions où l'upwelling persiste (Clarke, 1983).

Récemment, une attention particulière a été donnée aux différents types de El Niño : El Niño Pacifique Est (EP) et El Niño Pacifique Central (CP), qui diffèrent selon les emplacements des anomalies maximales de température de surface de la mer (SST), dans le EP et le CP, respectivement. Kao et Yu, 2009 ; Capotondi et al., 2015 ont montré que El Niño peut être compris comme résultant de ces deux régimes et qui inclue les deux types d'événements différents (Yeh et al., 2009, Takahashi et al., 2011). Les réponses de la circulation atmosphérique (i.e. la position et l'extension longitudinale de la circulation de Walker) à ces deux régimes (Kug et al., 2009 ; Zheleznova et Gushchina, 2015 ; Andreoli et al., 2016) sont très différentes. El Niño EP (CP) est lié au déplacement vers le sud (position dominante dans le Pacifique centre-est) de la zone de convergence intertropicale du Pacifique -ITCZ- reliée à un mouvement ascendant sur le Pacifique et à une subsidence dans le nord et le nord-est de l'Amérique du Sud (60 ° W) étant plus forte dans El Niño EP que dans le El Niño CP (Tedeschi et al., 2013, Andreoli et al., 2016, Sulca et al., 2017). Au Pérou, El Niño EP et CP sont associés à des précipitations extrêmes dans le nord et jusqu'à la région côtière centrale et à des déficits pluviométriques dans les Andes, respectivement (Bourrel et al., 2015, Rau et al., 2017, Sulca et al., 2017). Au Pérou, El Niño EP et CP sont associés à des précipitations extrêmes dans la région côtière du nord au centre et déficit pluie dans les Andes, respectivement (Bourrel et al., 2015 ; Rau et al., 2017 ; Sulca et al., 2017).

Dans les forts événements El Niño, les anomalies SST positives sur le Pacifique Centre-Est conduisent à une évaporation plus forte que la normale entraînant une augmentation du flux d'humidité (Mayer et al., 2013). Il est clairement observé une convection dans le Pacifique

Central et un transport d'humidité vers l'est (Paixao et al., 2005 ; Boers et al., 2014; Xu et al., 2015). Le flux ou le transport d'humidité suit le déplacement vers l'est du réchauffement de la SST équatoriale de deux régimes El Niño qui sont associés à des régimes de circulation atmosphérique distincts conduisant à des patrons d'anomalies pluviométriques différents (Gu et al., 2016). Ce transport d'humidité de l'Océan vers le continent et la topographie des Andes conduisent à la production de pluies sur les côtes de l'Équateur et du Pérou (Gimeno et al., 2016).

Ce transport d'humidité de l'Océan vers le continent apparaît comme la composante principale de la branche atmosphérique du cycle de l'eau et forme le lien entre l'évaporation de l'Océan et les précipitations sur les continents (Peixoto and Oort, 1992).

Le transport de l'humidité nous aide à comprendre les principales caractéristiques du transport de l'humidité depuis sa source. Ce transport comme une composante du cycle de l'eau, et le cycle comme part du cycle énergétique global, joue un rôle fondamental dans la détermination de la circulation à grande échelle et des patrons de précipitation. En particulier, il existe une association entre le transport de l'humidité et les précipitations extrêmes (Lin et al., 2013, Swales et al., 2016), suggérant que le transport de l'humidité peut être utilisé pour fournir une indication et un aperçu plus approfondi des événements de précipitations extrêmes, en raison de la haute prévisibilité du transport de l'humidité relatif à la précipitation et de la forte relation entre eux. Cependant, la convergence du transport d'humidité semble être le meilleur indicateur de la précipitation car elle a des effets plus directs sur l'humidité disponible dans une zone que le transport d'humidité (Q), qui ne mesure principalement que l'humidité traversant une zone (Wei et al., 2016).

Le forçage à grande échelle susmentionné, perturbé par El Niño EP, induit des précipitations extrêmes dans le Centre-Nord péruvien. Il est nécessaire d'expliquer le pourquoi de ces différences dans les impacts de la pluie (extension et magnitude) des forts événements El Niño (similaires dans le Niño 3.4) sur le PPB qui est la question centrale de la présente thèse. Notre principale motivation est de fournir une évaluation des impacts forts d'El Niño sur les précipitations qui peuvent être utilisés pour identifier les principaux schémas de circulation climatique responsables de son évolution et magnitude différentes. Ces schémas clés sont très importants pour le diagnostic et la prévision des événements El Niño forts, afin de réduire les impacts de ENSO sur l'économie péruvienne.

2. MOTIVATIONS DE L'ÉTUDE

Les mécanismes d'advection d'humidité à grande échelle et d'activation de la convection locale dus aux conditions de réchauffement de la température de surface de l'eau lors des événements El Niño forts conduisent à différents patrons de précipitations le long du PPB qui ne sont pas encore bien compris. Il y a des évidences que l'advection d'humidité à grande échelle associée aux forts événements El Niño de 1982/1983 et 1997/1998 incluent un processus de transport d'humidité qui atteint la côte nord du Pérou qui est canalisé par les montagnes et qui détermine les précipitations particulièrement sur le versant des Andes (Goldberg et Tisnado 1987). Ces événements forts semblent également inclure un processus de précipitations locales de convection, déclenché par des eaux anormalement chaudes le long des côtes du nord du Pérou (Horel et Cornejo-Garrido, 1986, Goldberg et al., 1987, Bendix et Bendix 1998, Takahashi, 2004).

D'autres mécanismes d'activation de la convection locale associés au « El Niño côtier » comme le fort El Niño de 1925 (Murphy, 1926) présentent une dynamique différente caractérisée par des conditions chaudes dans le Pacifique Est, mais des conditions froides ailleurs dans le Pacifique central. Ce réchauffement local implique une dynamique de rétroaction couplée mer-atmosphère méridional associée à la ZCIT, aux vents du nord, et à l'asymétrie SST nord-sud dans le Pacifique Est qui conduit à une extension du cycle saisonnier et qui a produit cet événement côtier. Le réchauffement de l'Océan implique probablement une combinaison du mécanisme du vent- de l'évaporation - de la SST, et de l'advection chaude océanique vers le sud. Cet El Niño de dynamique méridionale locale a conduit à très fortes précipitations le long de la côte du PPB (Murphy, 1926, Takahashi et al., 2017).

Il est également à noter que ce mécanisme n'a pas évolué comme un type El Niño EP pour le El Niño 2015/2016, bien que cet événement dans les régions Niño3 et Niño4 ait atteint une amplitude importante d'anomalies SST dépassant 4 °C, comme pour l'événement extrême précédent de 1997/98 (Hu et Fedorov., 2017), mais que dans le Pacifique Est, il a été considérablement plus faible comparé à 1982/1983 et 1997/1998 (L'Heureux et al., 2017), avec des anomalies de pluies plus faibles le long de la côte nord du Pérou (Sanabria et al., 2018).

Deux mécanismes (les grands événements El Niño de 1982/1983 et 1997/1998, et le très fort «El Niño côtier» comme 1925) apparemment associés à des rétroactions convectives non linéaires mais présentant une dynamique très différente lors des événements El Niño contrôlent les caractéristiques principales de la variabilité interannuelle. L'occurrence d'autres

événements, comme celui de 2015/2016, sont associés à une dynamique combinant des processus de type EP El Niño et CP El Niño (Paek et al., 2017) ont ajouté à la complexité de ces caractéristiques de la variabilité interannuelle. Ce qui constitue une motivation supplémentaire pour étudier la variabilité interannuelle des précipitations le long du PPB afin de mieux comprendre ces mécanismes qui déterminent les différents patrons de précipitations associés aux événements El Niño forts. Une autre motivation est l'augmentation des occurrences des événements extrêmes El Niño à l'avenir en réponse au réchauffement climatique (gaz à effet de serre) (Cai et al., 2014). Mais ces projections futures proviennent de l'augmentation de la SST qui ne sont pas toujours liées au développement d'un EP El Niño et aux fortes précipitations le long du PPB comme pour El Niño 2015/2016 : il y a donc d'autres facteurs clés qui doivent être pris en compte.

Les différents mécanismes El Niño associés aux différents régimes de précipitations extrêmes (extension et magnitude) le long du PPB doivent être mieux compris. Dans ce contexte, l'objectif de la thèse est de fournir une évaluation des forts impacts d'El Niño sur les précipitations qui pourront être utilisés pour identifier les divers patrons de circulation climatique clé responsables de leur évolutions et magnitudes différentes. Ces patrons clés sont très importants pour le diagnostic et la prévision des événements El Niño forts, et ce afin de réduire les impacts socio-économiques de des événements El Niño le long du versant Pacifique Péruvien.

2.1 OBJECTIFS

L'objectif principal est de documenter la variabilité interannuelle des précipitations dans le PPB et de l'interpréter à la lumière des progrès récents dans notre compréhension de l'ENSO, en particulier la notion de diversité ENSO (voir section 1.4). Nous évaluons également la mesure dans laquelle les données de réanalyses peuvent rendre compte des détails des patrons de téléconnection ENSO dans le PPB et recherchons le mécanisme atmosphérique mis en œuvre lors du développement des événements extrêmes El Niño.

2.1.1 LES OBJECTIFS SPECIFIQUES

Les objectifs spécifiques sont :

- I. Analyser l'observation in situ sur la période 1964-2016
- II. Documenter l'évolution saisonnière des événements El Niño forts

Nous évaluons la relation entre ENSO et les précipitations lors d'événements

El Niño forts en observant si ces événements peuvent être caractérisés par différentes évolutions. Une telle dispersion de l'évolution et de la magnitude est susceptible de se refléter dans les précipitations le long de la côte et des pentes du PPB. En particulier, nous documentons la relation entre l'évolution temporelle des événements El Niño forts et les précipitations le long de la côte du Pérou pour acquérir des connaissances sur les facteurs locaux et à grande échelle qui déterminent l'étendue et la magnitude des précipitations. Nous avons pris en compte les quatre événements El Niño forts qui ont eu lieu au cours des cinq dernières décennies (événements de 1972/1973, 1982/1983, 1997/1998 et 2015/2016 El Niño) et qui ont provoqué des précipitations importantes au Pérou.

Trois propositions sont utilisées pour atteindre cet objectif :

- Estimer les modes de variabilité des précipitations du PPB en utilisant la méthodologie de rotation des modes EOF.
- Évaluer la saisonnalité des modes de précipitations et établir un lien avec ENSO.
- Analyser les différences entre les événements forts

III. Évaluer les données de réanalyses atmosphérique en fonction de l'état moyen et de sa variabilité interannuelle

L'une des principales difficultés pour aborder les processus atmosphériques concernant le lien entre le transport de l'eau atmosphérique et les précipitations sont les différences significatives entre les différentes réanalyses disponibles qui permettent d'évaluer cette réanalyse et de fournir un choix raisonnable pour mieux représenter ce processus atmosphérique. Si la réanalyse des précipitations est générée par son modèle d'équilibre de l'eau atmosphérique (cohérent avec les précipitations observées), nous suggérons alors que la réanalyse simule bien le transport de l'humidité. Singulièrement, nous analysons la comparaison entre la variabilité pluviométrique dans la région du PPB pour trois produits de réanalyse (ERA-Intérim, CFSR et JRA-55) et la variabilité des précipitations observée, ce qui nous permettra d'identifier le biais de réanalyse et la capacité à reproduire la variabilité in situ.

Nous nous concentrons sur la capacité de la réanalyse à reproduire les modèles spatiaux qui caractérisent la variabilité des précipitations, et aussi à reproduire l'évolution des quatre plus forts événements El Niño survenus au cours des cinq

dernières décennies : El Niño 1972/1973, 1982/1983, 1997/1998 et 2015/2016.

Nous visons à répondre à la question suivante :

- Comment la variabilité des précipitations est reproduite par les trois produits de réanalyses ?

IV. Documenter le transport de l'humidité dans les produits de réanalyses les plus complets durant les trois derniers événements El Niño forts et fournir une compréhension des mécanismes des événements de précipitations dans le PPB.

Le quatrième chapitre examine comment le transport l'humidité contribue à différents types de précipitations sur le PPB pendant les fortes conditions El Niño (1983, 1998 et 2016). Nous étudions comment les régimes de précipitations, dans la région du PPB, associés à El Niño peuvent conduire à des réponses différentes (i.e. phases d'anomalie opposées), et si ces différences sont basées sur la variabilité locale (e. g. Niño 1 + 2). Nous examinons également comment les changements dans la circulation atmosphérique régionale et à grande échelle affectent ces régimes de précipitations. Nous émettons l'hypothèse que les précipitations dans le PPB peuvent connaître des tendances déphasées dans des événements El Niño similaires, telles que mesurées par El Niño 3.4. Cependant, ces modèles doivent satisfaire l'équilibre hydrique sur l'Amérique du Sud tropicale. Ainsi, nous testons cette hypothèse en analysant les variations liées au transport de l'humidité en suivant les changements dans les précipitations et la circulation atmosphérique. Nos approches considèrent que les précipitations observées et l'équilibre de l'eau atmosphérique (convergence du flux d'humidité intégré verticalement) sont comparables (Paixao et al., 2005 ; Wei et al., 2016).

Notre approche méthodologique combine l'utilisation de l'analyse statistique classique telle que l'EOF et l'analyse diagnostique des sorties de réanalyses au travers de l'estimation de la convergence et du transport de l'humidité.

Chapter 2: Rainfall along the coast of Peru during strong El Niño events

Preamble

In order to investigate the mechanisms associated to the rainfall distribution during extreme El Niño events, it is necessary to document the details of the rainfall variability in the PPB, that is, its seasonal evolution of rainfall and its spatial distribution. This is done here in this chapter based on station data covering the period 1964-2016. Over this period, 4 strong El Niño events took place (1972/1973, 1982/1983, 1997/1998 and 2015/2016). These events were classified as strong event according to the NOAA definition (see Chapter 1, section 1.7). However, these events produced distinct rainfall anomalies and societal impacts in Peru, which needs to be understood.

This Chapter is thus viewed as a prerequisite for addressing the mechanistic understanding of the ENSO teleconnection over the PPB during strong events. A detailed analysis of the evolution of precipitation during these events was performed using gauge records from 1964 to 2016 from a network of 145 meteorological stations located along the Peruvian Pacific region. We show that the precipitation in the PPB exhibits a large dispersion in evolution among the strong El Niño events and the impact of these events can be understood in terms of their teleconnection patterns associated to the two types of El Niño. The results led us also to discuss physical mechanisms producing heavy rainfall during Pacific El Niño events.

This page intentionally left blank

Rainfall along the coast of Peru during strong El Niño events

Janeet Sanabria,^{a,b*}  Luc Bourrel,^a Boris Dewitte,^{c,d,e} Frédéric Frappart,^{a,c} Pedro Rau,^a Olimpio Solis^b and David Labat^a

^a UMR 5563 GET, Université de Toulouse - CNRS - IRD - OMP - CNES, France

^b SENAMHI, Lima, Peru

^c UMR 5566 LEGOS, Université de Toulouse - CNRS - IRD - OMP - CNES, France

^d Centro de Estudios Avanzado en Zonas Áridas, Coquimbo, Chile

^e Departamento de Biología, Facultad de Ciencias del Mar, Universidad Católica del Norte, Coquimbo, Chile

ABSTRACT: While, climatologically, most areas of the Peruvian Pacific region do not experience precipitation, they can be affected by heavy rain and flooding during strong El Niño events with severe socio-economic impacts. Only four strong El Niño events took place within the last five decades (1972/1973, 1982/1983, 1997/1998 and 2015/2016) which led to significant rainfall events in the northern part of Peru. Here a detailed analysis of the evolution of precipitation during these events was performed using gauge records from 1964 to 2016 from a network of 145 meteorological stations located along the Peruvian Pacific region. Through empirical orthogonal function analysis, the rainfall anomalies variability is interpreted as resulting from the combination of a meridional see-saw mode (North–South) (Ep mode) and a zonal see-saw mode (East–West) (Cp mode) that represent, respectively, 34 and 21% of the explained variance. It is shown that the extreme 1982/1983 and 1997/1998 El Niño events have a dominant projection on the Ep mode that has a strong loading in the northern region, while the 1972/1973 and 2015/2016 El Niño events have a relatively weak projection onto the Ep mode (about ten times less at the peak rainy season than the extreme events) and mostly project onto the Cp mode. Also, it is shown that while all events are associated with positive rainfall anomalies in the northern part of Peru which is accounted for by the Ep mode, the evolution of rainfall anomalies along the Cp mode exhibits a significant dispersion. This suggests that the impact of strong El Niño events on the highlands along the coast cannot solely be inferred from the magnitude of the sea surface temperature anomalies in the central equatorial Pacific. Overall, our study illustrates the nonlinearity of the ENSO teleconnection on the rainfall along the coast of Peru during strong El Niño events.

KEY WORDS strong El Niño events; rainfall anomalies variability; rainfall anomalies modes; rainfall; Peruvian Pacific coast; highlands

Received 24 January 2017; Revised 5 July 2017; Accepted 18 August 2017

1. Introduction

The El Niño Southern Oscillation (ENSO) is the largest mode of climate variability at the interannual time scale. It has a strong impact on many regions surrounding the Pacific Ocean. The ENSO phenomenon influences the regional climate remotely through so-called teleconnections. First, ENSO is associated with the release of adiabatic heat to the troposphere, modifying main atmospheric pathways, leading to the so-called atmospheric teleconnections (Bjerknes, 1969; Horel and Wallace, 1981; Keshavamurthy, 1982; Philander, 1985; Trenberth *et al.*, 1998; Diaz *et al.*, 2001). The atmospheric ENSO teleconnections have been extensively studied as they can provide a mechanism by which the main mode of interannual variability in the tropics, that is ENSO, can impact regional climate over the globe. For the coast of Peru where dry mean conditions usually prevail south of 7°S, these are

particularly spectacular during strong El Niño events, because the coastal region experiences heavy rainfall as far south as the Lima region (Takahashi and Martinez, 2017). Second, ENSO is associated with planetary oceanic wave activity along the equator (i.e. Kelvin wave) which can propagate along the coasts of South America and alter the local oceanic circulation in regions which usually experience a persistent upwelling (Clarke, 1983). Countries such as Ecuador and Peru are particularly sensitive to this type of teleconnection, known as oceanic teleconnection. Previous studies have shown in particular that when the sea surface temperature (SST) off Païta (5°S) reaches ~26 °C, episodes of heavy rainfall can take place suggesting formation of deep local convection under coastal warm SST like what happens in the central western Pacific at large scale (e.g. Woodman, 1999).

Northern Peru has previously experienced devastating rainfall events during El Niño events. For instance, the cost on society and economy associated with the 1982/1983 El Niño event has been estimated at US\$ 3.283 million while the 1997/1998 El Niño event exceeded US\$ 3.500 million; these values equate to 11.6 and 6.2% of the

*Correspondence to: J. Sanabria, UMR 5563 GET, Université de Toulouse - CNRS - IRD - OMP - CNES, Toulouse 31400, France. E-mail: janeet.sanabria@get.omp.eu

respective annual gross domestic product (GDP) (Vargas, 2009).

While it is expected that strong El Niño events impact rainfall in the north of Peru, there is still uncertainty on the magnitude and extent of anomalous rainfall patterns during those events (Rau *et al.*, 2017). This is due to the complex of physical processes at work and the limited number of registered strong events (only four since the 1950s) preventing robust statistics. Another limitation is attributed to the diversity of ENSO. Recent studies pointed out that ENSO can be understood as resulting from at least two distinct regimes (Kao and Yu, 2009; Takahashi *et al.*, 2011; Capotondi *et al.*, 2015) which encompass the two different types of events (Yeh *et al.*, 2009; Takahashi *et al.*, 2011). Extreme El Niño events tend to be characterized by peak SST anomalies in the far eastern Pacific and are referred to as eastern Pacific (EP) El Niño, whereas a different type of event consists in peak SST anomalies confined to the central Pacific (CP). These events are referred as CP event (Kug *et al.*, 2009). Because the SST warming is located at a different place along the equator, these two types of El Niño events are associated with a distinct atmospheric teleconnection (Hastenrath, 1978; Ropelewski and Halpert, 1987; Barsugli and Sardeshmukh, 2002; Frauen *et al.*, 2014; Capotondi *et al.*, 2015). They are also associated with different oceanic teleconnections particularly in the absence of a persistent coastal warming off Peru during CP El Niño events, conversely to that during EP El Niño events (Dewitte *et al.*, 2012).

Recent studies have pointed out that the impact on rainfall along the coast of Peru is distinct during these two types of El Niño events (Lavado and Espinoza, 2014; Bourrel *et al.*, 2015; Rau *et al.*, 2017). EP El Niño events are associated with heavy rainfall in northern Peru while CP El Niño produces dryer conditions upstream along the Pacific slope. These studies focused on the average rainy season and on the peak phase of ENSO while events can differ in their evolution. Here we take a closer look at the relationship between ENSO and rainfall during strong El Niño events by observing that these events have different evolutions. Four strong El Niño events took place over the last five decades and produced noticeable rainfall in Peru: the 1972/1973, 1982/1983, 1997/1998 and 2015/2016 El Niño events. While not fully documented yet, we include in our analysis the recent 2015/2016 El Niño event as it has been recorded as the largest El Niño event to date since 1997. The selection of these events is based on the Niño3.4 index (i.e. SST anomalies averaged from 5°S to 5°N and 170° to 120°W). All these events had a comparable value of the Niño3.4 index at the peak phase of the event (1.9, 2.1, 2.3 and 2.3 °C, respectively, for December). While these events have comparable magnitudes, they present a different evolution and projection on SST anomalies in the tropical Pacific, which is thought to be influential on their teleconnections over Peru.

To illustrate the former statement, we present Figure 1 which shows the evolution of the so-called *C* and *E* indices defined by Takahashi *et al.* (2011) for these four events. The *E* and *C* indices are based on the first two PC time

series of the empirical orthogonal function (EOF) analysis of SST over the tropical Pacific and account for the variability of the EP and CP El Niño events, respectively (see Section 2.3 for details). The composite evolution of the composite of the other 12 moderate El Niño events over the period 1950–2016 is also presented as a benchmark for comparison.

First, Figure 1 shows that the EP El Niño events are distinct from the CP El Niño events because the *E* index is characterized by large anomalies for EP El Niño, which is not the case for CP El Niño events. For the *C* index, the magnitude is comparable for both types of events although there is a tendency for lower values for EP El Niño than for CP El Niño events. The striking feature in Figure 1 is the large dispersion in the evolution of the *E* index for strong events with for instance, the 1997/1998 El Niño event peaking in December 1997, while the 1982/1983 presents a double peak, one in December 1982 and the other one in June 1983. The 1972/1973 El Niño peaked earlier in the year in August 1972 with still a secondary peak in December 1972, with also significantly lower values of the *E* index. The 2015/2016 El Niño event is more comparable to the 1972/1973 El Niño in terms of the magnitude of the *E* index, although it peaked in January 2016 while the 1972 El Niño peaked twice [in August (0) and December (0)]. Such dispersion in evolution and magnitude is likely to reflect onto precipitation along the coast, which is the focus of this article. In particular, we document the relationship between the temporal evolution of strong El Niño events and rainfall along the coast of Peru to gain knowledge in the local and large-scale factors that determine the extent and magnitude of rainfall. Our study can be viewed as an extension of former studies (Lavado and Espinoza, 2014; Bourrel *et al.*, 2015; Rau *et al.*, 2017) that focused on the impact of the two types of El Niño on rainfall. While these studies used the *E* and *C* indices to account for the ENSO variability at basin scale and investigate how rainfall in Peru projected onto these modes, our purpose is here to document the rainfall variability without assuming any *a priori* relationship with ENSO diversity. Our study is also motivated by the societal demand and the need to provide an interpretation of recent precipitation conditions in Peru associated with the 2015/2016 El Niño event that has been categorized as a strong event by the international community (L'Heureux *et al.*, 2017) while having much less dramatic consequences than the 1997/1998 El Niño for instance (SENAMHI, 2015). In that sense our study is also aimed at evaluating the nonlinearity of the ENSO teleconnection over Peru during strong El Niño event.

This article is structured as follows. Sections 2 and 3 provide a description of the study region, the *in situ* rainfall observed data set and El Niño indices, as well as the method for deriving the two main modes of variability in rainfall along the coast of Peru. Section 4 describes the characteristics of the modes and documents their statistical properties and relationship with ENSO. The four strong El Niño events are documented in the light of the obtained indices. Section 5 summarizes the results and discusses perspectives of this work.

RAINFALL ALONG THE COAST OF PERU DURING STRONG EL NIÑO EVENTS

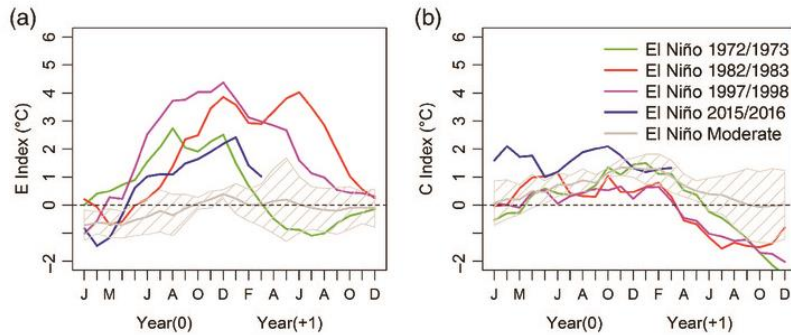


Figure 1. Evolution of the (a) E and (b) C indices of the four strong El Niño events (1972/1973, 1982/1983, 1997/1998 and 2015/2016) and the composite of moderate events. The E and C indices are defined as in Takahashi *et al.* (2011) from the HadISST data set over the period 1950–2016. The composite for moderate events includes 12 events from 1950 to 2016 (i.e. years 1957/1958, 1963/1964, 1965/1966, 1968/1969, 1969/1970, 1977/1978, 1987/1988, 1991/1992, 1994/1995, 2002/2003, 2004/2005 and 2009/2010). The hatching in grey line represents the dispersion (standard deviation) among the 12 moderate El Niño events. [Colour figure can be viewed at [wileyonlinelibrary.com](#)].

2. Study area and data sets

2.1. Study area

The Peruvian Pacific region is located from the shores of the eastern tropical Pacific to the west side of the Andes Mountains, between 3.5° and 18.5°S latitude and 69.5° and 80°W longitude (Figure 2). It presents an altitudinal west–east gradient that ranges from sea level to 4000 m above sea level (masl). It comprises a coastal strip as well as part of the Andes. The study area can be divided into an upper and lower region separated by an altitudinal level of around 1000 m (Brack and Mendiola, 2000; Rundel *et al.*, 2007). The lower region, that is, the coastal strip, is characterized by an arid climate with very low rainfall. The higher region exhibits a low mean annual rainfall of about 300 mm year^{-1} ; average rainfall values increase with altitude and decrease with latitude progressing from northern to central areas. Large increases in rainfall are associated with the influence of oceanic warming in the EP during extreme El Niño events (Horel and Cornejo, 1986; Goldberg *et al.*, 1987; Tapley and Waylen, 1990; Bendix and Bendix, 2006; Douglas *et al.*, 2009; Cai *et al.*, 2014; Lavado and Espinoza, 2014; Bourrel *et al.*, 2015; Tedeschi *et al.*, 2015).

2.2. Monthly rainfall data set

The rainfall data set is composed of records from 145 meteorological stations distributed in lower and higher areas, ranging from sea level to 4406 m elevation, in the Peruvian Pacific region. These data were made available by the National Service of Meteorology and Hydrology of Peru (SENAMHI). The data set is composed of monthly rainfall data recorded over 52 years from 1964 to 2016 (see Figure 2 for the location of the stations). Missing data represent approximately 5% of the total data set. Quality control and homogenization of the data set were performed earlier by Bourrel *et al.* (2015) and Rau *et al.* (2017) using the regional vector method (taking into consideration elevation, watershed boundaries and latitude) and the significant correlation between the neighbouring stations.

A previous study on the north-central Peruvian Pacific (Bourrel *et al.*, 2015) presented a regionalization which defined nine regions (R1–R9) based on rainfall variability (see map of Figure 7). R1 and R3 correspond to the lower region located along the coast. R2 and R4–R9 represent highlands localized on the slopes of the Andes. Each climatically homogeneous region follows a rainfall regime based on proximal and homogeneous pluviometric stations and physiographic/topographical pattern constraints according to the regional vector methodology [RVM; Brunet-Moret (1979) cited by Bourrel *et al.* (2015)]. Rau *et al.* (2017) redefined these regions as a regionalized product along the whole Peruvian Pacific slope and coast following the RVM methodology combined with a k -means cluster analysis. This product showed the main modes of influence of the ENSO that influence the rainfall variability at seasonal and interannual time scales.

2.3. El Niño indices

In this study, we use the E and C indices as defined by Takahashi *et al.* (2011) based on SST data from the HadISST data set (Rayner *et al.*, 2003). These two indices are derived from the first two dominant principal components (PC) time series (PC1 and PC2) of the EOF analysis of SST over the tropical Pacific, as follows: $E = \frac{\text{PC1} + \text{PC2}}{\sqrt{2}}$ and $C = \frac{\text{PC1} - \text{PC2}}{\sqrt{2}}$.

They are independent by construction and depict the variability of EP El Niño (120° – 90°E , 15°S – 15°N) and CP El Niño events (170°E – 100°W), respectively. These have been used in previous relevant studies to document ENSO teleconnections on rainfall in Peru (Lavado and Espinoza, 2014; Bourrel *et al.*, 2015; Rau *et al.*, 2017).

3. Methodology

3.1. Interpolation of rainfall

The quality-checked rainfall from the 145 meteorological stations was gridded at a spatial resolution of 0.5° using Cressman technique (Cressman, 1959; Doty, 1995). This

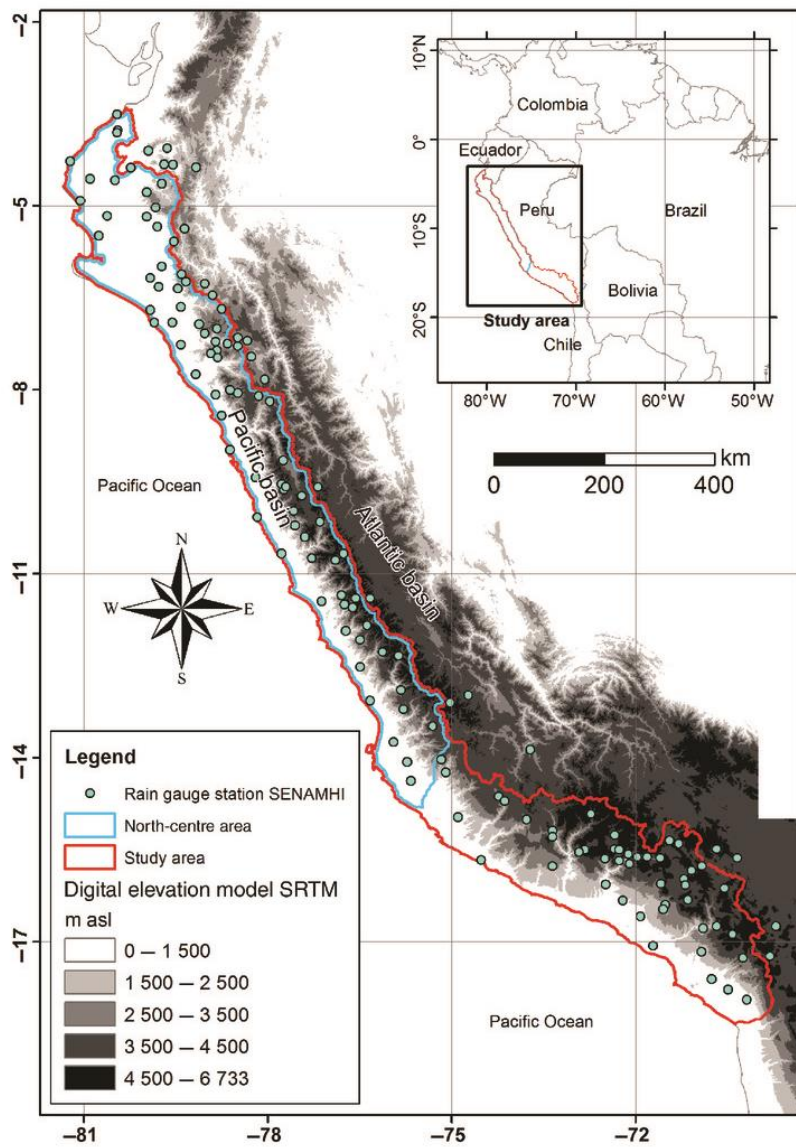


Figure 2. Map of the Peruvian Pacific slope (red outline) and north centre area (blue outline) (Bourrel *et al.*, 2015) and location of the 145 meteorological stations (turquoise dots) provided by the National Service of Meteorology and Hydrology of Peru (SENAMHI) from 1964 to 2016. [Colour figure can be viewed at wileyonlinelibrary.com].

spatial resolution was chosen as it represents the average distance between every station to its closest neighbours. The rainfall anomalies ($P - \bar{P}$), where P represents the observed monthly rainfall and \bar{P} the mean climatology of rainfall, were computed over two distinct periods (1964–1977 and 1978–2016) to take into account the climate shift in the Pacific Ocean of the 1970s (Trenberth and Stepaniak, 2001), so that anomalies are referred to the mean seasonal cycle calculated over two different periods for the periods after and before 1977. Note that it was verified that has little impact on the results but still allows emphasizing anomalous events prior to 1977.

3.2. EOF analysis of the rainfall data set

In order to characterize the rainfall variability, we use the EOF analysis. EOF modes are statistical modes that are aimed to grasp aspects of the physical mechanisms. However, sometimes some modes arise to satisfy the orthogonality conditions and do not necessarily have a simple physical interpretation. It is sometimes convenient to linearly combine EOF modes, which is equivalent to rotate the EOF modes, to infer mode patterns and associated time series that correspond readily to an observed process. The rotation is aimed at maximizing the variance along preferred directions that correspond to peculiar evolutions of

some events. In the case of our data set a strong positive skewness of the distribution is observed which corresponds to the impact of extreme ENSO events. It is therefore convenient to describe the variability along the direction of the evolution of extreme events from the first rotated mode. The second rotated mode more arises from the orthogonality condition and therefore accounts for the rainfall variability associated with moderate events. The angle of the rotation can be determined objectively from an EOF analysis in the space of the PC time series of the previous EOF analysis of the data.

Here, for precipitation data, the maximization procedure yields a rotation of 60° to be performed on the original EOF modes (PC1 and PC2). The corresponding indices are thus defined as follows: $Ep = \frac{PC1 - \sqrt{3} \cdot PC2}{2}$ and $Cp = \frac{\sqrt{3} \cdot PC1 + PC2}{2}$. The corresponding patterns are obtained by projecting the data onto these two indices through bilinear regression analysis. Regression analysis as a function of calendar month is also used to relate the Ep and Cp indices to the E and C indices, noting that they have a distinct seasonal evolution and seasonal phase locking. The significance of the regression coefficients was estimated using a t -test and retaining the 95% confidence level. At last, we also calculated composite evolution of precipitation anomalies based on the results of the EOF analysis that is averaging the associated time series of the rotated modes for extreme ENSO events over the time period covering the temporal evolution of the events (i.e. over 2 years). While the significance level is difficult to estimate for strong El Niño events (because they are too few), it was estimated for the composite of moderate El Niño events based on a bootstrap method (Efron and Tibshirani, 1993). The latter consisted in randomly selecting 7 events among the 12 events and calculate the composite. The operation is repeated 1000 times which allows estimating the PDF of the mean Cp and Ep values as a function of calendar month, yielding the threshold for the 95% significance level. These moderate 12 events were selected from Yu and Kim (2013).

4. Results

4.1. Modes of rainfall variability

As a first step, the rainfall variability is described based on the estimate of the two rotated EOF modes (Section 3.2). Figure 3(a) presents the phase space of the rotated EOF time series while Figure 3(b) displays the mode patterns. By construction the rainfall during extreme El Niño events should be accounted for by the Ep mode [x-axis of Figure 3(a)]. However, the striking feature of Figure 3(a) is that only the 1997/1998 and 1982/1983 El Niño events align along the x-axis during their developing phase (with little component on the y-axis), while the 1972/1973 and 2015/2016 El Niño events have their variance dominantly explained by the Cp mode (main projection along the y-axis). The 1972/1973 and 2015/2016 El Niño events

exhibit weak or moderate rainfall anomalies along the Cp mode, while the 1997/1998 and 1982/1983 El Niño events exhibit significant anomalous rainfall conditions along the Ep mode for at least 3 months (January–March).

The mode patterns (Figure 3(b)) reveal that the Ep mode that explains 34% of the explained variance has a strong loading in the northern Peru (Piura region) and consists in a meridional see-saw with a node at the latitude of $\sim 12^\circ\text{S}$ (Lima). To the south of this critical latitude, rainfall anomalies during extreme El Niño events tend to be negative in the highland but still positive near the coast. The second mode pattern (Cp) explains 21% of the variance in rainfall anomalies and is characterized by a zonal east–west gradient that is more pronounced south of 15°S . This mode has its stronger loading in the inner domain indicating it is more related to high-altitude rainfall variability. The PC time series of the Ep (Cp) mode is correlated to the E (C) index at 44% (21%), which is significant at the 95% level. These relatively low values of correlation are likely associated with the distinct seasonality of rainfall and SST anomalies in the tropical Pacific during ENSO. This is investigated further in the subsequent section.

4.2. Seasonality and link with ENSO

While El Niño events tend to peak in austral summer [September (Y0) to January (Y1)], the rainy season in northern Peru concentrates around February (Y1) to April (Y1) (Bourrel *et al.*, 2015). There is thus a strong seasonal phase locking of the relationship between rainfall anomalies and ENSO. The seasonality of the relationship between ENSO and rainfall anomalies is investigated based on the rainfall and ENSO indices described previously. Figure 4 indicates that the peak variance for the Ep mode takes place in March while the Cp mode peaks in February. We note a sharp increase in rainfall variability from December to January for the Ep mode, which corresponds to the onset of the rainy season. The variance of the Cp mode also reduces earlier than that of the Ep mode suggesting more oceanic influence for the Ep mode, particularly associated with oceanic Kelvin wave activity (Bourrel *et al.*, 2015). By construction the Ep mode is positively skewed (skewness of $Ep = 6.18$) and thus relates the most to the E mode while the Cp mode is much more symmetric (skewness of $Cp = 0.87$). A bilinear regression analysis of the Ep and Cp modes onto the E and C indices provides the approximate Ep and Cp indices explained by E and C : $Ep = 0.44*E + 0.04*C$ and $Cp = 0.15*E - 0.24*C$, which indicates that the Ep mode is mostly related to the E mode, while the Cp mode is influenced by both the E and C modes. Note the negative coefficient over C for Cp meaning that during a CP El Niño event (i.e. $C > 0$), Cp is negative so that the highlands along the coast experience a deficit of precipitation (Figure 3(b), right). In order to refine this analysis and take into account the marked seasonality in both the ENSO and rainfall indices (Figure 4), the climatological regression coefficients of the Ep and Cp indices onto the E and C indices are estimated, which consists in carrying the aforementioned regression analysis for each calendar month (Figure 5). The results of

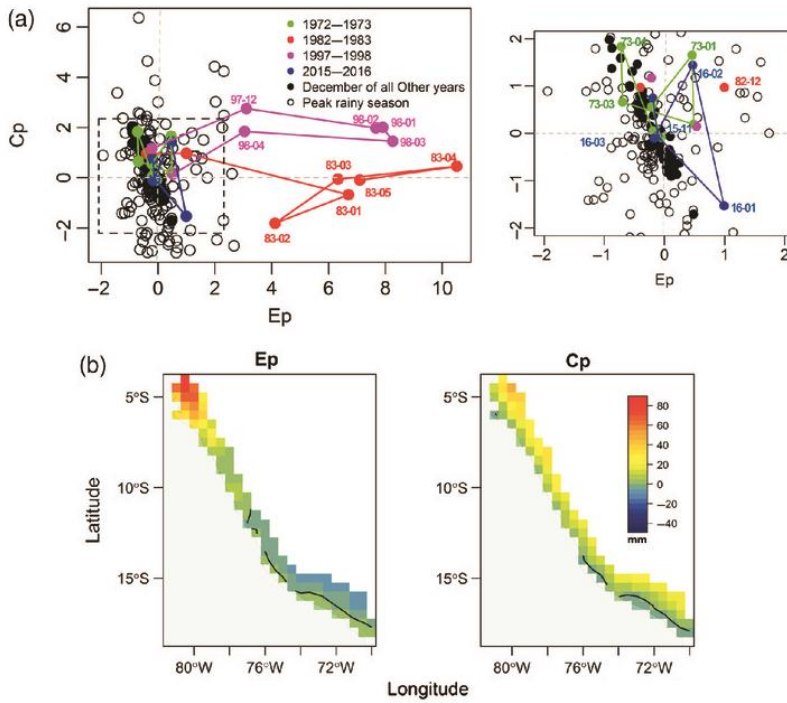


Figure 3. (a) Phase space of the evolution of the Ep and Cp modes. The evolution of the four strong El Niño event is highlighted with lines connecting the dots for the months between January of the first year J(Y0) and December of the second year D(Y1). (Y0: developing El Niño, Y1: decaying El Niño). The dots in black line correspond to the December value (Y1) of all other El Niño events. Zoom: (a) in interval $[-2, 2]$ (right-hand side). (b) Associated patterns (Ep and Cp) of rainfall anomalies over the period 1964–2016. Ep mode (first mode) (left-hand side) and Cp mode (second mode) (right-hand side). The thick black line indicates the zero contour. [Colour figure can be viewed at wileyonlinelibrary.com].

Figure 5 indicate that the Ep mode is tightly linked to the E index in March that is at the peak month of the rainy season. Interestingly, the Cp mode is also strongly related to the C index in February, which consists in an inverse relationship. Extreme El Niño events thus tend to yield a deficit in precipitation in the highland at the onset of the rainy season. Interestingly, the regression coefficient linking the Ep index to the C index peaks in April, which suggests that the magnitude of the SST anomalies in the CP (i.e. C mode) tends to determine the persistence of rainfall anomalies during extreme El Niño event in the northern region of Peru. On the other hand, strong EP El Niño event (E index) can also be influential on the Cp mode increasing precipitation in the highlands in April and December. In light of these results, in the following we take a closer look at the differences between the evolutions of the strong events.

4.3. Differences between strong events

Figure 6 shows the evolution of the Ep and Cp indices during the four strong El Niño events. The composite evolution of moderate El Niño events is also displayed so as to highlight the anomalous conditions during strong events. Clear differences in the evolution of the strong El Niño events can be observed. A striking feature revealed in Figure 6 is the large difference in the magnitude of the Ep

index at the peak of the events, with the 1997/1998 ($Ep \approx 8$ in March) and 1982/1983 ($Ep \approx 6$ in January and $Ep \approx 10$ in April) being associated with a much larger rainfall anomaly in the northern part of Peru and an extended period of anomalous rainy conditions (lasting until June 1998 and July 1983) than the 1972/1973 and 2015/2016 El Niño events ($Ep \leq \pm 1$). The 1972/1973 and 2015/2016 El Niño events also differ in terms of their projection on the Cp mode as the 1972/1973 event exhibits a positive value of the Cp index in January (Y1) while the 2015/2016 has a negative value of the Cp index, a situation that is inverted in the subsequent month [February (Y1)]. The evolution of the 1972/1973 and 2015/2016 El Niño events thus falls within the error for the composite of moderate El Niño events. Note also that the 1982/1983 and 2015/2016 El Niño events have a comparable negative value of the Cp mode at the peak phase, which is similar to the composite of the moderate El Niño events. This means that these two strong El Niño events were associated with a deficit in rainfall over the highlands. On the other hand, the 1997/1998 El Niño event also has a marked projection on the Cp but positive values during the rainy season, indicating that the highlands are associated with excess rainfall.

We now consider the regionalized product of Bourrel *et al.* (2015) in order to provide more details on the spatial variability of the impact of the strong El Niño events on

RAINFALL ALONG THE COAST OF PERU DURING STRONG EL NIÑO EVENTS

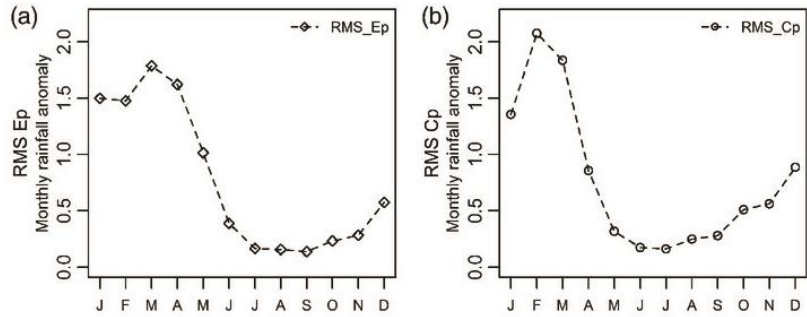


Figure 4. Climatological root mean square (RMS) of (a) the Ep mode and (b) Cp mode.

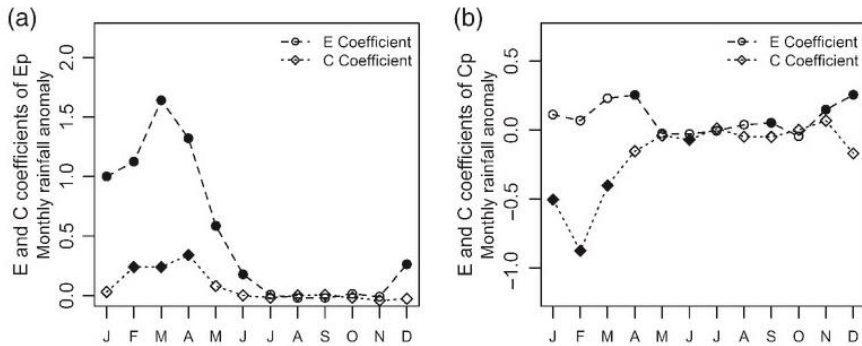


Figure 5. Climatological regression coefficients between (a) the Ep mode and the *E* and *C* indices (round), and the (b) Cp mode and the *E* and *C* indices (losange). The values of the coefficient that are statistically significant at the 0.05 level (*p*-value) are with filled symbol.

the precipitation responses. This is also considered a consistency check of the relevance of the Ep and Cp modes for depicting the rainfall anomalies associated with the strong El Niño events. Figure 7 provides the evolution of the Ep and Cp indices during the strong El Niño events along with the rainfall anomalies for the nine climatological homogeneous regions (Table 1) Bourrel *et al.* (2015). It indicates that the evolution of the Ep and Cp modes during the strong El Niño grasps in general the peculiarities of the homogeneous regions, with, in particular, the Ep mode accounting to a large extent for the rainfall anomalies in the R1, R2 and R3 regions during the 1997/1998 and 1982/1983 El Niño events, while the rainfall anomalies in the highland regions (R4–R9) evolving like the Cp mode for all events except during the 1982/1983 El Niño in R5–R7 and during the 2015/2016 El Niño. During the latter event, the Cp mode accounts for the evolution of rainfall anomalies only in the R1 region although the magnitude of the anomalies is underestimated by the Cp mode.

5. Discussion and conclusions

While El Niño events are generally classified from the amplitude of some indices at their peak phase (classically the NIÑO3.4 index), they can exhibit significant differences in their evolution, which is influential on their teleconnections and local impact. We have showed here that

the four strongest El Niño events of the last five decades are associated with a distinct rainfall anomaly evolution along the Pacific coast and slope. The different rainfall anomaly evolution during these El Niño events is interpreted as resulting from the contribution of two modes, the first mode accounting for heavy precipitation in the northern part of Peru and slight rainfalls in coastal zones southward, and characterized by a meridional see-saw pattern (Ep) with a node at the latitude of Lima (12°S), and the second mode associated with high variability (dryer and wet conditions) in the highlands along the coast and characterized by a marked zonal contrast (Cp). We show that the evolution of these two modes exhibits a large dispersion in evolution among strong El Niño events, with in particular the 1982/1983 and 1997/1998 El Niño events having the strongest impact by far over the northern region of Peru. The 1972/1973 and 2015/2016 El Niño events have a much weaker rainfall anomaly in the northern part of Peru and are statistically hardly distinguishable from the moderate El Niño events. The strong El Niño events are also in general associated with driest conditions over the highlands and to the South, with the 1982/1983 and 2015/2016 El Niño events exhibiting comparable negative anomalies of the Cp mode than the moderate El Niño composite. However, the 1997/1998 El Niño event was associated with significant positive rainfall anomalies over the highlands. The impact of the strong El Niño events over the highlands is thus also diverse.

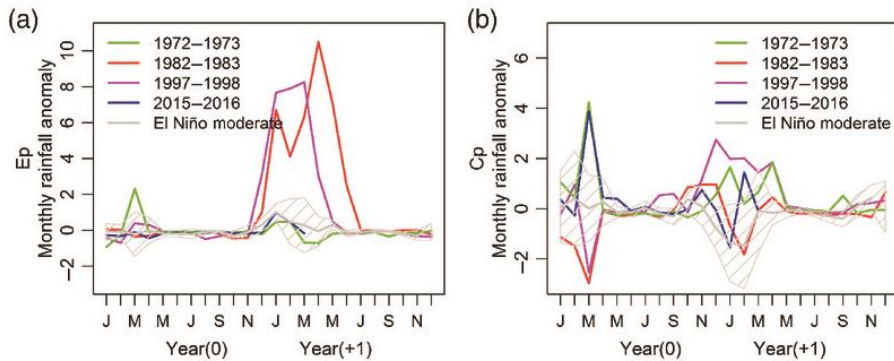


Figure 6. Evolution of the Ep and Cp modes during the four strong El Niño events and the composite of moderate events: Ep mode (left-hand side) and Cp mode (right-hand side). The composite for moderate events includes the same events than in Figure 1(b). The hatching in grey line represents the dispersion (standard deviation) among moderate El Niño events. [Colour figure can be viewed at wileyonlinelibrary.com].

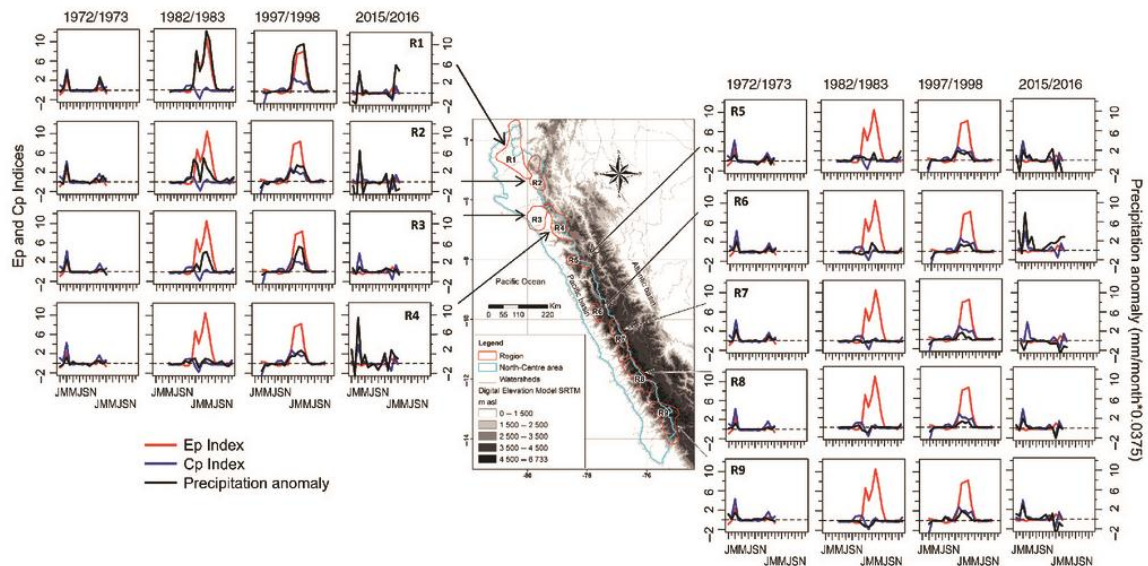


Figure 7. Evolution of the Ep and Cp indices and precipitation anomaly in the homogeneous regions during the four strong El Niño events 1972/1973, 1982/1983, 1997/1998 and 2015/2016. [Colour figure can be viewed at wileyonlinelibrary.com].

Overall, our results illustrate the nonlinear nature of the ENSO teleconnection of the rainfall over the western coast of Peru and the difficulty to predict anomalous rainfall conditions during strong El Niño events, which has a strong societal relevance. In particular, small changes in rainfall over highland areas can affect agriculture, water reservoir storage level and hydroelectric resources (BCRP, 2016). Our approach has been to model the complex of physical processes operating in nature with a linear statistical relationship between SST and rainfall variability during ENSO, which, although convenient for forecasting purpose, can be considered, oversimplified due to the diversity in forcing mechanisms of the anomalous rainfall in this region. Still our model takes into account the nonlinear evolution of ENSO through the consideration of the two ENSO regimes, which add a dimension to the commonly used approach. Among

the physical mechanisms producing heavy rainfall during strong EP Pacific El Niño events, the one associated with the deep convection triggered by SST when the latter is above $\sim 26^{\circ}\text{C}$ (Woodman, 1999) can be used for the interpretation of the differences among events. The characteristics of SST along the coast of Peru during such events are likely influential on the distribution and magnitude of rainfall. As an illustration, we present Figure 8 that shows the evolution of the Niño1+2 index (based on total SST) during the four events. It shows that during the 1982/1983 and 1997/1998 El Niño events, the total temperature in the Niño1+2 region was above 26°C for almost 6 months while during the 2015/2016 El Niño event, it only hardly reaches 26°C during 1 month. The pattern of SST anomalies was also distinct between events (Figure 9), which could also drive mesoscale low-level atmospheric circulation and influence the distribution

RAINFALL ALONG THE COAST OF PERU DURING STRONG EL NIÑO EVENTS

Table 1. Observed monthly rainfall with respect to mean climatology (M. C. over the 1964–2016 period) during the El Niño events of 1972/1973, 1982/1983, 1997/1998 and 2015/2016 [between January of the developing year J(Y0) and December of the decaying year D(Y1)]. The dark green colour represents rain values above 80% of the monthly mean climatology. [Colour table can be viewed at wileyonlinelibrary.com].

	J	F	M	A	M	J	J	A	S	O	N	D	J	F	M	A	M	J	J	A	S	O	N	D	
	Year (0)												Year (+1)												
M. C.	46	78	125	58	21	5	1	0	0	1	2	12	46	78	125	58	21	5	1	0	0	1	2	12	
R1	1972/1973	5	60	355	23	8	9	0	2	0	0	2	6	206	87	96	20	3	0	1	0	1	0	0	2
	1982/1983	2	2	0	16	1	0	0	0	0	1	5	90	597	372	509	893	707	266	26	0	3	2	0	12
	1997/1998	4	37	116	58	18	5	3	0	9	9	46	479	670	755	785	381	89	2	0	0	1	3	0	2
	2015/2016	18	59	259	78	43	3	1	0	0	3	4	3	35	271	263	—	—	—	—	—	—	—	—	—
M. C.	118	194	257	152	40	15	4	6	13	29	31	65	118	194	257	152	49	15	4	6	13	29	31	65	
R2	1972/1973	109	140	476	150	70	27	4	12	8	8	39	105	101	251	251	239	72	25	7	10	26	8	18	69
	1982/1983	90	115	39	118	48	2	2	0	5	65	80	387	380	223	601	348	182	58	16	0	23	69	44	143
	1997/1998	72	117	185	142	10	9	1	0	51	37	75	237	243	446	473	358	134	10	0	7	27	40	35	42
	2015/2016	108	95	444	90	47	4	2	0	0	31	78	4	168	172	229	—	—	—	—	—	—	—	—	—
M. C.	14	25	54	15	4	1	0	1	1	3	3	3	14	25	54	15	4	1	0	1	1	3	3	3	
R3	1972/1973	2	28	224	10	0	1	0	0	1	1	1	4	47	37	20	17	1	1	0	1	5	0	1	0
	1982/1983	1	4	1	7	0	0	0	0	1	4	7	16	126	52	308	297	155	19	0	0	1	9	0	1
	1997/1998	0	13	8	16	1	1	0	1	1	1	8	55	240	376	371	57	9	1	0	0	2	2	0	3
	2015/2016	38	23	81	27	9	1	0	1	5	11	24	20	20	49	40	—	—	—	—	—	—	—	—	—
M. C.	103	131	171	106	48	22	14	17	44	80	61	68	103	131	171	106	48	22	14	17	44	80	61	68	
R4	1972/1973	62	90	242	71	68	11	4	21	36	40	55	82	140	104	178	202	46	42	22	37	71	72	46	71
	1982/1983	62	74	57	87	59	6	6	4	43	115	78	136	164	92	196	184	107	51	13	22	73	59	28	87
	1997/1998	42	159	76	90	25	24	0	4	38	53	123	183	197	309	360	255	72	12	3	8	44	97	36	60
	2015/2016	173	83	435	111	99	1	5	5	6	75	122	41	170	192	209	—	—	—	—	—	—	—	—	—
M. C.	114	136	168	93	30	12	7	10	28	67	49	74	114	136	168	93	30	12	7	10	28	67	49	74	
R5	1972/1973	115	143	256	102	36	11	6	11	11	27	40	74	182	75	203	204	61	23	21	8	68	93	82	86
	1982/1983	61	55	90	105	28	0	7	3	13	104	80	125	156	159	165	200	16	17	0	2	23	102	78	212
	1997/1998	41	182	49	107	36	6	1	3	28	59	109	213	215	235	275	144	13	7	0	8	25	72	37	60
	2015/2016	139	82	217	111	54	6	7	0	15	55	87	144	56	153	88	—	—	—	—	—	—	—	—	—
M. C.	68	92	122	43	8	1	1	2	6	27	29	41	68	92	122	43	8	1	1	2	6	27	29	41	
R6	1972/1973	83	107	255	20	7	1	3	6	6	6	17	38	127	74	153	70	19	0	6	6	18	26	29	76
	1982/1983	26	54	53	29	2	0	0	1	0	4	5	4	57	78	241	112	0	0	0	0	4	8	17	18
	1997/1998	51	104	26	25	7	0	0	0	7	19	57	148	142	183	206	61	9	4	0	0	6	36	9	40
	2015/2016	177	81	333	82	83	0	3	0	19	56	79	87	118	175	199	—	—	—	—	—	—	—	—	—
M. C.	91	106	118	40	9	2	1	3	10	30	33	61	91	106	118	40	9	2	1	3	10	30	33	61	
R7	1972/1973	71	100	286	63	0	1	5	5	21	22	24	57	152	113	148	85	21	0	3	5	30	44	41	100
	1982/1983	94	114	52	24	0	0	1	0	1	43	42	37	77	81	120	44	2	6	0	0	2	13	24	57
	1997/1998	67	115	39	22	2	0	0	1	12	18	51	140	189	128	135	31	3	1	0	0	6	36	19	42
	2015/2016	84	52	102	39	10	1	0	3	1	12	22	48	24	73	72	—	—	—	—	—	—	—	—	—
M. C.	76	91	99	29	5	1	1	2	5	15	18	50	76	91	99	29	5	1	1	2	5	15	18	50	
R8	1972/1973	89	101	179	33	2	0	1	0	6	16	11	49	99	83	130	49	11	0	0	3	15	17	9	84
	1982/1983	58	92	56	18	2	1	2	1	4	29	47	19	20	26	115	19	6	2	1	2	2	3	13	80
	1997/1998	69	113	39	12	1	0	0	1	7	11	37	111	158	152	176	32	0	0	1	2	6	5	40	
	2015/2016	94	84	152	48	2	1	0	4	2	10	24	58	22	109	96	—	—	—	—	—	—	—	—	—
M. C.	97	112	118	37	8	3	2	5	9	16	20	50	97	112	118	37	8	3	2	5	9	16	20	50	
R9	1972/1973	178	115	226	68	5	0	1	1	21	26	23	76	105	101	106	61	5	1	0	5	13	11	26	54
	1982/1983	73	117	64	6	1	0	0	0	13	13	2	13	28	51	41	3	0	0	0	0	0	0	13	45
	1997/1998	100	95	61	33	9	0	0	59	23	27	30	107	225	217	174	53	0	15	0	7	15	31	51	59
	2015/2016	122	134	186	49	7	4	1	5	20	42	16	83	3	95	71	—	—	—	—	—	—	—	—	—

of deep convection. The mechanisms associated with SST changes along the coast of Peru during El Niño events are tightly linked to both the El Niño equatorial dynamics (remote forcing) and upwelling dynamics (local forcing), which could thus be sources of the differences in rainfall between events. A recent study (Paek *et al.*, 2017) indicates for instance that the 2015/2016 El Niño event dynamics can be interpreted as resulting from processes

associated with both the EP and CP El Niño events, conversely to the 1997/1998 El Niño that is diagnosed as a ‘pure’ EP El Niño event. Other factors explaining the differences between events include the distinct characteristics between El Niño events of processes associated with synoptic variability due to either the Madden–Julian oscillation (Madden and Julian, 1972) or the extra-tropical storm activity of

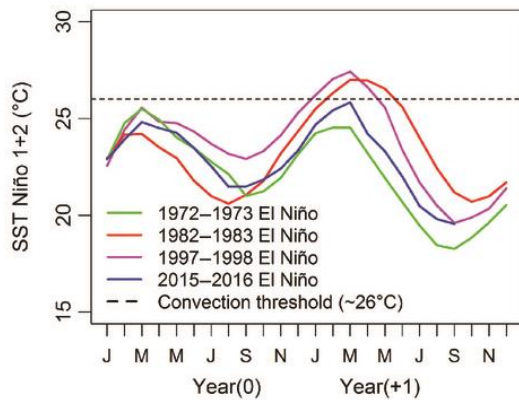


Figure 8. Evolution of the SST in the Niño 1+2 region during the fourth strong El Niño events. The horizontal line indicates the convection threshold temperature ($\sim 26^{\circ}\text{C}$). SST is obtained from the HadISST data set over the period 1950–2016. [Colour figure can be viewed at wileyonlinelibrary.com].

the mid-latitudes that are influential on the along-shore winds along the coast of Peru (Dewitte *et al.*, 2011) or the South Pacific meridional mode (Zhang *et al.*, 2014). Local processes of air-sea interactions are also thought to be at work during El Niño events in this region (B. Dewitte, 2017; personal communication). While local SST anomalies are not likely to be the only factor

influencing the rainfall conditions during strong El Niño events (Takahashi and Martinez, 2017), our study calls for investigating the sensitivity of the rainfall distribution and evolution to the regional oceanic conditions, which could be through the use of a regional atmospheric model. This is planned for future work.

Noteworthy, while extreme El Niño events are forecasted to increase in frequency in a warmer climate (Cai *et al.*, 2014), our study suggests that there might not be a straightforward relationship with the rainfall events over Peru considering the dispersion between events documented here over the observational record. In addition, one aspect that is not currently well accounted for in global coupled models is the regional SST anomalies along the coast of Peru and Ecuador (Takahashi *et al.*, 2014), which calls for investigating regional physical processes explaining such a diverse response of rainfall under strong El Niño conditions. Considering the likely impact of decadal variability on the relationship between ENSO and rainfall in Peru (Bourrel *et al.*, 2015; Segura *et al.*, 2016), the investigation of such processes would have to consider the influence of decadal variability.

Acknowledgements

This work was supported by Peruvian Ministry of Education (MINEDU-PRONABEC, scholarship). The authors would like to thank SENAMHI (National Service of

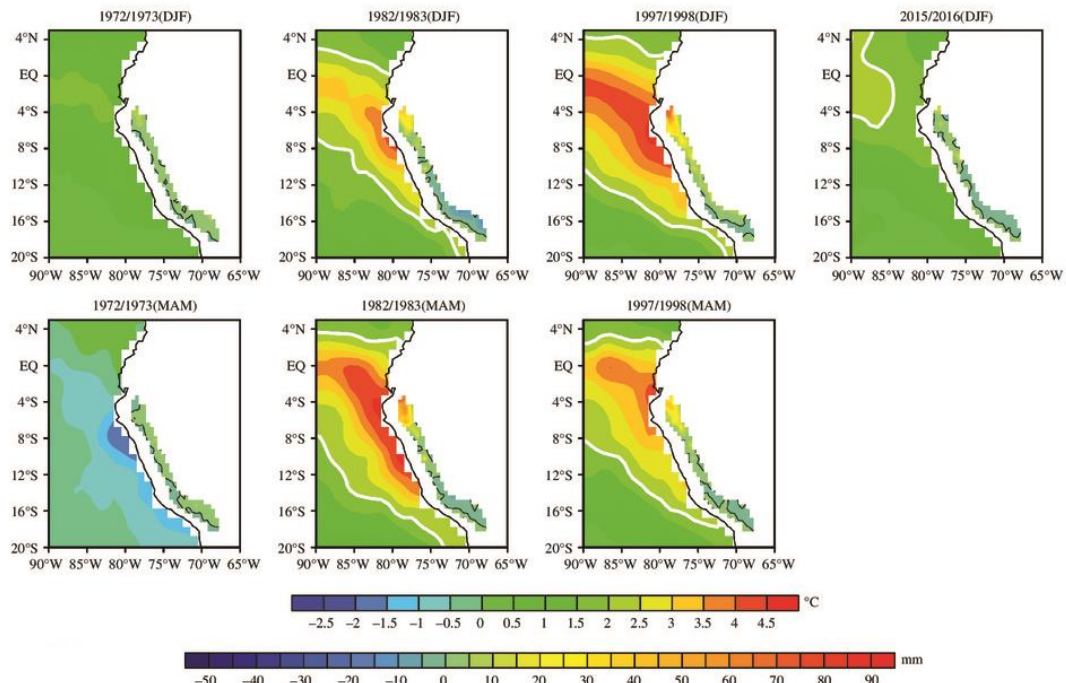


Figure 9. Evolution of SST and precipitation anomalies during the fourth strong El Niño events. Monthly averaged anomalies for (top) D(0)JF(+1) and (bottom) MAM(+1). Unit is in $^{\circ}\text{C}$ for SST (in the bottom right-hand corner) and in mm for precipitation (in the top right-hand corner for precipitation). For precipitation, the thick black line indicates the zero contour. For SST the contour in white line indicates the 2°C isotherm. Anomalies are relative to the seasonal cycle calculated over the period 1964–1977 (1978–2008) for the 1972/1973 El Niño (the 1982/1983 and 1997/1998 El Niño). [Colour figure can be viewed at wileyonlinelibrary.com].

Meteorology and Hydrology of Peru) for providing the raw data set. B. Dewitte acknowledges supports from FONDECYT (projects 1151185 and 1171861). The two anonymous reviewers are thanked for their constructive comments.

References

- Barsugli JJ, Sardeshmukh PD. 2002. Global atmospheric sensitivity to tropical SST anomalies throughout the Indo-Pacific basin. *J. Clim.* **15**(23): 3427–3442.
- BCRP. 2016. Actividad Económica (Marzo, abril y setiembre). Banco Central de Reserva del Perú (Central Reserve Bank of Peru). *Notas Estudio* **35**: 2–3 43: 2–3, 80: 2–4.
- Bendix A, Bendix J. 2006. Heavy rainfall episodes in Ecuador during El Niño events and associated regional atmospheric circulation and SST patterns. *Adv. Geosci.* **6**: 43–49.
- Bjerknes J. 1969. Atmospheric teleconnections from the equatorial Pacific. *Mon. Weather Rev.* **97**: 163–172.
- Bourrel L, Rau P, Dewitte B, Labat D, Lavado W, Coutaud A, Vera A, Alvarado A, Ordoñez J. 2015. Low-frequency modulation and trend of the relationship between ENSO and precipitation along the northern to centre Peruvian Pacific coast. *Hydro. Processes* **29**(6): 1252–1266.
- Brack A, Mendiola C. 2000. *Ecología del Perú*. Editorial Brújula: Lima.
- Brunet-Morel Y. 1979. Homogénéisation des précipitations. Cahiers ORSTOM. Serie. *Hydro.* **16**: 3–4.
- Cai W, Borlace S, Lengaigne M, van Rensh P, Collins M, Vecchi G, Timmermann A, Santoso A, McPhaden MJ, Wu L, England MH, Wang G, Guilyardi E, Jin F-F. 2014. Increasing frequency of extreme El Niño events due to greenhouse warming. *Nat. Clim. Change* **5**(2): 1–6. <https://doi.org/10.1038/nclimate2100>.
- Capotondi A, Wittenberg AT, Newman M, Di Lorenzo E, Yu J-Y, Braconnot P, Cole J, Dewitte B, Giese B, Guilyardi E, Jin F-F, Karinauskas K, Kirtman B, Lee T, Schneider N, Xue Y, Yeh S-W. 2015. Understanding ENSO diversity. *Bull. Am. Meteorol. Soc.* **96**(June): 921–938.
- Clarke AJ. 1983. The reflection of equatorial waves from oceanic boundaries. *J. Phys. Oceanogr.* **13**(7): 1193–1207.
- Cressman GP. 1959. An operational objective analysis system. *Mon. Weather Rev.* **81**: 367–374.
- Dewitte B, Illig S, Renault L, Goubanova K, Takahashi K, Gushchina D, Mosquera K, Purca S. 2011. Modes of covariability between sea surface temperature and wind stress intraseasonal anomalies along the coast of Peru from satellite observations (2000–2008). *J. Geophys. Res.* **116**: C04028. <https://doi.org/10.1029/2010JC006495>.
- Dewitte B, Vazquez-Cuervo J, Goubanova K, Illig S, Takahashi K, Cambon G, Purca S, Correa D, Gutierrez D, Sifeddine A, Ortieb L. 2012. Change in El Niño flavours over 1958–2008: implications for the long-term trend of the upwelling off Peru. *Deep Sea Res. II: Trop. Stud. Oceanogr.* **77–80**: 143–156.
- Diaz HF, Hoerling MP, Eischeid JK. 2001. ENSO variability, teleconnections and climate change climate variability; El Niño-Southern Oscillation (ENSO); teleconnections. *Int. J. Climatol.* **21**(15): 1845–1862.
- Doty B. 1995. *The Grid Analysis and Display System-GrADS*. Center for Ocean-Land-Atmosphere Studies: Calverton, MD, 148 pp.
- Douglas MW, Mejia J, Ordinola N, Boustead J. 2009. Synoptic variability of rainfall and cloudiness along the coasts of northern Peru and Ecuador during the 1997/98 El Niño event. *Mon. Weather Rev.* **137**: 116–136.
- Efron B, Tibshirani RJ. 1993. *An Introduction to the Boot Strap*. Chapman and Hall: New York, 456 pp.
- Frauen C, Dommenget D, Tyrell N, Rezny M, Wales S. 2014. Analysis of the nonlinearity of El Niño-Southern Oscillation teleconnections. *J. Clim.* **27**(16): 6225–6244.
- Goldberg RA, Tisnado GM, Scofield RA. 1987. Characteristics of extreme rainfall events in northwestern Peru during the 1982–1983 El Niño period. *J. Geophys. Res.* **92**(C13): 14225–14241.
- Hastenrath S. 1978. On modes of tropical circulation and climate anomalies. *J. Atmos. Sci.* **35**: 222–223.
- Horel JD, Cornejo GA. 1986. Convection along the coast of northern Peru during 1983: spatial and temporal variation of clouds and rainfall. *Mon. Weather Rev.* **114**: 2091–2105.
- Horel JD, Wallace JM. 1981. Planetary-scale atmospheric phenomena associated with the Southern Oscillation. *Mon. Weather Rev.* **109**: 813–829.
- Kao HY, Yu JY. 2009. Contrasting eastern Pacific and central Pacific types of ENSO. *J. Clim.* **22**(3): 615–632.
- Keshavamurti RN. 1982. Response of the atmosphere to sea surface temperature anomalies over the equatorial Pacific and the teleconnections of the Southern Oscillation. *J. Atmos. Sci.* **39**: 1241–1259.
- Kug JS, Jin FF, An SI. 2009. Two types of El Niño events: cold tongue El Niño and warm pool El Niño. *J. Clim.* **22**(6): 1499–1515.
- Lavado W, Espinoza JC. 2014. Impactos de El Niño y La Niña en las lluvias del Perú (1965–2007). *Rev. Brasil. Meteorol.* **29**(2): 171–182.
- L'Heureux ML, Takahashi K, Watkins AB, Barnston AG, Becker EJ, Di Liberto TE, Gamble F, Gottschalk J, Halpert MS, Huang B, Mosquera-Vásquez K, Wittenberg AT. 2017. Observing and predicting the 2015–16 El Niño. *Bull. Am. Meteorol. Soc.* **98**: 1363–1382. <https://doi.org/10.1175/BAMS-D-16-0009.1>.
- Madden R, Julian P. 1972. Description of global-scale circulation cells in the tropics with a 40–50 day period. *J. Atmos. Sci.* **29**: 1109–1123.
- Paek H, J-Y Y, Qian C. 2017. Why were the 2015/16 and 1997/98 extreme El Niños different? *Geophys. Res. Lett.* **44**: 1848–1856. <https://doi.org/10.1002/2016GL071515>.
- Philander SGH. 1985. El Niño and La Niña. *J. Atmos. Sci.* **42**: 2652–2662.
- Rau P, Bourrel L, Labat D, Melo P, Dewitte B, Frappart F, Lavado W, Felipe O. 2017. Regionalization of rainfall over the Peruvian Pacific slope and coast. *Int. J. Climatol.* **37**(1): 143–158.
- Rayner NA, Parker DE, Horton EB, Folland CK, Alexander LV, Rowell DP, Kent EC, Kaplan A. 2003. Global analyses of sea surface temperature, sea ice, and night marine air temperature since the late nineteenth century. *J. Geophys. Res.* **108**(D14): 4407.
- Ropelewski CF, Halpert MS. 1987. Global and regional scale precipitation patterns associated with El Niño/Southern Oscillation. *Mon. Weather Rev.* **115**: 1606–1626.
- Rundel PW, Villagra PE, Dillon MO, Roig-Junent SA, Debandi G. 2007. Arid and semi-arid ecosystems. In *The Physical Geography of South America*, Veblen TT, Young K, Orme AE (eds). Oxford University Press: Oxford, UK, 158–183.
- Segura H, Espinoza JC, Junquias C, Takahashi K. 2016. Evidencing decadal and interdecadal hydroclimatic variability over the Central Andes. *Environ. Res. Lett.* **11**(9): 1–8. <https://doi.org/10.1088/1748-9326/11/9/094016>.
- SENAMHI. 2015. Escenarios de Peligros Hídricos en el Perú ante la ocurrencia de Eventos Niño Extraordinarios. Documento técnico elaborado por la Dirección General de Hidrología y Recursos Hídricos. Servicio Nacional de Meteorología e Hidrología del Perú, Lima, Peru.
- Takahashi K, Martínez AG. 2017. The very strong El Niño in 1925 in the far-eastern Pacific. *Clim. Dyn.* <https://doi.org/10.1007/s00382-017-3702-1>.
- Takahashi K, Montecinos A, Goubanova K, Dewitte B. 2011. ENSO regimes: reinterpreting the canonical and Modoki El Niño. *Geophys. Res. Lett.* **38**: L10704.
- Takahashi K, Martínez R, Montecinos A, Dewitte B, Gutiérrez D, Rodriguez-Rubio E. 2014. Regional applications of observations in the eastern Pacific: Western South America. Whitepaper for TPOS2020, No. 8a, California, 1–31.
- Tapley TD, Waylen PR. 1990. Spatial variability of annual precipitation and ENSO events in western Peru. *Hydro. Sci. J.* **35**(4): 429–446.
- Tedeschi RG, Grimm AM, Cavalcanti IFA. 2015. Influence of central and east ENSO on extreme events of precipitation in South America during austral spring and summer. *Int. J. Climatol.* **35**: 2045–2064.
- Trenberth KE, Stepaniak DP. 2001. Indices of El Niño evolution. *J. Clim.* **14**: 1697–1701.
- Trenberth KE, Branstator GW, Karoly D. 1998. Progress during TOGA in understanding and modeling global teleconnections associated with tropical sea surface temperatures. *J. Geophys. Res.* **103**(C7): 14291–14324.
- Vargas P. 2009. El Cambio Climático y sus Efectos en el Perú. Working Papers, World Bank, Washington, DC.
- Woodman R. 1999. Modelo estadístico de pronóstico de las precipitaciones en la costa norte del Perú. El Fenómeno El Niño. Investigación para una proyección, 1er encuentro de Universidades del Pacífico Sur: Memoria 93–108, Piura-Perú.
- Yeh SW, Kug JS, Dewitte B, Kwon MH, Kirtman BP, Jin F-F. 2009. El Niño in a changing climate. *Nature* **461**(7263): 511–514.
- Yu JY, Kim ST. 2013. Identifying the types of major El Niño events since 1870. *Int. J. Climatol.* **33**(8): 2105–2112.
- Zhang H, Clement AC, DiNezio P. 2014. The South Pacific meridional mode: a mechanism for ENSO-like variability. *J. Clim.* **27**: 769–783. <https://doi.org/10.1175/JCLI-D-13-00082.1>.

This page intentionally left blank

Chapter 3: Comparison of rainfall reanalysis data to develop atmospheric scenarios during extreme El Niño events (observations and evaluations)

3.1 REANALYSIS

The climate research community uses reanalysis data sets to understand a wide range of processes and variability in the climatic system (see Fig. 3.1), yet different reanalysis may give very different results for the same diagnostics.

Reanalysis is a climate or weather model simulation of the past that includes data assimilation of historical observations. The group reanalyses.org (NOAA/ESRL Physical Sciences Division, the NOAA climate Program Office and the US Department of Energy's Office of Science-BER) define climatic reanalysis as a scientific method for developing a comprehensive record of how weather and climate are changing over time. In it, observations and a numerical model that simulates one or more aspects of the Earth system are combined objectively to generate a synthesized estimate of the state of the system. A reanalysis typically extends over several decades or longer and covers the entire globe from the Earth's surface to well above the stratosphere. Reanalysis products are used extensively in climate research and services, including for monitoring and comparing current climate conditions with those of the past, identifying the causes of climate variations and change, and preparing climate predictions. Information derived from reanalysis is also being used increasingly in commercial and business applications in sectors such as energy, agriculture, water resources, and insurance.

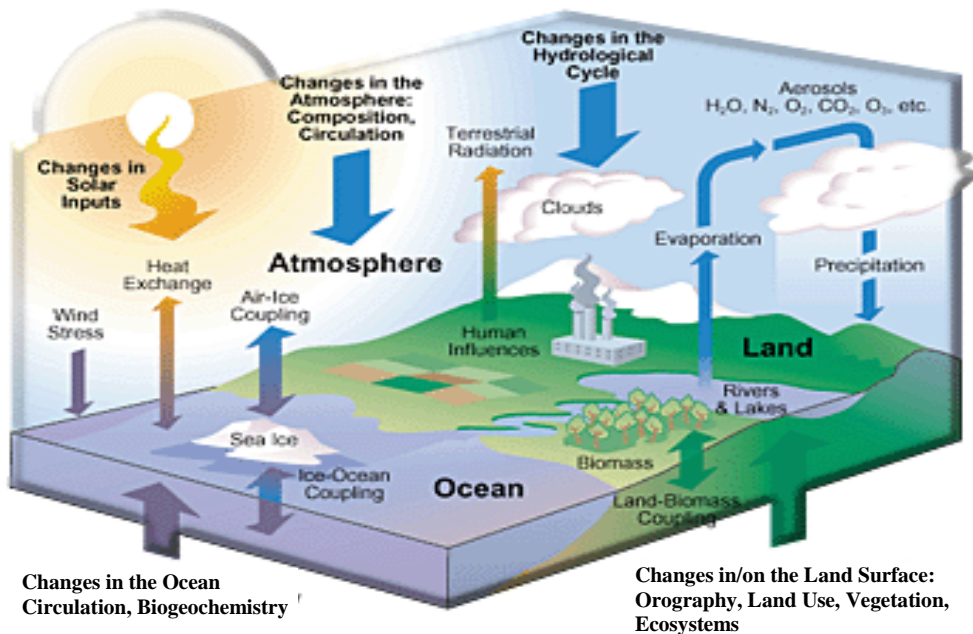


Figure 3.1. Global climatic system components (atmosphere, land, Ocean, and cryosphere) and their main interactions. The climate system data are used for the production of global reanalysis. Reanalysis data covers the globe from the Earth's surface to beyond the stratosphere. Credit: European Reanalysis of the Global Climate System. <http://www.era-clim.eu/ERA-CLIM2/>

3.2 ATMOSPHERIC REANALYSIS

The scope of this chapter is mainly dedicated to compare the current reanalysis of the atmosphere. An atmospheric reanalysis system consists of a global forecast model, input observations, and an assimilation scheme, which are used in combination to produce best estimates (analyses) of past atmospheric states (including temperature, wind, geopotential height, and humidity fields). The forecast model propagates information forward in time and space from previous analyses of the atmospheric state.

The atmospheric reanalysis are useful tools for examining climate processes because they provide greater coverage than observations alone, combine information from a diverse range of sources, and adjust for biases that may exist in any specific set of observations. However, they must be used cautiously because the quantity, quality and type of observations being included in the reanalysis have changed over time, which can produce artificial trends (Dee et al., 2011). However, considerable advancement in the data assimilation techniques and model physics results in reduction of biases and errors in the new generation of reanalysis.

3.2.1 Reanalysis system

The first three major reanalysis efforts started in the late 1980s, conducted by NASA, ECMWF, and a joint effort between the NMC (now NCEP) and NCAR (e.g. Edwards, 2010). Currently make available more than 10 global atmospheric reanalysis data sets which basic specifications for each of the reanalysis as the released year, temporal coverage, horizontal grid spacing, vertical levels, top level and boundary conditions (externally supplied forcings) are show in Table 1 and 2.

3.2.1.1 ECMWF reanalysis

The European Centre for Medium-range Weather Forecasts (ECMWF) Interim reanalysis (ERA Interim) lead three major reanalysis of the global atmosphere: the first the ERA-40 project generated reanalysis from September 1957 to August 2002.

The second, ERA-Interim (Dee et al., 2011), cover the period 1979 until present. A full-input reanalysis of satellite dates that includes several corrections and modifications to the system used for ERA-40 (Uppala et al., 2005). An atmospheric weather forecast model with a fixed configuration is physically constrained by observations using four-dimensional data assimilation. Vertical profiles of temperature and water vapor from satellite and conventional observations are used by the assimilation system, and the resulting analysis provides comprehensive diagnostics of atmospheric and surface properties (Dee et al., 2011). While some variables are strongly constrained by assimilated variables, such as water vapor and temperature, others such as cloud and precipitation are dependent upon the realism of the model parametrizations. The water vapor profiles and transports are strongly dependent upon the assimilation of water vapor variables. Major focus areas during the production of ERA-Interim included achieving more realistic representations of the hydrologic cycle relative to ERA-40, as well as improving the consistency of the reanalysis products in time.

The performance of ERA-Interim over South America has been analyzed by Lorenz et al., 2012 and Solman et al., 2013 who showed a low uncertainty in precipitation, and also by Knippertz et al., 2013; Drumond et al., 2014 who showed a reliable representation of the moisture source over the tropical zone. The appropriate representation of the hydrological cycle by ERA-Interim supposes an increase in forecast quality compared to previous ERA reanalysis (Trenberth et al., 2011).

The third, ERA-20C (Poli et al., 2015, 2016) uses a 4D-Var data assimilation system but takes its spatially and temporally varying background errors from a prior ensemble data assimilation (Isaksen et al., 2010; Poli et al., 2013). Because ERA-20C directly assimilates only surface

pressure and surface wind observations, it can generate reanalysis of the climate state that extend further back in time (in this case to the beginning of the 20th century).

3.2.1.2 JMA reanalysis (Japanese Meteorological Agency) (JMA)

JRA-25 (Onogi et al., 2007) is a full-input reanalysis of the satellite ERA and the first reanalysis produced by JMA. JRA-55 (Japanese global atmospheric reanalysis conducted by JMA) (Kobayashi et al., 2015) is the most recent reanalysis that applies a 4D-Var data assimilation scheme to upper-air data during the pre-satellite ERA, besides has incorporated many improvements relative to its predecessor JRA-25 (Onogi et al. 2007).

In particularly, JRA-55 offers improvements in the representation of the phenomena on a wide range of space-time scales (i.e. Equatorial Waves), still the amplitudes of equatorial waves and the MJO (Madden and Julian Oscillation) are weaker than in the other reanalysis (Harada *et al.*, 2016). Also, water vapor fluxes account into the continent linked to regional circulation still need to be well resolved by this product (Kobayashi *et al.*, 2015).

3.2.1.3 NASA GMAO reanalysis

MERRA (Rienecker et al., 2011) is a full-input reanalysis of the satellite ERA developed by American Space Agency NASA's GMAO using the GEOS-5 data assimilation system. MERRA is an offline replay of MERRA (Rienecker et al. 2011) land model component with two major changes: an updated land surface model and improved precipitation forcing based on gauge-based National Oceanic and Atmospheric Administration (NOAA) Climate Prediction Centre (CPC) with the MERRA precipitation. This reanalysis was conceived with the intention of leveraging the large amounts of data produced by NASA's Earth Observing System (EOS) satellite constellation and improving the representations of the water and energy cycles relative to earlier reanalysis. MERRA-2 (Bosilovich et al., 2015) is a full-input reanalysis of the satellite ERA from NASA's GMAO. The Project focuses on historical analyses of the hydrological cycle on a broad range of weather and climate time scales and places the NASA EOS suite of observations in a climate context.

3.2.1.4 NOAA/NCEP and related reanalysis

NCEP–NCAR R1 (Kalnay et al., 1996; Kistler et al., 2001) is produced using a modified 1995 version of the NCEP forecast model. NCEP–DOE R2 (Kanamitsu et al., 2002) is a 1998

version of the same model and covers the satellite ERA (1979–present) including corrections for some important errors and limitations identified in R1.

Climate Forecast System Reanalysis (CFSR) (Saha et al., 2010) is a full-input reanalysis of the satellite ERA that uses a 2007 version of the NCEP CFS. CFSR contains a number of improvements relative to R1 and R2 as a better forecast model and data assimilation system, including higher horizontal and vertical resolutions, a higher model top, more sophisticated model physics, and the ability to assimilate satellite radiances directly. CFSR is also the first global reanalysis of the coupled atmosphere–Ocean–sea-ice system. Being this migrated to the operational CFSv2 analysis system (Saha et al., 2014) which has a different horizontal resolution and includes minor changes to physical parametrizations.

Over South America CFSR produce greatly improves tropical intraseasonal rainfall (Wang et al., 2012) and a well-represented regional climatology of South American besides the signals of anomalous heavy rainfall over the northern Peru and Ecuador during El Niño (Eichler and Londoño, 2013). Although the heavy precipitation between the Andes and the coast is simulated by local model topography of CFSR (Eichler and Londoño, 2013) still CFSR has substantial bias along large topographical gradient (Silva et al., 2011; Eichler and Londoño, 2013; Blacutt et al., 2015).

NOAA–CIRES 20CR v2 (Compo et al., 2011) is the first reanalysis to span more than 100 years. Like ERA-20C, 20CR is a surface-input reanalysis. Unlike ERA-20C, which uses a 4D-Var approach to assimilate surface pressure and surface winds, 20CR uses an ensemble Kalman filter (EnKF) approach and assimilates only surface pressure. The forecast model used in 20CR is similar in many ways to that used in CFSR, but with much coarser vertical and horizontal resolutions. The major limitation in 20CR, similar to other global atmospheric reanalysis products of shorter duration, is its poor representation of the precipitation features at regional and local scale.

Reanalysis system	Reference	Description	Model*	Horizontal grid spacing	Vertical levels	Top level
ERA-40	Uppala et al. (2005)	Centre: ECMWF Coverage: September 1957 to August 2002	IFS Cycle 23r4 (2001)	N80 (TL159): ~125 km	60 (hybrid σ -p)	0.1 hPa
ERA-Interim	Dee et al. (2011)	Centre: ECMWF Coverage: January 1979 to present	IFS Cycle 31r2 (2007)	N128 (TL255): ~79 km	60 (hybrid σ -p)	0.1 hPa
ERA-20Ca	Poli et al. (2016)	Centre: ECMWF Coverage: January 1900 to December 2010	IFS Cycle 38r1 (2012)	N80 (TL159): ~125 km	91 (hybrid σ -p)	0.01 hPa
JRA-25/JCDAS	Onogi et al. (2007)	Centre: JMA and CRIEPI (JRA-25) Coverage: January 1979 to January 2014	JMA GSM (2004)	F80 (T106): 1.125°	40 (hybrid σ -p)	0.4 hPa
JRA-55	Kobayashi et al. (2015)	Centre: JMA Coverage: January 1958 to present	JMA GSM (2009)	N160 (TL319): ~55 km	60 (hybrid σ -p)	0.1 hPa
MERRA	Rienecker et al. (2011)	Centre: NASA GMAO Coverage: January 1979 to February 2016	GEOS 5.0.2 (2008)	1/2° latitude x 2/3° longitude	72 (hybrid σ -p)	0.01 hPa
MERRA-2	Bosilovich et al. (2015)	Centre: NASA GMAO Coverage: January 1980 to present	GEOS 5.12.4 (2015)	0.5° latitude x 0.625° longitude	72 (hybrid σ -p)	0.01 hPa
NCEP-NCAR R1	Kalnay et al. (1996)	Centre: NOAA/NCEP and NCAR R1 Kistler et al. (2001) Coverage: January 1948 to present	NCEP MRF (1995)	F47 (T62): 1.875°	28 (σ)	3 hPa
NCEP-DOE R2	Kanamitsu et al. (2002)	Centre: NOAA/NCEP and the DOE AMIP-II project (R2) Coverage: January 1979 to present	Modified MRF (1998)	F47 (T62): 1.875°	28 (σ)	3 hPa
CFSR	Saha et al. (2010)	Centre: NOAA/NCEP (CDAS-T382) Coverage: January 1979 to December 2010	NCEP CFS (2007)	F288 (T382): 0.3125°	64 (hybrid σ -p)	~0.266 hPa
CFSv2	Saha et al. (2014)	Centre: NOAA/NCEP (CDAS-T574) Coverage: January 2011 to present	NCEP CFS (2011)	F440 (T574): 0.2045°	64 (hybrid σ -p)	~0.266 hPa
NOAA-CIRES 20CR v2d	Compo et al. (2011)	Centre: NOAA and the University of Colorado CIRES (20CR) Coverage: November 1869 to December 2012	NCEP GFS (2008)	F47 (T62): 1.875°	28 (hybrid σ -p)	~2.511 hPa

Table 3.1. List of global atmospheric reanalysis systems. Approximate longitude grid spacing is reported in degrees for models with regular Gaussian grids (Fn) and in kilometers for models with reduced Gaussian grids (Nn). Wavenumber truncations for models with Gaussian grids are reported in parentheses. * Year in parentheses indicates the year for the version of the operational analysis system that was used for the reanalysis.

Reanalysis system	Reference	Grid	Time	Reference
ERA-40	HadISST1 (Sep 1957–Nov 1981) NCEP 2DVar (Dec 1981–Jun 2001) NOAA OISSTv2 (Jul 2001–Aug 2002)	1° 1° 0.25°	monthly weekly daily	Rayner et al. (2003) Reynolds et al. (2002) Reynolds et al. (2007)
ERA-Interim NOAA OISSTv2 (Jul 2001–Dec 2001) NCEP RTG (Jan 2002–Jan 2009)	HadISST1 (Sep 1957–Nov 1981) NCEP 2DVar (Dec 1981–Jun 2001) OSTIA (Feb 2009–present)	1° 1° 0.25° 0.083° 0.05°	monthly weekly daily daily daily	Rayner et al. (2003) Reynolds et al. (2002) Reynolds et al. (2007) Gemmell et al. (2007) Donlon et al. (2012)
ERA-20C	HadISSTv2.1.0.0 _	0.25°	daily	Titchner and Rayner (2014)
JRA-25/JCDAS	COBE	1°	daily	Ishii et al. (2005)
JRA-55	COBE	1°	daily	Ishii et al. (2005)
MERRA	Hadley Centre (Jan 1979–Dec 1981) NOAA OISSTv2 (Jan 1982–present)	1° 1°	monthly weekly	none (personal communication Reynolds et al. (2002))
MERRA-2	AMIP-II (Jan 1980–Dec 1981) NOAA OISSTv2 (Jan 1982–Mar 2006) OSTIA (Apr 2006–present)	1° 0.25° 0.05°	monthly daily daily	Taylor et al. (2000) Reynolds et al. (2007) Donlon et al. (2012)
NCEP-NCAR R1	Met Office GISST (Jan 1948–Oct 1981) NOAA OISSTv1 (Nov 1981–Dec 1994) NOAA OISSTv1 (Jan 1995–present)	1° 1° 1°	monthly weekly daily	Parker et al. (1995) Reynolds and Smith (1994) Reynolds and Smith (1994)
NCEP-DOE R2	AMIP-II (Jan 1979–15 Aug 1999) NOAA OISSTv1 (16 Aug 1999–Dec 1999) NOAA OISSTv1 (Jan 2000–present)	1° 1° 1°	monthly monthly daily	Taylor et al. (2000) Reynolds and Smith (1994) Reynolds and Smith (1994)
CFSR	HadISST1.1 (Jan 1979–Oct 1981) NOAA OISSTv2 (Nov 1981–present)	1° 0.25°	monthly daily	Rayner et al. (2003) Reynolds et al. (2007)
CFSv2	HadISST1.1 (Jan 1979–Oct 1981) NOAA OISSTv2 (Nov 1981–present)	1° 0.25°	monthly daily	Rayner et al. (2003) Reynolds et al. (2007)
NOAA-CIRES 20CR v2d	HadISST1.1	1°	monthly	Rayner et al. (2003)

Table 3.2. Sources of SST used in reanalysis.

3.3 Reanalysis rainfall over the Peruvian Pacific Basin (PPB)

Over South America the different reanalysis shows differences in patterns of rainfall changes (Donat *et al.*, 2014; Angélil *et al.*, 2016). The biases present generally large magnitude, and there are also regional differences in the observations biases especially in areas of large topographical gradients (Eichler *et al.*, 2016). Comparison of reanalysis on the Pacific basin of South America has been little documented. The recent development of temporal and spatial high-resolution third-generation reanalysis datasets allows a better representation over coarse and complex terrain. Besides offers an opportunity to better evaluate the rainfall variability and climatologic diversity of the South American continent. The third-generation reanalysis that adopt a sophisticated assimilation show a robustness identifying coupled ocean–atmosphere anomalies (Ruiz-Barradas *et al.*, 2017). They have also a high similarity for describe the principal mode of the variability of water vapor though there is main discrepancy in the multiyear global distribution, variation of interannual cycle and long-term trend (Yu *et al.*, 2015). In South America, this third-generation reanalysis have shown improved performance in the rainfall variability during the austral summer (Albuquerque de Almeida *et al.*, 2018). In particular, ERA-Interim is better correlated than CFSR (Lorenz *et al.*, 2012 and Solman *et al.*, 2013; Knippertz *et al.*, 2013; Drumond *et al.*, 2014; Blázquez and Solman, 2017 Albuquerque de Almeida *et al.*, 2018) and presents a wide ability to reproduce the main factors that control rainfall in South America (Blázquez and Solman, 2017).

One of the main difficulties for addressing the atmospheric processes regarding the link of atmospheric water transport and precipitation is the significant difference between reanalysis which leads to evaluate them and choosing the reliable reanalysis. Through the robustness of rainfall quantification in reanalysis we can say with confidence that moisture transport and large-scale and regional circulation from atmospheric reanalysis are correctly modeling. The comparison of reanalysis rainfall in the PPB is supported in the following paper (“**Rainfall during the strong El Niño events from Reanalysis ERA-interim, CFSR and JRA-55 in the Pacific Peruvian basin**”).

RESEARCH WORK (RESEARCH ARTICLE)

Rainfall during the strong El Niño events from Reanalysis ERA-interim, CFSR and JRA-55 in the Pacific Peruvian basin (manuscript to be submitted to *Atmospheric Research Journal*)

Preamble

This section is dedicated to the comparison of the three most recent third-generation reanalysis (ERA-Interim, CFSR and JRA55) regarding which of them is most sustainable for studies of extreme rainfall associated with the strong El Niño events. Monthly rainfall reanalysis was compared with rainfall observed for the common period from 1979 to 2009. A statistical analysis was also performed using correlation, bias and Mean Square Error (MSE) indexes. Likewise, the rainfall variability was compared taking into account the main rainfall patterns observed and the evolution of strong El Niño events observed. We show that the precipitation ERA-Interim shows better performance for reproducing rainfall variability in the PPB in terms of the spatial pattern (Ep and Cp Mode). In addition, the three reanalysis better reproduce the evolution of Ep mode than the Cp mode. Furthermore, these reanalysis well agree also with the different projections of rainfall peak though they have still deficiencies in the exact reproduction of peak magnitude.

**Rainfall during the strong El Niño events from Reanalysis ERA-
Interim, CFSR and JRA-55 in the Pacific Peruvian basin (manuscript
to be submitted to *Atmospheric Research Journal*)**

Janeet Sanabria^{1,2}, Luc Bourrel¹, David Labat¹

¹*UMR 5563 GET, Université de Toulouse - CNRS - IRD - OMP - CNES, Toulouse, France.*

²*SENAMHI, Jirón Cahuide 785, Lima 11, Peru.*

*Correspondence to: J. Sanabria, UMR 5563 GET, Université de Toulouse -CNRS-IRD -OMP-CNES,Toulouse 31400, France. E-mail: janeet.sanabria@get.omp.eu

Rainfall during the strong El Niño events from Reanalysis ERA-Interim, CFSR and JRA-55 in the Pacific Peruvian basin

Abstract

The focus of this research is to analyze the ability of three reanalysis ERA-Interim, Climate Forecast System Re-analysis (CFSR) and JRA-55 to reproduce observed rainfall variability in the Peruvian Pacific Basin (PPB) with emphasis in the extreme rainfall associated with the strong El Niño events, using reanalysis and observed rainfall time series from 1979 to 2016. The rainfall statistics (correlation, bias and Mean Square Error) indicate that ERA-Interim is more realistic reproducing the rainfall in low and highlands areas of the PPB while the other two reanalysis products have more difficulty to reproduce rainfall in Andes Mountains with a high variance for JRA-55 than CFSR. Interestingly, ERA-Interim reproduced better the two main modes that characterize the rainfall variability mainly the Ep mode linked with heavy rainfall whereas JRA-55 and CFSR disagrees to reproduce the Cp mode linked with moderate rainfall in highlands. In particular, the three reanalysis closely reproduce the differences among the strong El Niño events, such as the intensity of rainfall peak (extreme events about ten times more than moderate events) and the evolution of the 1982/1983 and 1997/1998 events on the Ep mode which better agree than the events 1972/1973 and 2015/2016 on Cp mode. Although, these reanalysis well agree with the different projections of rainfall peak of the events still they have deficiencies in the exact reproduction of peak magnitude. Finally, these reanalysis agree that the strong El Niño events are the result of two modes due to the projected modes in each event. These results help better understand the rainfall variability difference among the three reanalysis products and observed records, and allow us to choose the more appropriate for different research requirements.

Key Points:

- ERA-Interim shows better performance for reproducing rainfall variability in the PPB in terms of the spatial pattern (Ep and Cp Mode).
- The three reanalysis better reproduce the evolution of 1982/1983 and 1997/1998 events (Ep mode) than the 1972/1973 and 2015/2016 (Cp mode).
- These reanalysis well agree with the different projections of rainfall peak still they have deficiencies in the exact reproduction of peak magnitude.

1. Introduction

Rainfall anomalies during the strong El Niño events (i.e. extreme rainfall events over coastal and slope areas and high rainfall variability in highlands) over the Peruvian Pacific Basin (PPB) (Sanabria *et al.*, 2018) affect population and several productive sectors (agriculture, energy, transport, miner and other) (BCRP 2017) and have a significant impact on the Peruvian economic growth (i.e. Gross Domestic Product GDP) (Vargas, 2009). One of the main difficulties for addressing atmospheric mechanisms that explain the rainfall variability during the strong El Niño events are the significant differences between Reanalysis (besides the scarcity of *in situ* data) as was already pointed out by previous studies (Mcglone and Vuille, 2012; Kumar *et al.*, 2012; Eichler and Londoño, 2013). Reanalysis (datasets from global and regional atmospheric retrospective analysis models) are climate and weather numerical model simulations of the past that includes data assimilation of historical observations (Uppala *et al.*, 2008). They estimate climatological mean values of the state of the Earth system. Being reanalysis one of the best method for evaluating climate processes (e.g., Dee *et al.*, 2011; Saha *et al.*, 2010) and their recent development of high-resolution datasets offer an opportunity to better evaluate the rainfall variability of in smaller-scale regions.

The three most recent third-generation reanalysis products as the European Centre for Medium-Range Weather Forecasts (ECMWF) Reanalysis (ERA-Interim), NCEP/Climate Forecast System Reanalysis (CFSR) and the Japanese 55-year Reanalysis (JRA-55) have been widely evaluated as an alternative to the earlier versions of global atmospheric reanalysis (e.g. Kumar *et al.*, 2012; Mayer *et al.*, 2013; Quadro *et al.*, 2013, Angélil *et al.*, 2016). These reanalysis incorporate a more suitable atmosphere-Ocean-land-sea ice coupled model (Yu *et al.*, 2015; Ruiz-Barradas *et al.*, 2017) and also an advanced assimilation system of observed dates from various networks allowing them a better prediction and analysis in a finer space-temporal resolution. In South America, this third-generation reanalysis have shown improved performance in the rainfall variability during the austral summer (Albuquerque de Almeida *et al.*, 2018). The performance of ERA-Interim over South America has been analyzed by Lorenz *et al.*, 2012 and Solman *et al.*, 2013; Blázquez and Solman, 2017 who showed a low uncertainty in precipitation, and also by Knippertz *et al.*, 2013; Drumond *et al.*, 2014; who showed a reliable representation of the moisture source over the tropical zone. The appropriate representation of the hydrological cycle by ERA-Interim supposes an increase in forecast quality compared to previous ERA reanalysis (Trenberth *et al.*, 2011). In addition, although CFSR produce greatly improves tropical intraseasonal rainfall (Wang *et al.*, 2012) and a well-represented regional climatology of South America besides the signals of anomalous heavy rainfall over the northern Peru and Ecuador during El Niño (Eichler and Londoño, 2013). Although the

heavy precipitation between the Andes and the coast is simulated by local model topography of CFSR (Eichler and Londoño, 2013) still CFSR has substantial bias along large topographical gradient (Silva et al., 2011; Eichler and Londoño, 2013; Blacutt et al., 2015). As well as JRA-55 offers improvements in the representation of the phenomena on a wide range of space-time scales (i.e. Equatorial Waves), still the amplitudes of equatorial waves and the MJO (Madden and Julian Oscillation) are weaker than in the other reanalysis (Harada et al., 2016). Also, water vapor fluxes account into the continent linked to regional circulation still need to be well resolved by this product (Kobayashi et al., 2015).

In this study, we analyze the rainfall variability in the PPB for three reanalysis products compared with the observed data which will allow identifying the reanalysis bias and ability to reproduce this variability. The focus is to show the skill of the reanalysis to reproduce the spatial patterns that characterize rainfall variability, and also the evolution of four different strong El Niño events which took place over the last five decades: the 1972/1973, 1982/1983, 1997/1998 and 2015/2016 El Niño events (selected events from ONI index -Nino 3.4- NOAA). The rainfall patterns of this variability in reanalysis are obtained following the methodology as used in the observed climatic variability (Sanabria et al., 2018). We aim to address the following questions: (1) how rainfall variability is performed in the three reanalysis products (ERA-Interim, CFSR and JRA-55) (2) what is the relevant difference between the rainfall variability of reanalysis in relation to the observed rainfall? The reanalysis and observed data are described in Section 2. Results of the comparison among reanalysis and observations are presented in Section 3 and the discussion and conclusions are provided in Section 4.

2. Data and Methodology

2.1 Dataset

2.1.1 Observed rainfall Dataset

Observed monthly rainfall data used in this study are obtained from 145 meteorological stations located in the PPB, provided by the Peruvian National Service of Meteorology and Hydrology (SENAMHI), over the 1964-2016 period. These data have been validated and homogenized following the regional vector methodology used in Bourrel et al., 2015 and Rau et al., 2017. These observed station rainfalls were then gridded at $0.5^\circ \times 0.5^\circ$ resolution by interpolation using Cressman technique (Cressman, 1959; Doty, 1995).

2.1.2 Reanalysis

ERA-Interim uses the Integrated Forecast System, at a horizontal resolution of $0.75^\circ \times 0.75^\circ$ (~80 km) with 37 vertical pressure levels extending from the surface to 1 hPa. ERA-Interim produces a reanalysis with an improved atmospheric model and assimilation system that replaces those used in ERA-40 (Dee *et al.*, 2011). Data is available from <http://apps.ecmwf.int/datasets/data/interim-full-moda/levtype=sfc/>. Complementary reanalysis information is described in <https://www.ecmwf.int/en/research/climate-reanalysis/era-interim>. CFSR is the National Centers for Environmental Prediction (NCEP) derived from a coupled atmosphere–Ocean–land surface– sea ice system. The atmosphere resolution is T382 (~40 km) with 64 vertical levels extending from the surface to 0.26 hPa. CFSR adopts a three-dimensional variational (3D-Var) model that includes various upgrades in model physic and assimilation algorithms (Saha *et al.*, 2010). JRA-55 is the second Japanese global atmospheric reanalysis conducted by Japanese Meteorological Agency (JMA) with a resolution grid size of about ~55 km (TL319L60) with 60 vertical levels as well it is the first to apply 4D-Var to the 1958 to 2013 period. JRA-55 was extensively improved compared to the previous reanalysis (JRA-25) product mainly with revised long wave radiation scheme, four-dimensional variational analysis (4D-Var) and variational bias correction for satellite radiances (Kobayashi *et al.*, 2015).

Reanalysis monthly data products obtained at different resolutions were homogenized at the same resolution ($0.5^\circ \times 0.5^\circ$;~50 km) as the observed grid data, and then compared with the observed data for the 30 years common available period (1979 – 2009).

2.2 Methodology

2.2.1 EOF rainfall analysis

The rotated EOF methodology to determine the mainly rainfall patterns that characterize of the observed rainfall variability (Sanabria *et al.*, 2018) is used in the rainfall from reanalysis. The original EOF modes of rainfall from reanalysis will be rotated 60° as observed rainfall. The rotation maximizes the variance along preferred directions that correspond to peculiar evolutions of some events. The first rotated mode describes the variability along the direction of the evolution of the extreme events, and the second rotated mode account the variability associated to moderate events. Significance level for the modes was estimated based on a bootstrap method (Efron and Tibshirani, 1993) (see Sanabria *et al.*, 2018 for details). As well, it was calculated composite spatial and temporal evolution of rainfall anomalies along the

modes from reanalysis. The temporal evolution of the events is over the time period covering El Niño episode (i.e. two years).

In addition, monthly rainfall anomalies in reanalysis like the observed are calculated over two distinct periods (1964-1977 and 1978-2016) to take into account the 70s climate shift in the Pacific Ocean (Trenberth and Stepaniak, 2001). These anomalies are used in the rotated EOF and in other indices.

2.2.2 Statistic indices

We used the well know statistical parameters such as Mean Square Error (MSE) that measure the quality of the reanalysis error through the variability of reanalysis (precision) and its BIAS (accuracy), smaller values for MSE indicate closer agreement between reanalysis and observed results. It is expressed as:

$$MSE = (Sd_{reanalysis})^2 + bias^2 \quad (1)$$

where $Sd_{reanalysis}$ is the standard deviation of reanalysis and $bias$ is a systematic error referred to the tendency of a sample statistic to systematically over or under estimate the observed dates

$$Bias = \sum_1^n \frac{(P_{reanalysis} - P_{observed})}{n} \quad (2)$$

where P : monthly precipitation (mm) and n :number of month. $Bias = 0$ indicates that the reanalysis rainfall data are the same as the observed rainfall data; $Bias < 0$ indicates that the reanalysis rainfalls are smaller than the observed rainfall tending to a underestimation; $Bias > 0$ indicates that the reanalysis rainfall tend to an overestimation of the observed rainfall.

Correlation describes the degree of relationship between reanalysis and observed, and the direction of the relationship (positive or negative). Reanalysis and observed climatology were also compared.

3. Results and discussion

3.1 Statistical analysis and climatology

In order to test the accuracy of rainfall reanalysis and its spatial-temporal coherence (Kutner et al., 2003), correlation analysis was performed. The average correlations of rainfall data grid-point series between ERA-Interim CFSR and JRA-55 reanalysis and observed data were 72, 72 and 68% respectively. This result indicates that reanalysis dataset reproduces fairly well observed rainfall pattern and explain the observed rainfall variability (Fig. 1). Using MSE, a more useful measure that considers sensitivity to error magnitude (Murphy, 1988), it is observed during rainy period that ERA-Interim fits very well the observed rainfall with smallest MSE (5%), while JRA-55 shows high deviations along Andes with large MSE and a great change in magnitude (20% to 50%). CFSR also exhibits slight deviations in southern Andes with a MSE from 20% to 30% (Fig. 2a). This suggests that rainfall representation may have more uncertainty in JRA-55 than CFSR. Consistently, the bias analysis illustrates the difficulty of JRA-55 and CFSR to make accurate estimates of rainfall in the Andes. Both show a rainfall overestimation around 5 to 10 mm/day (e.g. CFSR with a multiplied factor of 50000) while rainfall bias in ERA-Interim are rather small underestimating in 1mm/day suggesting its reliability (Fig. 2b). In addition, climatology is described by a monthly climatic mean and exhibits spatial (west to east zonal gradient) and temporal (peaking in February and March) variability of the rainfall annual cycle. Being it fairly well reproduced by the three-reanalysis showing their intrinsic overestimations evident in CFSR that exacerbates real value of rainfall (Fig. 3). In CFSR, this overestimation may be due to local circulation created by the topographic model (Eichler and Londoño 2013). These results suggest that ERA-interim precipitation is more realistic than JRA-55 and CFSR because it fits better with the observed rainfall, showing its ability to better represent the slope and range of the Andes Cordillera in the PPB.

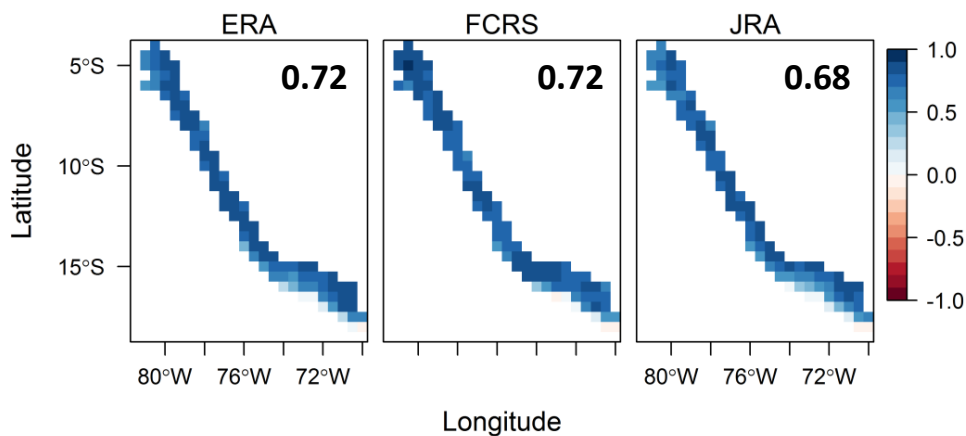


Figure 1: Correlation between the observed and reanalysis (ERA-Interim, CFSR and JRA-55) rainfall. The average value and value for each point grid (scale of values) of the correlation

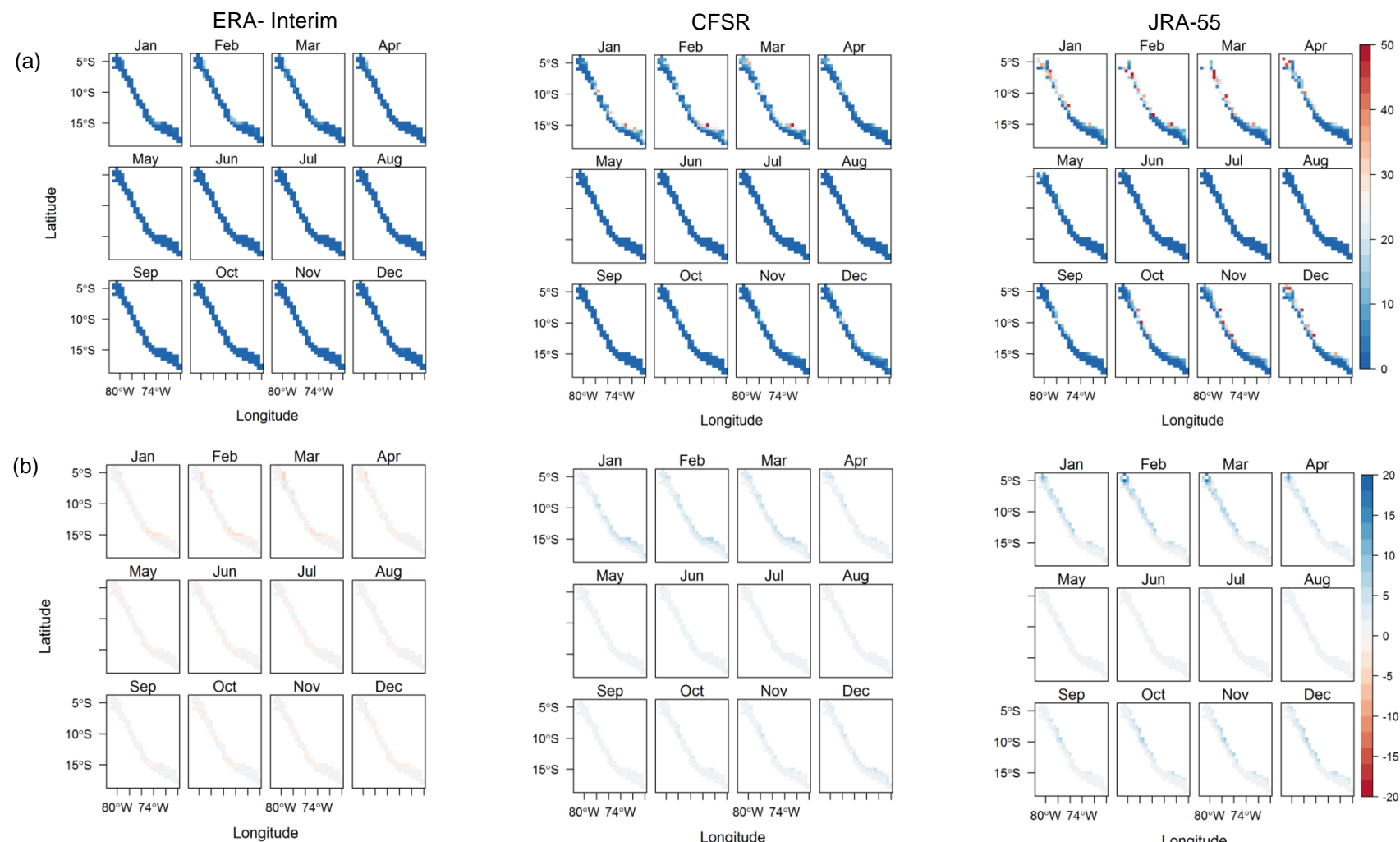


Figure 2: (a) Mean square error (b) of observed and reanalysis (ERA-Interim, CFSR and JRA-55) rainfall anomalies. Period 1979-2009. Bias CFSR *50000

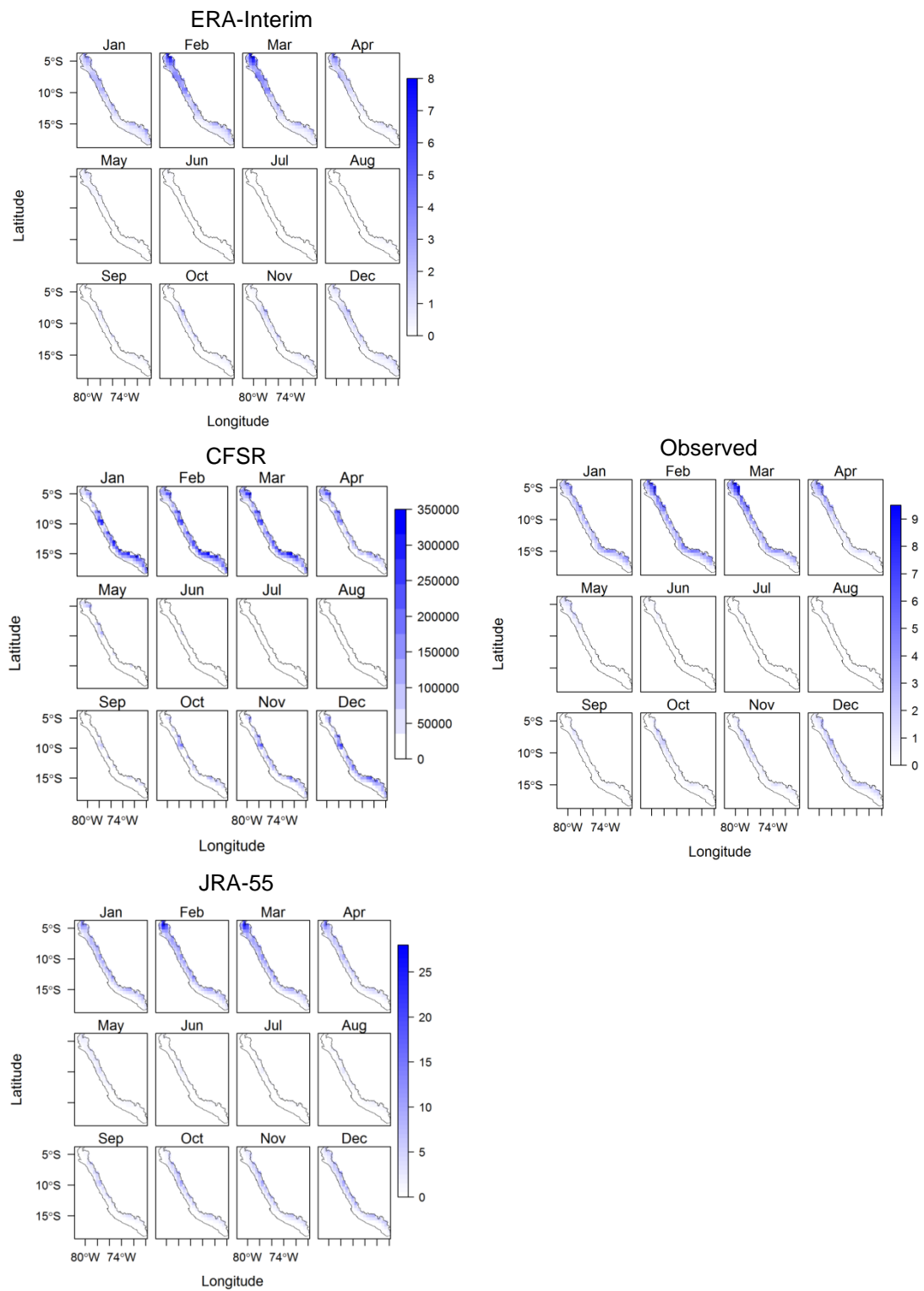


Figure 3: Climatology of observed and reanalysis (ERA-Interim, CFSR and JRA-55) rainfall over the period 1979-2009.

3.2 Major patterns of the rainfall variability – ENSO

In Figure 4, rainfall variability is shown through the estimates of the two rotated EOF modes (see section 2.2.1). The two main modes or rainfall patterns are better reproduced by ERA-Interim than JRA-55 and CFSR. Ep mode (first mode) with distinctive feature such as the meridional (North to South) see-saw and a node at the latitude of $\sim 12^{\circ}\text{S}$ (near to Lima) are well described. The Cp mode (second mode) features a zonal (West to East) see-saw and is also described closely with the observed rainfall but with slight rainfall overestimation in the North-Central coast of the PPB. However, the distinctive signal of strong loading in northern PPB of the Ep mode is captured by the three reanalysis. On the other hand, the Cp pattern characterized with the west-east altitudinal gradient of rainfall, does not show much agreement among the reanalysis such that CFSR (and JRA-55) which underestimates (overestimates) rainfall in northern (southern) PPB. This suggests a limited skill of the reanalysis to reproduce the Cp pattern. Differences in rainfall anomalies can be observed between the three reanalysis and observed rainfall patterns. In ERA-Interim are closer to the observed and its underestimates nearly at 1mm/day, whereas JRA-55 overestimates nearly at 2,5 mm/day. In the same way CFSR overestimates with very far values from the observed value (40000 mm/day). These results indicate that ERA-Interim agrees fairly well with the main characteristic of rainfall patterns in the PPB.

Figure 5 shows the phase space of the modes time series. The three reanalysis can relatively represent the tendency of phase space of the Ep and Cp mode. It is worth noting that by construction the rainfall during extreme El Niño events should be account by the Ep mode. The striking feature in the reanalysis is that only 1997/1998 and 1982/1983 events align along the Ep mode during their developing phase associated with strong rainfall, while other moderate events are projected on the Cp mode associated with weak to moderate rainfall which well agreement with the observed. However, the projection of 1972/1973 and 2015/2016 events are poor represented they seem fall over the Ep mode when is opposite to observed although are associated with weak rainfall. Despite that those differences in projections between the events are well represented (strong projections for 1997/1998 and 1982/1983 events, and moderate projections for 1972/1973 and 2015/2016 events), there is no agreement on the magnitude of rainfall peak respect to the observed (i.e. the 1997/1998 event with a greater magnitude than 1982/1983 when this is opposite in the observed). In general, these reanalysis underestimate rainfall peak during the extremes El Niño events up to 50% (i.e. CFSR in El Niño 1982/1983). The result indicates that the projection of the extreme 1982/1983 and 1997/1998 El Niño events along the Ep mode better agree than the 1972/1973 and 2015/2016 El Niño events.

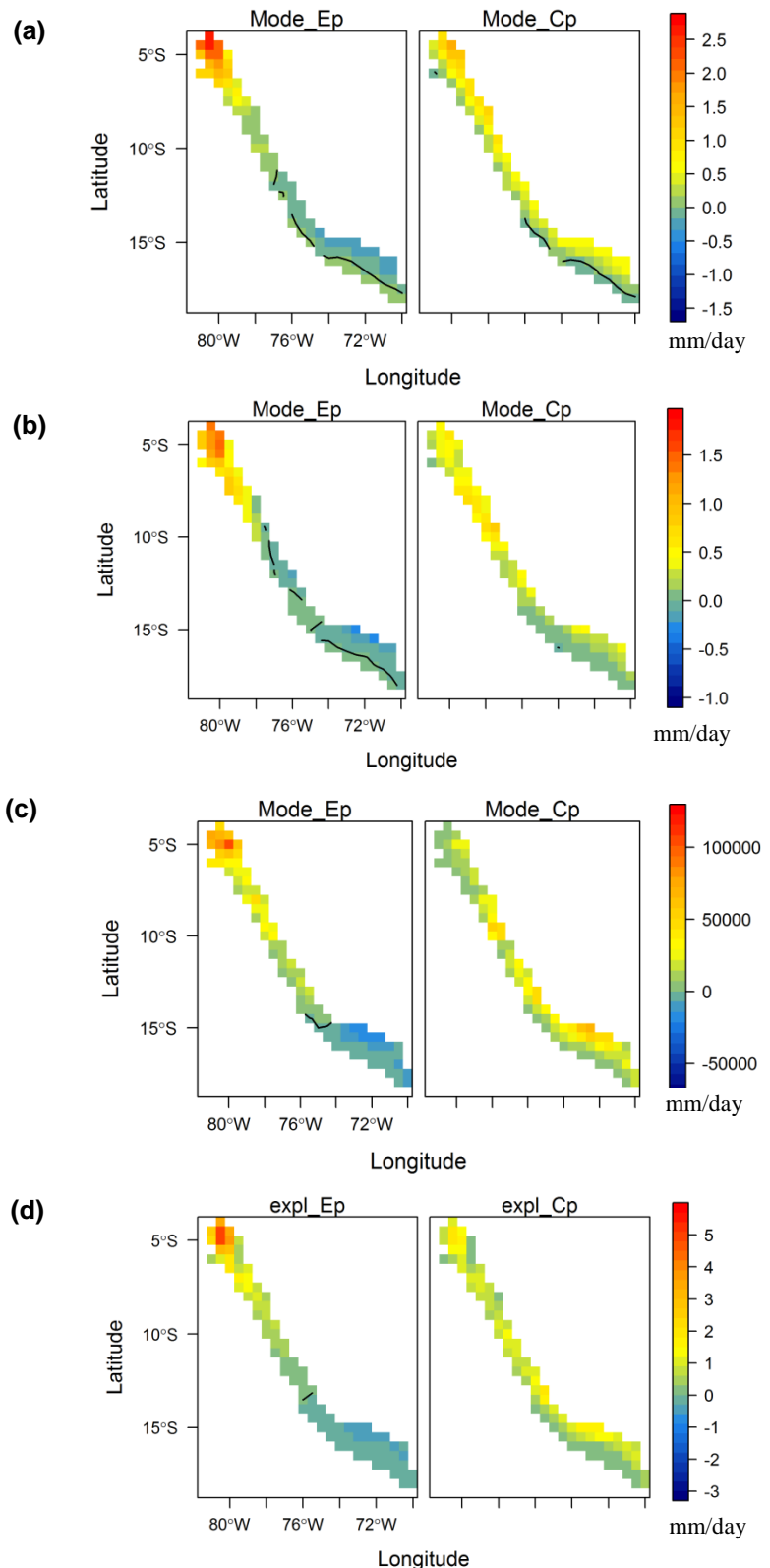


Figure 4: Associated patterns (Ep and Cp) of rainfall anomalies over the period 1979–2009. Ep mode (first mode) (left-hand side) and Cp mode (second mode) (right-hand side). The thick black line indicates the zero contour. (a) Observed (b) ERA-Interim (c) CFSR (d) JRA-55.

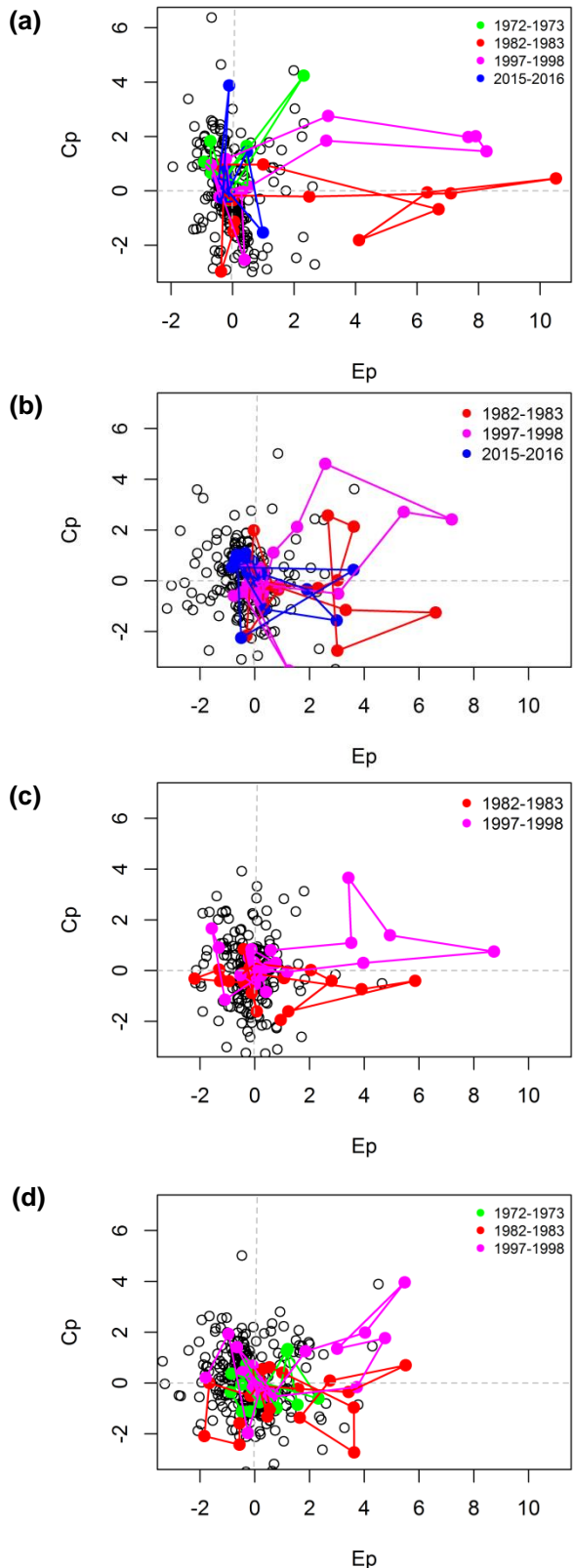


Figure 5: Phase space of the evolution of the Ep and Cp modes. The evolution of the four strong El Niño event is highlighted with lines connecting the dots for the months between January of the first year J(Y0) and December of the second year D(Y1). (Y0: developing El Niño, Y1: decaying El Niño). (a) Observed (b) ERA-Interim (c) CFSR (d) JRA-55

3.3 Differences between strong El Niño events

The differences in the evolution of events projected on the Ep and Cp mode can be visually highlighted in the figure 6 that illustrates the evolution of the Ep and Cp indices during the strong El Niño events from reanalysis and observed rainfall. Clear differences in the evolution of the strong El Niño events are observed. The most striking features revealed are the large difference in the magnitude of Ep mode at the peak of the events of 1997/98 ($Ep \approx 8$ in March) and 1982/1983 ($Ep \approx 6$ in January and $Ep \approx 10$ in April) being associated with a much larger rainfall anomaly, and the extended period of anomalous rainy conditions (lasting until June 1998 and July 1983) which are better reproduced by ERA-Interim than CFSR and JRA-55. The events reach their peak in the corresponding months of the observed. In particular, the three reanalysis reproduce the peak magnitude of the 1997/98 event better than the 1982/1983 event. The first and second peaks of the 1982/1983 event are significantly underestimated by ERA-Interim with $Ep \approx 6$ and 4, CFSR with $Ep \approx 2$ and 6, and JRA-55 with $Ep \approx 4$ and 6, respectively.

On the other hand, there exist notorious differences in terms of the projection on the Cp mode of the 1972/1973 and 2015/2016 El Niño events (i.e. 1972/1973 event exhibits a positive value of the Cp index while the 2015/2016 has a negative value of the Cp index, in January (Y1)). There is a well agreement with ERA-Interim and JRA-55. However, these reanalysis do not well reproduce the evolution of these events that fall within the deviation of the moderate El Niño events due to their projection on the Ep mode. This indicates a rainfall overestimation over the Peruvian Pacific coast. Interestingly, projection on the Cp mode of the 1982/1983 (negative Cp) and 1997/98 (positive Cp) events which are associated with deficiency and excess rainfall in highlands respectively, is fairly well agreement with the three reanalysis. These results indicate that although the reanalysis relatively well agree with the different projections among the strong El Niño events, distinguishing them as different events, there are still deficiencies in reproducing exactly the peak magnitude of extreme events.

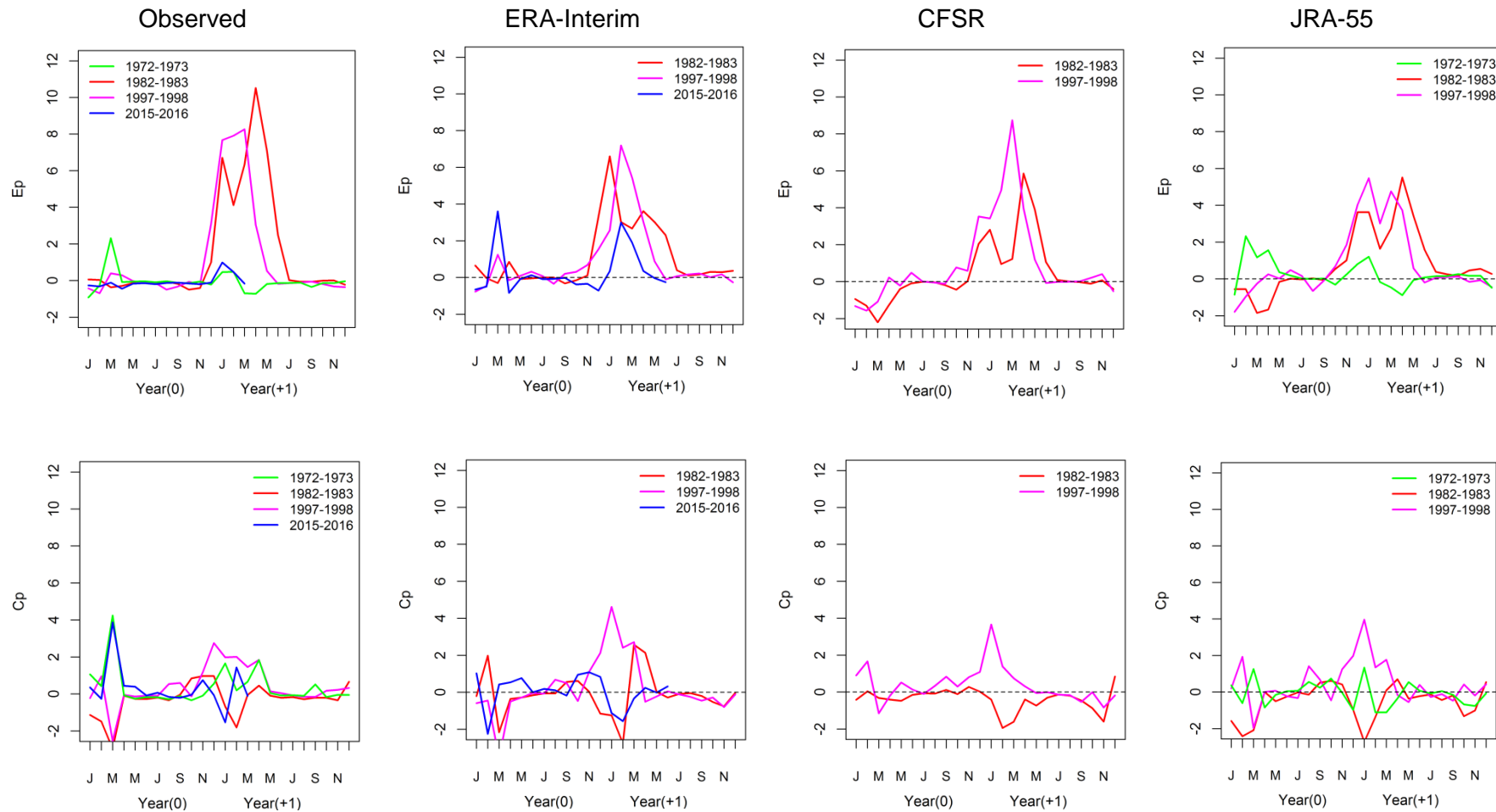


Figure 6: The temporal evolution of the strong El Niño events on the Ep and Cp mode observed in the three reanalysis (ERA-Interim, CFSR and JRA-55). January of the first year J(Y0) and December of the second year D(Y1).

4. Discussion and Conclusion

Reproducing rainfall variability with a focus in the strong El Niño events over the PPB has been evaluated using three reanalysis products (ERA-interim, CFSR and JRA-55) and observed rainfall time series. Patterns of rainfall variability were obtained with the rotated EOF methodology. Results have showed that ERA-interim agree fairly well with observed rainfall, it is based on statistics of high correlation and small RMS and bias than their predecessors CFSR and JRA-55. Interestingly, ERA-interim reproduce well the spatial patterns that characterize the rainfall variability mainly the extreme El Niño events (Ep mode; first mode). Whereas JRA-55 and CFSR still have difficulties to reproduce the moderate El Niño events (Cp mode; second mode) which are associated with west to east zonal gradient of rainfall over the Andes Mountains. This is coherent with other studies over the Andean region, which have shown systematic overestimations during the wet season (Urrutia and Vuille 2009; Eichler and Londoño 2013; Blacutt *et al.*, 2015; Manz *et al.*, 2016). These differences of rainfall overestimation in the Andes, in JRA-55 is attributed to large moistening increment and vorticity problems (Kobayashi *et al.*, 2015) and a lower overestimation in CFSR (Eichler and Londoño 2013), while the best skill in ERA-interim is due to an improved representativity of the topography in the atmospheric model (Dee *et al.*, 2011).

The three reanalysis closely reproduce differences among the strong El Niño events such as the 1982/1983 and 1997/1998 events evolve along the Ep mode associated with heavy rainfall whereas the 1972/1973 and 2015/2016 events seem to evolve most on the Ep mode which is opposite to the observed. As well, the reanalysis relatively well agrees with the different projections among the strong El Niño events, distinguishing them as different events, however still there are deficiencies in reproducing exactly the peak magnitude of extreme events. Lastly, these reanalyses similar to observed assume that these strong El Niño events are the results of both modes due to the projected modes in each event. This suggests that the reanalysis take into account a remote oceanic influence linked to the Ep mode and other regional factors for the CP mode (Sanabria *et al.*, 2018). However, there is still no clear understanding of regional and large-scale atmosphere processes for precipitation, and how their interactions may shape precipitation. These results would help to better understanding rainfall variability differences among the three reanalysis and recommend in a proper way the use of ERA-Interim rainfall datasets for research requirements in the region. Through the robustness of ERA-Interim reanalysis reflected in precipitation we can assume with confidence that large-scale and regional circulation field from atmospheric reanalysis are correctly modeling.

References

- Angélil O, Perkins-Kirkpatrick S, Alexander L V., Stone D, Donat MG, Wehner M, Shiogama H, Ciavarella A, Christidis N. 2016. Comparing regional precipitation and temperature extremes in climate model and reanalysis products. *Weather and Climate Extremes*. Elsevier 13: 35–43. DOI: 10.1016/j.wace.2016.07.001.
- BCRP 2017. Actividad Economica (Febrero, Marzo, Abril). Banco Central de Reserva del Peru (Central Reserve Bank of Peru). *Notas de Estudio* 29: 2-4,36: 2-4 y 45: 2-4.
- Bendix A and Bendix J. 2006. Heavy rainfall episodes in Ecuador during El Niño no events and associated regional atmospheric circulation and SST patterns, *Advances in Geosciences.*, 6, 43–49, doi:10.5194/adgeo-6-43-2006.
- Blacutt LA, Herdies DL, de Gonçalves LGG, Vila DA, Andrade M. 2015. Precipitation comparison for the CFSR, MERRA, TRMM3B42 and Combined Scheme datasets in Bolivia. *Atmospheric Research*. The Authors 163: 117–131. DOI: 10.1016/j.atmosres.2015.02.002.
- Bourrel L, Rau P, Dewitte B, Labat D, Lavado W, Coutaud A, Vera A, Alvarado A, Ordoñez J. 2015. Low-frequency modulation and trend of the relationship between ENSO and precipitation along the northern to centre Peruvian Pacific coast. *Hydrological Processes* 29(6): 1252–1266. DOI: 10.1002/hyp.10247.
- Dee D P, Uppala S M, Simmons A J, Berrisford P, Poli P, Kobayashi S, Andrae U, Balmaseda M A, Balsamo G, Bauer P, Bechtold P, Beljaars A C M, van de Berg L, Bidlot J, Bormann N, Delsol C, Dragani R, Fuentes M, Geer A J, Haimberger L, Healy S B, Hersbach H, Hólm E V, Isaksen L, Kållberg P, Köhler M, Matricardi M, McNally A P, Monge-Sanz B M, Morcrette J J, Park B K, Peubey C, de Rosnay P, Tavolato C, Thépaut J N, Vitart F. 2011. The ERA-Interim reanalysis: Configuration and performance of the data assimilation system. *Q J R Meteorol Soc*, 137: 553–597.
- Drumond A, Marengo J, Ambrizzi T, Nieto R, Moreira L, Gimeno L. 2014. The role of the Amazon Basin moisture in the atmospheric branch of the hydrological cycle: A Lagrangian analysis. *Hydrology and Earth System Sciences* 18(7): 2577–2598. DOI: 10.5194/hess-18-2577-2014.
- Eichler TP, Londoño AC. 2013. South American climatology and impacts of El Niño in NCEP's CFSR data. *Advances in Meteorology* 2013. DOI: 10.1155/2013/492630.
- Harada Y, Kamahori H, Kobayashi C, Endo H, Kobayashi S, Ota Y, Onoda H, Onogi K, Miyaoka K, Takahashi K. 2016. The JRA-55 Reanalysis: Representation of Atmospheric Circulation and Climate Variability. *Journal of the Meteorological Society of Japan. Ser. II* 94(3): 269–302. DOI: 10.2151/jmsj.2016-015
- Knippertz P, Wernli H, Gläser G. 2013. A global climatology of tropical moisture exports. *Journal of Climate* 26(10): 3031–3045. DOI: 10.1175/JCLI-D-12-00401.1.
- Kobayashi S, Ota Y, Harada Y, Ebita A, Moriya M, Onoda H, Onogi K, Kamahori H, Kobayashi C, Endo H, Miyaoka K, Takahashi K. 2015. The JRA-55 Reanalysis: General Specifications and Basic Characteristics. *Journal of the Meteorological Society of Japan. Ser. II* 93(1): 5–48. DOI: 10.2151/jmsj.2015-001.
- Kumar A, Zhang L, Wang W. 2013. Sea Surface Temperature–Precipitation Relationship in Different Reanalyses. *Monthly Weather Review* 141(3): 1118–1123. DOI: 10.1175/MWR-D-12-00214.1.

Kutner MH, Nachtsheim C, Neter J. 2003. Applied Linear Regression Models, 4th edn. McGraw-Hill Higher Education, Irwin: New York, NY, USA.

Lorenz C, Kunstmann H. 2012. The hydrological cycle in three state-of-the-art reanalyses: Intercomparison and performance analysis. *Journal of Hydrometeorology* 13(5): 1397–1420. DOI: 10.1175/JHM-D-11-088.1.

Manz B, Buytaert W, Zulkafli Z, Lavado W, Willems B, Robles LA, Rodríguez-Sánchez J-P. 2016. High-resolution Satellite-Gauge Merged Precipitation Climatologies of the Tropical Andes. *Journal of Geophysical Research: Atmospheres* (JANUARY): n/a-n/a. DOI: 10.1002/2015JD023788.

Mcglone D, Vuille M. 2012. The associations between El Niño–Southern Oscillation and tropical South American climate in a regional climate model. *Journal of Geophysical Research* 117. DOI: 10.1029/2011JD017066.

Murphy A H. 1988. Skill scores based on the mean square error and their relationships to the correlation coefficient. *Monthly Weather Review*, 116: 2417–2424.

Peixoto JP, Oort AH. 1992. Physics of Climate. MIT press: San Diego, CA.

Quadro MFL, Berbery EH, Dias MAFS, Herdies DL, Gonçalves LG. 2013. The atmospheric water cycle over south America as seen in the new generation of global reanalyses. AIP Conf. Proc. 1531:732-735, doi: 10.1063/1.4804874.

Rau P, Bourrel L, Labat D, Melo P, Dewitte B, Frappart F, Lavado W, Felipe O. 2017. Regionalization of rainfall over the Peruvian Pacific slope and coast. *International Journal of Climatology* 37(1): 143–158. DOI: 10.1002/joc.4693.

Saha S, Moorthi S, Pan H L, Wu X, Wang J, Nadiga S, Tripp P, Kistler R, Woollen J, Behringer D, Liu H, Stokes D, Grumbine R, Gayno G, Wang J, Hou Y T, Chuang H Y, Juang H M, Sela J, Iredell M, Treadon R, Kleist D, Van Delst P, Keyser D, Derber J, Ek M, Meng J, Wei H, Yang R, Lord S, Van den Dool H, Kumar A, Wang W, Long C, Chel-liah M, Xue Y, Huang B, Schemm J K, Ebisuzaki W, Lin R, Xie P, Chen M, Zhou S, Higgins W, Zou C Z, Liu Q, Chen Y, Han Y, Cucu- rull L, Reynolds R W, Rutledge G, Goldberg M. 2010. The NCEP climate forecast system reanalysis. *Bull Amer Meteorol Soc*, 91: 1015–1057.

Sanabria J, Bourrel L, Dewitte B, Frappart F, Rau P, Solis O, Labat D. 2018. Rainfall along the coast of Peru during strong El Niño events. *International Journal of Climatology* 38 (4): 1737 – 1747.

Silva VBS, Kousky VE, Higgins RW. 2011. Daily precipitation statistics for South America: an intercomparison between NCEP reanalyses and observations. *Journal of Hydrometeorology*. 12: 101–117. <http://dx.doi.org/10.1175/2010JHM1303.1>.

Solman SA, Sanchez E, Samuelsson P, da Rocha RP, Li L, Marengo J, Pessacq NL, Remedio ARC, Chou SC, Berbery H, Le Treut H, de Castro M, Jacob D. 2013. Evaluation of an ensemble of regional climate model simulations over South America driven by the ERA-Interim reanalysis: Model performance and uncertainties. *Climate Dynamics* 41(5-6): 1139–1157. DOI: 10.1007/s00382-013-1667-2.

Trenberth K E, Stepaniak D P, Hurrell J W, Fiorino M. 2001. Quality of reanalyses in the tropics. *Journal of Climate*, 14: 1499–1510.

Trenberth K E, Fasullo J T, Mackaro J. 2011. Atmospheric moisture transports from ocean to land and global energy flows in reanalyses. *Journal of Climate*, 24: 4907–4924. DOI:

10.1175/2011JCLI4171.1.

Uppala SD, Dee S, Kobayashi P, Berrisford, Simmons A. 2008. Towards a climate data assimilation system: status update of ERA- Interim. ECMWF Newsletter, 115, 12-18 pp. [Available at <http://old.ecmwf.int/publications/newsletters/pdf/115.pdf>].

Urrutia R, Vuille M. 2009. Climate change projections for the tropical Andes using a regional climate model: temperature and precipitation simulations for the end of the 21st century. *Journal of Geophysical Research* 114:D02108. doi:10.1029/2008JD011021.

Vargas P. 2009. El Cambio Climatico y sus Efectos en el Peru. Working Papers, World Bank, Washington, DC.

Wang J, Wang W, Fu X, Seo KH. 2012. Tropical intraseasonal rainfall variability in the CFSR. *Climate Dynamics* 38(11-12): 2191–2207. DOI: 10.1007/s00382-011-1087-0.

This page intentionally left blank

Chapter 4: Large scale and local atmospheric factors that controls the rainfall variability along the Peruvian Pacific slope and coast during strong El Niño events

4.1 STRONG EL NIÑO EVENTS WITH REGARD TO THE TRANSPORT OF MOISTURE AND ATMOSPHERIC FACTORS

In recent years, moisture transport and large-scale Ocean-atmosphere dynamics is better understood. The moisture transport is based in the requirements of water vapor in the atmosphere that reflects the behavior of the general circulation in the hydrological cycle in lower half of the atmosphere and its convergence describe the atmospheric pathway of the hydrological cycle (Peixoto and Oort, 1992). This convergence is an important component of the water balance in the atmospheric branch of the hydrological cycle through the balance by the difference between net surface precipitation (P) and evaporation (E) : the moisture transport forms the connection between evaporation from the Ocean and precipitation over the continents. The variations in moisture sinks ($E < P$) associated with the evaporative sources ($E > P$) reproduce the major patterns of variation of large-scale atmospheric and precipitation systems (Dirmeyer and Brubaker, 2007; Gimeno et al. 2010; Knippertz et al., 2013).

El Niño influences on the sources of moisture in size and position (Castillo et al., 2014; Andreoli et al., 2016). As in the extreme El Niño events is noted an enhanced intertropical convergence zone (ITCZ) connected to the displacements of the Walker Cell system over the Equatorial Pacific Ocean and consequent alterations in the Hadley cell system (Ambrizzi et al., 2005) and accompanied by changes in precipitation patterns. In South America these changes are associated with the displacement of equatorial Pacific rainfall toward the eastern basin linked to ITCZ (Castillo et al., 2014; Cai et al., 2015) and the weakening of the major South American Summer Monsoon (SASM) (Moura and Shukla 1981; Kousky et al., 1984; Grimm et al., 1998; Lau and Zhou et al., 2003; Vera et al., 2005; Krishnamurthy and Vasubandhu, 2010; Liebmann and Mechoso, 2011; Vuille et al., 2012; Boers et al., 2014; Drumond et al., 2014) that lead to significant precipitation reductions on the north, northeast and central Brazil.

The ITCZ is one of the main meteorological structures of planetary scale transporting moisture (Gimeno et al., 2012; Knippertz et al., 2013) from the Ocean to the continent. During El Niño mature phase, the ITCZ migrates southward (Goldberg et al., 1987; Vecchi, 2006; Takahashi and Battisti, 2007; Tedeschi et al., 2013; Schneider et al., 2014) about 5°S (such as in 1983 and 1998) (Schneider et al., 2014) with respect to its normal position between 9°N and 2°N (Schneider et al., 2014), being associated with an increase in the evaporation of the Tropical Pacific that is dragged by the transport of moisture to the continents observing enhanced atmospheric convection and intensification of convergence toward eastern Pacific (Dai and Wigley, 2000, Castillo et al., 2014; Knippertz et al., 2013), and hence huge rainfall increases over Ecuador and North - Centre Peru (Garreaud et al., 2009; Sulca et al., 2017).

On the other hand, the South American Summer Monsoon (SASM) that also controls the climate of tropical South America, is fed, during the austral summer, by moisture influx from the ITCZ, Atlantic and Caribbean which contribute to its development (Zhou and Lau, 2001; Krishnamurthy and Misra; Vuille et al., 2012; Hoyos et al., 2017). During El Niño, the Tropical North Atlantic is strongly influenced with a delayed anomalous warming (Curtis and Hastenrath, 1995; Giannini et al., 2001) leading to decreases in rainfall in the north and northeast Brazil and in the Andes of Colombia. Over the north Amazon basin, the precipitation reduction is the result of a shifted Walker circulation, enhanced subsidence, and reduced convective activity (Liebmann and Marengo, 2001; Ronchail et al., 2002). These moisture influx reductions characterize the weakening of SASM.

The Bolivian High (BH) is due to the latent heat released by the cumulus convection over the Amazonian basin, appears in the austral summer over the Central Andes (200 hPa) (Lenters and Cook, 1997) and is connected to mid-upper level easterly winds which help to the transport of moist air continental, that is crucial for the development of deep convection over the Altiplano (Garreaud et al., 2003; Vuille and Keimig, 2004; Falvey and Garreaud, 2005, Garreaud et al., 2009). During El Niño the reduced latent heating from deficient rainfall over the Amazon Basin may reduce the intensity of the Bolivian High in austral summer and hence the weakening of the SASM (Silva Dias et al., 1983; Bell et al., 1999).

The easterly wind from the tropical Atlantic Ocean to the Amazon basin turn southward, being channeled between the eastern slope of the Andes and the Brazilian Plateau. This flux of orientation northerly exhibits a Low-Level Jet (LLJ) constituting a structure transporting large amounts of moisture that feed summertime convective storms over the subtropical plains as far south as 35°S (Saulo et al., 2000; Marengo et al., 2004; Cheng et al., 2013). The LLJ is important in regulating rainfall variability over subtropical South America, via moisture transport from the Amazon. During El Niño, the LLJ associated with the anomalous low-level anticyclone

south of the Amazon and the pressure gradient set up by the steep topography of the Andes can reinforce the LLJ (e.g. during El Niño 1997/1998, Lau and Zhou, 2003; Marengo *et al.*, 2004).

The South Hemisphere transient frontal system and mean low-level convergence lead to the formation of a diagonal band of convection and precipitation maxima, known the South Atlantic Convergence Zone (SACZ; Kodoma, 1992; Liebmann *et al.*, 1999; Carvalho *et al.*, 2004). The LLJ feeds the South Atlantic Convergence Zone (SACZ), extending from the southeastern Amazon basin toward the southeast out over the South Atlantic. The SACZ is more intense during summer when it is connected with the area of convection over the central part of the continent, producing episodes of intense rainfall over much of southeastern South America (Liebmann *et al.*, 1999). This convection band (SACZ) is a distinctive feature of the SAMS (Kodama, 1992). During El Niño, the SACZ moves southward of its climatological position (Robertson and Mechoso, 2000; Zhou and Lau, 2001; Carvalho *et al.*, 2004) and there is small impact on region that dominates with significant enhancement of convection around January and weakening in February (Grimm, 2003). The anticyclone over the southeastern Atlantic is likely to be affected by fluctuations of the Pacific–South America tele-connection linking the South Pacific and the South Atlantic by the upper-level jet stream in association with the displacement of the SACZ (Lau and Zhou, 2003). Also, the enhanced frontal activity in the SACZ could be associated with eastward shift of the South Pacific convergence zone which may be responsible of cool, dry, convectively unfavorable conditions in the central Andes (Cook, 2009).

The moisture transport follows the eastward shift of warm equatorial SST of two regimes El Niño (see Fig 4.1) which are associated with convection (see Fig 4.2) and moisture advected from Central Pacific Ocean (Paixao Veiga *et al.*, 2005 ; Boers *et al.*, 2014 ; Xu *et al.*, 2015) and distinct atmospheric circulation patterns leading to different rainfall anomaly patterns (Gu *et al.*, 2016).

Different are the responses of Atmospheric circulation anomalies (i.e. position and longitudinal extension of the Walker circulation) to these two regimes (Kug *et al.*, 2009; Zhelezova and Gushchina, 2015; Andreoli *et al.*, 2016) (see Fig.4.1 and 4.2). In the EP (CP) Niño linked with southward displacement (a dominate position in the central-eastern Pacific) of the Pacific ITCZ (InterTropical Convergence Zone) connected to ascent motion over the Pacific and subsidence over tropical South America (east of 60 °W) being these stronger in EP than CP El Niño (Tedeschi *et al.*, 2013; Andreoli *et al.*, 2016; Sulca *et al.*, 2017).

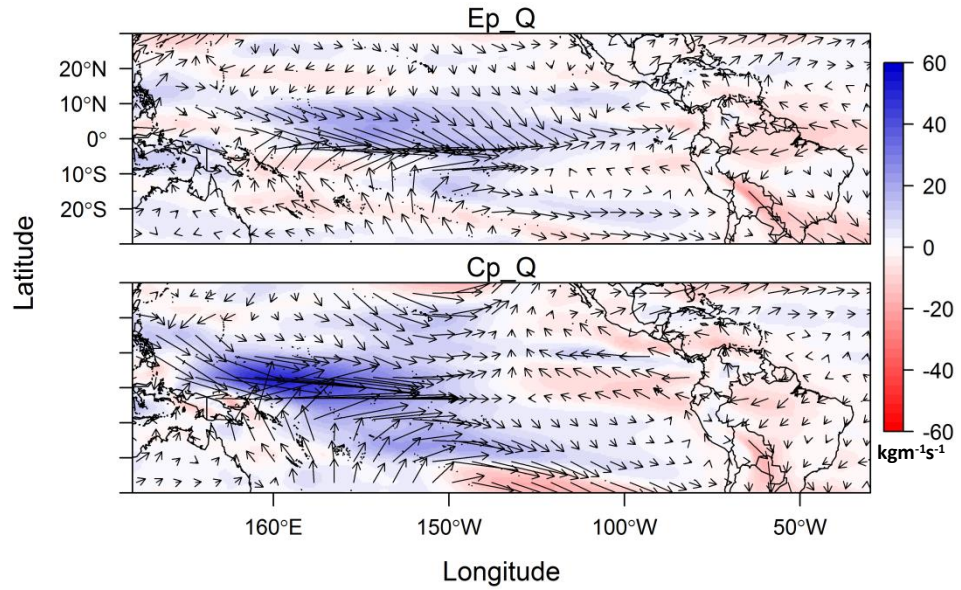


Fig 4.1. Moisture transport (Q) patterns associated with Eastern (EP) and Central (CP) Pacific El Niño. Patterns obtained from EOF regression 1964–2016. Q obtained from ERA-Interim reanalysis of the period 1979–2016. Source: Own elaboration.

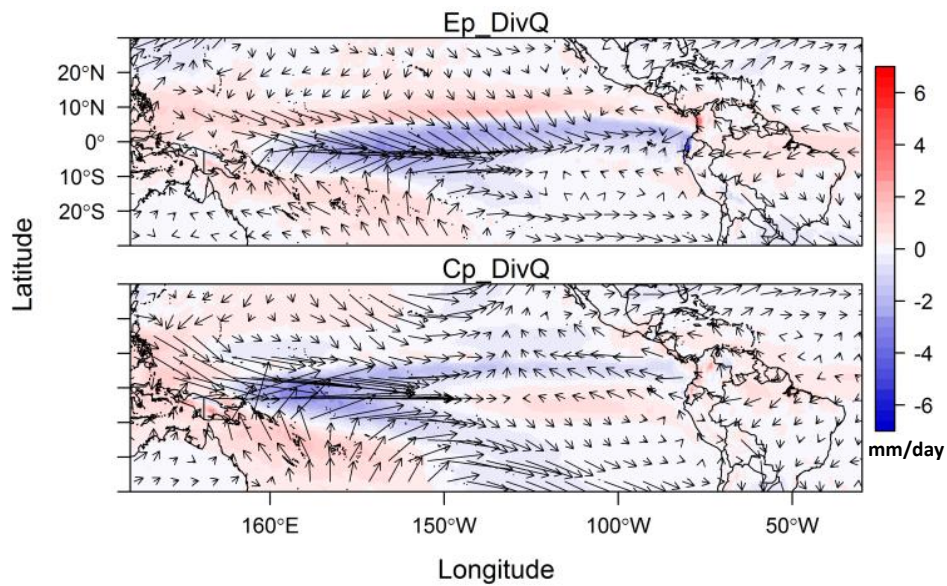


Fig 4.2. Moisture convergence ($-\nabla \cdot Q$) patterns associated with Eastern (EP) and Central (CP) Pacific El Niño. Patterns obtained from EOF regression. $-\nabla \cdot Q$ obtained from ERA-Interim reanalysis of the period 1979–2016. Source: Own elaboration.

4.2 MOISTURE TRANSPORT AND ITS CONVERGENCE

The connection between occurrence and activity of moisture transport and large-scale Ocean-atmosphere dynamics is better understood in recent years. The transport of moisture from oceanic sources to the continents forms the connection between evaporation from the Ocean and precipitation over the continents (Gimeno *et al.*, 2014) (see Fig. 4.3).

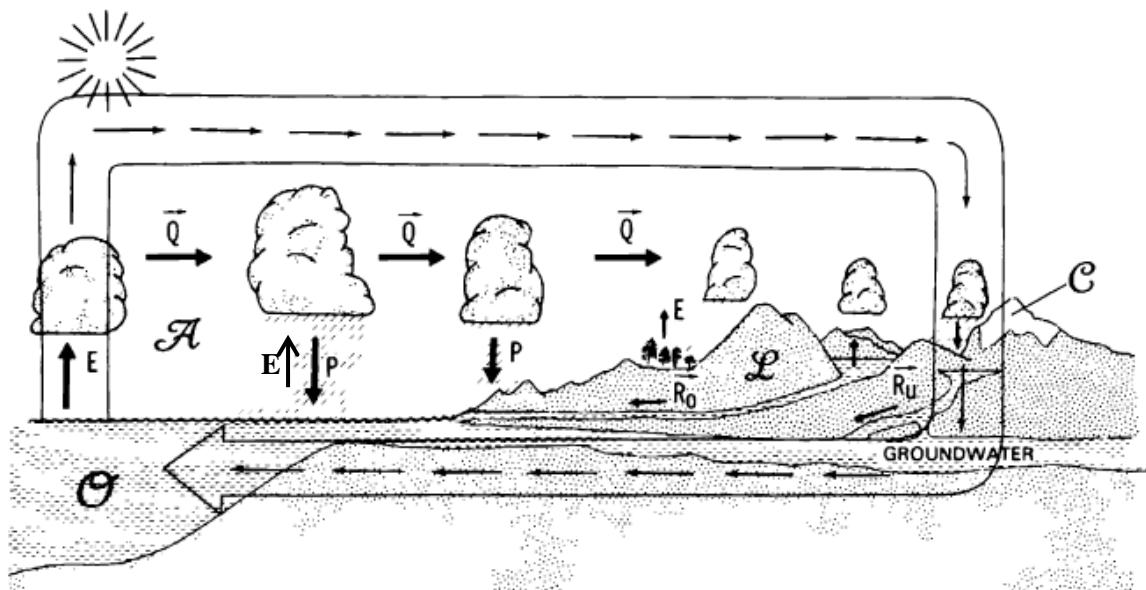


Figure 4.3. Schematic diagram of the atmospheric and terrestrial branches of the hydrological cycle: the importance of evaporation E , transport of water vapor in the atmosphere Q , precipitation P , river runoff R_o and underground runoff R_u . (Peixoto and Oort, 1992).

The moisture transport reflects the behavior of the general circulation in the hydrological cycle in lower half of the atmosphere (Peixoto and Oort, 1992) and its convergence describe the atmospheric pathway of the hydrological cycle through the balance by the difference between net surface precipitation (P) and evaporation (E). In particular, there is an association of extreme precipitation and moisture transport (Lin *et al.*, 2013; Lavers and Villarini, 2014; Swales *et al.*, 2016; Lavers *et al.*, 2016) suggesting that moisture transport can be used to provide an indication and deeper insight into extreme precipitation events, due to the higher predictability of moisture transport relative to precipitation and strong relationship between them.

However, the convergence of moisture transport ($-\nabla \cdot Q$) seems to be a better indicator for the precipitation because it has more direct effects on available moisture in an area than moisture transport (Q), which only measures the moisture passing through an area (Wei *et al.*, 2016).

Because of its close relationship with precipitation, $-\nabla \cdot \mathbf{Q}$ has been used for precipitation parameterization and forecasting (Banacos and Schultz 2005)., $-\nabla \cdot \mathbf{Q}$ has also stronger tie to the underlying atmospheric dynamic and less dependence on model parameterized processes (Castro *et al.*, 2001; 2007).

The moisture transport (or tropical moisture export denominated by Knippertz and Wernli, 2010) and its convergence ($-\nabla \cdot \mathbf{Q}$) aids to explain the origin of continental precipitation and its influence on local precipitation. Besides it helps to understand the role of moisture transport from its sources and large-scale and regional circulation on precipitation.

4.2.1 Approaches of the moisture transport and its convergence

One main approach used to detect moisture transport is the vertically integrated horizontal water vapor transport (\mathbf{Q}) between the earth's surface (1000 hPa) and the top of the atmosphere from atmospheric reanalysis. A further technique relates to the identification of hydrological extremes, such as extreme precipitation or floods, and then assessing the atmospheric state (e.g., \mathbf{Q} , specific humidity, and wind fields) to determine whether a moisture transport caused the extremes (e.g., Ralph *et al.*, 2006; Lavers *et al.*, 2011; Neimanetal., 2011).

To investigate the impact of moisture transport, we used the metric of the convergence ($-\nabla \cdot \mathbf{Q}$) of vertically integrated moisture transport (\mathbf{Q}). The $-\nabla \cdot \mathbf{Q}$ is an important component of the atmospheric water balance equation

$$\frac{\partial w}{\partial t} = E - P - \nabla \cdot \mathbf{Q} \quad \dots \dots \dots \quad (3)$$

Where w is the amount of water vapor in the atmospheric column which extends from the earth's surface to the top of the atmosphere. As the long- term mean of atmospheric moisture change is small ($\partial w / \partial t \approx 0$) (Sohn *et al.*, 2004; Trenberth *et al.*, 2011). While t is time, E is evaporation/evapotranspiration and P is precipitation.

\mathbf{Q} is integration of advection of water vapor in the atmosphere (w) (or integration of the horizontal transport of water vapor) with respect to pressure (p). \mathbf{Q} is measured by the vertically integrated water vapor transport which is a function of winds (u, v) and specific humidity (q). It is given (Peixoto and Oort, 1992) by the expression:

$$Qu = \frac{1}{g} \int_{1000}^1 qu dp \quad \dots \quad (4)$$

$$Qv = \frac{1}{g} \int_{1000}^1 qv dp \quad \dots \quad (5)$$

Qu and Qv are the zonal and meridional components of \mathbf{Q} :

$$Q = Qui + Qvj \quad \dots \quad (6)$$

$-\nabla \cdot \mathbf{Q}$ is Q convergence calculated as

$$-\nabla \cdot \mathbf{Q} = -\frac{1}{g} \nabla \cdot \int_{1000}^1 qv dp \quad \dots \quad (7)$$

where g is the gravitational acceleration (9.8ms^{-2}), p is pressure (hPa), q is specific humidity (KgKg^{-1}), v is wind vector (ms^{-1}).

Increases in specific humidity (q) and horizontal transport of moisture (\mathbf{Q}) are associated with heaviest daily rainfall events (Allan *et al.*, 2016). Locations where specific humidity anomalies are significant generally coincide with the regions of strong moisture transport (Dacre *et al.*, 2014). The specific humidity is particularly high in warm conditions, explained by the potential for higher water vapor content due to higher saturation vapor pressure (Seager *et al.*, 2010; Zvereva *et al.*, 2008). The rainfall amount (equation 7) is proportional to the vertically integrated product of specific humidity and horizontal mass convergence through the depth of the atmosphere (Banacos and Shultz, 2005).

$-\nabla \cdot \mathbf{Q}$ has more direct effects on available moisture in an area than moisture fluxes \mathbf{Q} which only measures the moisture passing through an area. Because of its close relationship with precipitation, $-\nabla \cdot \mathbf{Q}$ has been used for precipitation parameterization and forecasting (Banacos and Schultz 2005). In general, $-\nabla \cdot \mathbf{Q}$ is balanced by the difference between $P - E$ ($-\nabla \cdot \mathbf{Q} \approx P - E$) over a relatively long period since the temporal tendency of total precipitable water is small ($\partial w / \partial t \approx 0$).

4.3 RAINFALL AND MOISTURE PATTERNS ASSOCIATED WITH STRONG EL NIÑO EVENTS IN THE EASTERN PACIFIC REGION

We assess the moisture transport associated with extreme rainfalls during the El strong Niño events using ERA-Interim due to its better performance for reproducing rainfall variability in the PPB in terms of the spatial pattern (Ep and Cp Mode) and evolution in relation to the other two tested reanalysis. ERA-Interim precipitation is a model generated variable (Dee *et al.*, 2011), therefore, a coherent field representation of moisture flux is expected from the model. This assessment that attains the third specific objective of the thesis is developed in the following paper: *"Rainfall and moisture patterns associated with strong El Niño events in the eastern Pacific region"* to be submitted to Geophysical Research Letters.

RESEARCH WORK (RESEARCH ARTICLE)

Rainfall and moisture patterns associated with strong El Niño events in the eastern Pacific region (manuscript to be submitted to Geophysical Research Letters)

Preamble

This study evaluates whether moisture transport and other atmospheric forcing associated to El Niño can have a preferential response that may be responsible for extremes rainfall variability in the Eastern Pacific basin (EPB) (it includes the PPB). We evaluate how moisture transport (Q) (and its convergence, $-\nabla \cdot Q$) associated with large-scale and regional atmospheric circulation can explain the different patterns of rainfall over the Eastern Pacific basin (EPB) during the last three extreme El Niño events: 1983, 1998 and, 2016 with focus in Ecuador and northern Peru. This study uses 37 years (1979-2016) of monthly data from the ERA-interim reanalysis.

Our results indicate that although these three events recorded as strong in the Niño 3.4 region, presented similar large-scale circulation drivers (Niño 3.4) but they induced different rainfall patterns at a regional scale in the EPB. Fundamentally is the interplay of large-scale (moisture source contributors) and regional (modulate moisture influx in EPB) atmospheric factors. It should be noted large-scale atmospheric differences; thus, El Niño 2016 presents an atmospheric response opposite to the 1983 and 1998 events that are similar experiencing an out-of-phase convergence ($-\nabla \cdot Q$) associated with dominant subsidence in EPB and moisture transport from the Amazon. As well, the influence of upper level (100 to 300 hPa) meridional regional circulation on the amount entering of $-\nabla \cdot Q$ in the EPB, the role of topography stopping $-\nabla \cdot Q$, and the 600 to 400 hPa moisture transport on highlands which share the different rainfall patterns during the strong El Niño events are addressed in this paper. This study illustrates link of upper level regional mechanisms on the large-scale moisture transport in determining different rainfall patterns during these El Niño events.

Rainfall and moisture patterns associated with strong El Niño events in the eastern Pacific region

Janeet Sanabria^{1,2}, Luc Bourrel¹, Carlos M. Carrillo³, David Labat¹

¹*UMR 5563 GET, Université de Toulouse - CNRS - IRD - OMP - CNES, Toulouse, France.*

²*SENAMEHI, Jirón Cahuide 785, Lima 11, Peru.*

³*Earth and Atmospheric Sciences, Cornell University*

*Correspondence to: J. Sanabria, UMR 5563 GET, Université de Toulouse -CNRS-IRD -OMP-CNES,Toulouse 31400, France. E-mail: janeet.sanabria@get.omp.eu

Rainfall and moisture patterns associated with strong El Niño events in the eastern Pacific region

ABSTRACT

We studied how vertically integrated water vapor transport (Q) (and its convergence, $-\nabla \cdot Q$) associated with large-scale and regional atmospheric circulation can explain the different patterns of rainfall over the Eastern Pacific basin (EPB) during the last three strong El Niño events: 1983, 1998 and 2016 with focus in Ecuador and northern Peru. This study uses 37 years (1979-2016) of monthly data from the ERA-Interim reanalysis. Although these three events recorded as strong in the Niño 3.4 region, singularly El Niño 2016 presents an atmospheric response opposite to the first two events that are similar experiencing an out-of-phase $-\nabla \cdot Q$ pattern regarding those two events. El Niño 2016 also exhibits moisture transport from the Amazon opposite to the Amazonian subsidence that dominates in 1983 and 1998. However, in 1998 a weakened subsidence allows moisture transport from 600 to 400 hPa towards highlands. While the topography stops the $-\nabla \cdot Q$ concomitantly the amount entering the EPB is influenced by regional atmospheric circulation of upper level southerly or northerly winds (100 to 300 hPa) that can induce strengthening (or weakening) of subsidence allowing lower (greater) income from $-\nabla \cdot Q$ characterizing different enhanced $-\nabla \cdot Q$ transported by the EPB which are reflected in the different rainfall patterns. This enhanced transport in El Niño 1983, 1998 and 2016 reached about 10°S, 14°S and 6°S, founding the extremes and weak rainfalls anomalous, respectively in the North-Centre EPB. This study illustrates link of upper level regional mechanisms on the large-scale moisture transport in determining different rainfall patterns during these El Niño events.

1. Introduction

The three El Niño events (1983, 1998, and 2016) presented a global scale pattern that was observed in sea surface temperature (SST) anomalies in central Pacific Ocean. It drives typical temporal and spatial patterns of extreme rainfall in the eastern Pacific basin (EPB) along the vicinity of northern Peru and Ecuador. Extreme rainfall in the EPB is also associated with SST anomalies in El Niño 1+2 region. In the highlands along the Andes, the variability of rainfall (dryer and wet conditions) does not seem to be related to remote El Niño (Niño 3.4) only, and it might have influenced by other forcing (Sanabria *et al.*, 2018) such as moisture from the Amazon basin. Dry conditions in the Amazon basin is a common pattern during El Niño, however, highlands precipitation during El Niño might be influenced by water

vapor transport from the Amazon (Eichler *et al.*, 2013). Evidence of this source of moisture from the Amazon is known, but it has been little explored (Garreaud, 2009), so this study explore whether this transport can occur at a continental scale. During El Niño 1983 and 1998 (after here 1983-1998), the EPB exhibited positive precipitation anomalies over the Ocean with negative Sea Level Pressure (SLP) anomalies and northerly winds, consistent with the southward migration of the Intertropical Convergence Zone (ITCZ) (Goldberg *et al.*, 1987; Vecchi, 2006; Takahashi & Battisti, 2007; Tedeshi *et al.*, 2013; Schneider *et al.*, 2014). However, this atmospheric configuration was not the case during El Niño 2016, which showed opposed conditions, negative precipitation anomalies with high SLP (L'Heureux *et al.*, 2017; Levine & McPhaden; Paek *et al.*, 2017; Hu & Fedorov, 2017), and the ITCZ located northward of its El Niño climatology position. The different patterns of configuration during these recent El Niño events motivate to question what is the role of the regional atmospheric in the diverse response of rainfall under similar strong El Niño events? Or more fundamental, can the EPB have different responses with similar global El Niño as defined by SST.

During El Niño mature phase, extreme rainfall in EPB is associated with enhanced atmospheric convection due to the transport of moisture, and intensification of convergence toward eastern Pacific (Castillo *et al.*, 2014; Knippertz *et al.*, 2013). Transport of atmospheric moisture responds to the ENSO variability, which follows the eastward shift of warm equatorial sea surface temperature. This warm SST transport is connected with convection and moisture advected from Central Pacific Ocean (Paixao Veiga *et al.*, 2005 ; Boers *et al.*, 2014 ; Xu *et al.*, 2015), which is moduled by fast atmospheric Kelvin Waves (Yang & Hoskins, 2013). El Niño can be characterized in two regimes: East Pacific (EP) and Central Pacific (CP) ENSO (Kao & Yu, 2009;

Takahashi *et al.*, 2011; Capotondi *et al.*, 2015), as characterized by peaks of SST anomalies in East and Central Pacific. These ENSO-type patterns are also responsible for distinct pathways of moisture anomalies consistently being followed by different precipitation patterns (Gu & Adler, 2016). In Ecuador and northern Peru, transport of water vapor and local topography of the Andes lead rainfall production feed from Ocean toward continent (Gimeno *et al.*, 2016; Pineda *et al.*, 2013). Pineda *et al.*, 2013 and Gimeno *et al.*, 2016 suggest that water vapor and local topography of the Andes leads formation of heavy rainfall events in the coastal region. Westerly low-level moisture flux intersects the coastal area leading to orographic convection (Takahashi *et al.*, 2004).

How preferential moisture transport contributes to different patterns of rainfall over the EPB during strong El Niño conditions (1983, 1998 and 2016) is the focus of the present study. We

investigate whether pattern of rainfall, in the EPB, associated to El Niño can have different responses (i.e. opposite anomaly phases), and if these differences are based on local variability (e.g. Niño 1+2). Including how changes of the regional and large-scale atmospheric circulation impact these rainfall patterns. We hypothesize that rainfall in EPB can experience out-of-phase patterns in similar El Niño events as measured by the large-scale (El Niño 3.4), however, these patterns still must to agree with water balance in the tropical South America. Thus, we test this hypothesis by analyzing variations related to moisture transport following the changes in rainfall and atmospheric circulation. Our approach consider that observed rainfall and atmospheric water balance (convergence of vertically integrated moisture flux) are comparable (Paixao Veiga *et al.*, 2005).

2. Data and methodology

2.1 Precipitation

The study is based on monthly data that cover the period 1979-2016 and a spatial resolution of 0.5x0.5°). Observed raingage data were obtained from 145 meteorological stations (Peruvian National Service of Meteorology and Hydrology, SENAMHI) which were gridded for the same period and resolution using Cressman technique (Cressman, 1959; Doty, 1995). The quality control was performed early by Bourrel *et al.*, (2015) and Rau *et al.*, (2017) using the regional vector method (taking into consideration elevation, watershed boundaries and latitude). As well, precipitation data from the Climate Prediction Center (CPC) Merged Analysis of Precipitation (CMAP) (Xie and Arkin 1997) is used in this study. The anomalies were computed relative to a mean climatology cycle based on 37 years period 1979-2016.

2.2 Reanalysis

The European Centre for Medium-Range Weather Forecasts (ECMWF) interim Reanalysis (ERA-Interim) (Simmons *et al.* 2007; Dee *et al.*, 2011) is used to estimate moisture transport and verify atmospheric circulation changes during the strong El Niño events. ERA-Interim covers the period from 1979 to the present and has 37 divided pressure levels from 1000 to 1 hPa and a horizontal resolution 0.5°x0.5° (.50 km), its data is available from the website <http://apps.ecmwf.int/datasets/data/interim-full-modis/levtype=sfc/>. Detailed information is described on the website <https://www.ecmwf.int/en/research/climate-reanalysis/era-interim>. The performance of ERA-Interim over South America has been

analyzed by Lorenz & Kunstmann, 2012 and Solman *et al.*, 2013 who showed a low uncertainty in precipitation, and also by Knippertz *et al.*, 2012; Drumond *et al.*, 2014 who showed a reliable representation of the moisture source over the tropical zonal. The appropriate reproduction of the hydrological cycle by ERA-Interim supposes an increase in forecast quality compared to previous ERA reanalysis (Trenberth *et al.*, 2011).

2.3 Moisture transport

To investigate the impact atmospheric moisture transport on the rainfall, it was used the metric of the vertically integrated water vapor transport (Q) and its Q convergence ($-\nabla \cdot Q$) derived from ECMWF- ERA-Interim reanalysis. Zonal (u) and meridional (v) Q are available online as an integral over the atmospheric column (from the surface to 1 hPa). Q is a function of winds (u, v) and specific humidity (q) on 37 levels of mandatory pressure, defined as:

$$Qu = \frac{1}{g} \int_{1000}^1 qu dp \quad (1)$$

$$Qv = \frac{1}{g} \int_{1000}^1 qv dp \quad (2)$$

$$Q = Qui + Qvj \quad (3)$$

The Q convergence ($-\nabla \cdot Q$) is an important component of the atmospheric water balance equation $\frac{\partial w}{\partial t} + \nabla \cdot Q = E - P$ that describes the atmospheric pathway of the hydrological cycle expressed as the Q convergence ($-\nabla \cdot Q$) (or total columnar moisture convergence) which is the balance by the difference between net surface precipitation (P) and evaporation (E) and, in the opposite sense expressed as the total columnar moisture divergence ($\nabla \cdot Q$) where the E exceeds P . And w is the precipitable water (total column water vapor) that over a relatively long period since the temporal tendency are often assumed to be negligible (e.g., Sohn *et al.*, 2004; Trenberth *et al.*, 2011).

2.4 EOF regression of Q , $-\nabla \cdot Q$ and $\nabla \cdot Q$

The dominant moisture pathways that lead to rainfall over the EPB were analyzed using the orthogonal functions (EOF) regression technique. This technique consists in building a regression model using only a few most informative principal components (PCs) as their predictors, in order to find the direct correlation between the predictand and the

linearly independent PCs of the predictor fields. In our study the EOF regression denote as predictand to the Q and $-\nabla \cdot Q$ anomalies, and, for both, as predictors to the E and C indices and the predictor coefficients are the PCs. These indices depict the variability of EP and CP El Niño, respectively which were defined by Takahashi *et al.* (2011). This technique separates the moisture pathway associated with the two types of ENSO.

2.5 Composite analysis

The nonlinearity of strong El Niño events (1983, 1998 and 2016) on rainfall in the EPB is viewed in the composite of rainfall, Q convergence ($-\nabla \cdot Q$) and the vertical structure of q , vertical motion (ω) and winds. The Q convergence variability allows to examine the changes in atmospheric pathway of the hydrological cycle. The Q (vector) reflects the behavior of the general circulation in the hydrological cycle in lower half of the atmosphere (Peixoto and Oort, 1992). The vertical structures identify the atmospheric water input associated with anomalous global and regional scale circulation (convection, subsidence and low and high level circulation). This vertical structure was constructed for the north region (2°S and 7.5°S and 120°W and 30°W) and for south region (12°S and 17°S and 120°W and 30°W). The analysis was from the seasonal anomaly composites (JFMA rainy period). The comparison of observed and estimated ($-\nabla \cdot Q$) precipitation is helpful for the reliability of moisture transport variability.

3. Results

3.1 EOF modes of Q (vector), Q convergence ($-\nabla \cdot Q$) and rainfall variability

Based in EOF regression analysis (see section 2.4), Q , Q convergence ($-\nabla \cdot Q$), and rainfall variability associated with CP and EP ENSO types are described in phase space plots (Figs. 1a and 1b) and spatial mode patterns (Figs. 1c and 1d). In Figures 1a and 1b, the striking feature of El Niño 1983 and 1998 are projected onto the EP pattern ($CP \approx 0$) with significant positive values, while all other events included El Niño 2016 EP values are low or close to zero ($Cp \approx [-2.2]$). The $-\nabla \cdot Q$ follows similar behavior but with negative values due to a change in the sign of $\nabla \cdot Q$. In Figures 1c and 1d, the EOF mode patterns respond differently to the SST anomalies peak in the EP and CP. The EP and CP rainfall patterns match the trajectories of Q and $-\nabla \cdot Q$. The EP ENSO pattern expands over a broader range in the Eastern Pacific Ocean until reaching Ecuador and northern Peru, with predominant northwesterly Q anomalies flux (Fig. 1c) and significant positive rainfall anomalies consistent

with other studies (Castillo et al., 2014; Xu et al., 2015; Andreoli et al., 2016;). In the CP ENSO pattern, precipitation is confined to west Pacific extending towards the EPB north (around 5° N) associated with a weak $-\nabla \cdot Q$ and dominated by southeasterly Q anomaly fluxes (Fig. 1d). For both CP and EP patterns, the Amazonian region prevails dry (negative precipitation anomalies) the signal is stronger for EP. These results indicate that comparable moisture transport patterns come from Central Pacific Ocean that reaches the EPB, however, they present different magnitude and shifting location, which impact reflect onto rainfall along the EPB.

3.2 Observed rainfall, Q , and $-\nabla \cdot Q$ during strong El Niño events.

Figure 2 (panel a and b) shows that moisture convergence ($-\nabla \cdot Q$) and rainfall anomalies patterns are coherent, which represent that moisture transport leads to rainfall in the EPB during El Niño 1983, 1998 and 2016. In the first two El Niño events, the comparable belt of strong Q convergence ($-\nabla \cdot Q$) that reaches Ecuador and northern Peru (around 4°S) are channeled along the EPB and dissipates over the Andes. In the Amazon basin, along 4°S a dry divergent flow is predominant in both El Niño (1983 and 1998). Beside the orographic barrier of the Andes, the subsidence in Amazon is a dominant feature. On contrary, in the 2016 event the belt of $-\nabla \cdot Q$ (a weak case but significant) move far north (around 4°N and dry along 4°S) and is confined by the Andes until northern Peru (around 4°S; Figs. 2b and S1). A similar structure of convection along the Andes is observed in the three cases with a significant difference in the third case. The analysis suggests that local effect are dominant in this band along the Andes Mountains that migrates North-South modulated by the enhanced moisture transport ($-\nabla \cdot Q$) at the large-scale circulation. It was suggested that the local warming of the SST in the Niño 1+2 drive the diurnal cycle as land-sea breeze secondary circulation (Horel and Cornejo, 1986; Goldberg et al., 1987; Bendix, 2000) of westerly flow that facilitates orographic lifting and triggers convection (Takahashi, 2004; Douglas et al., 2009).

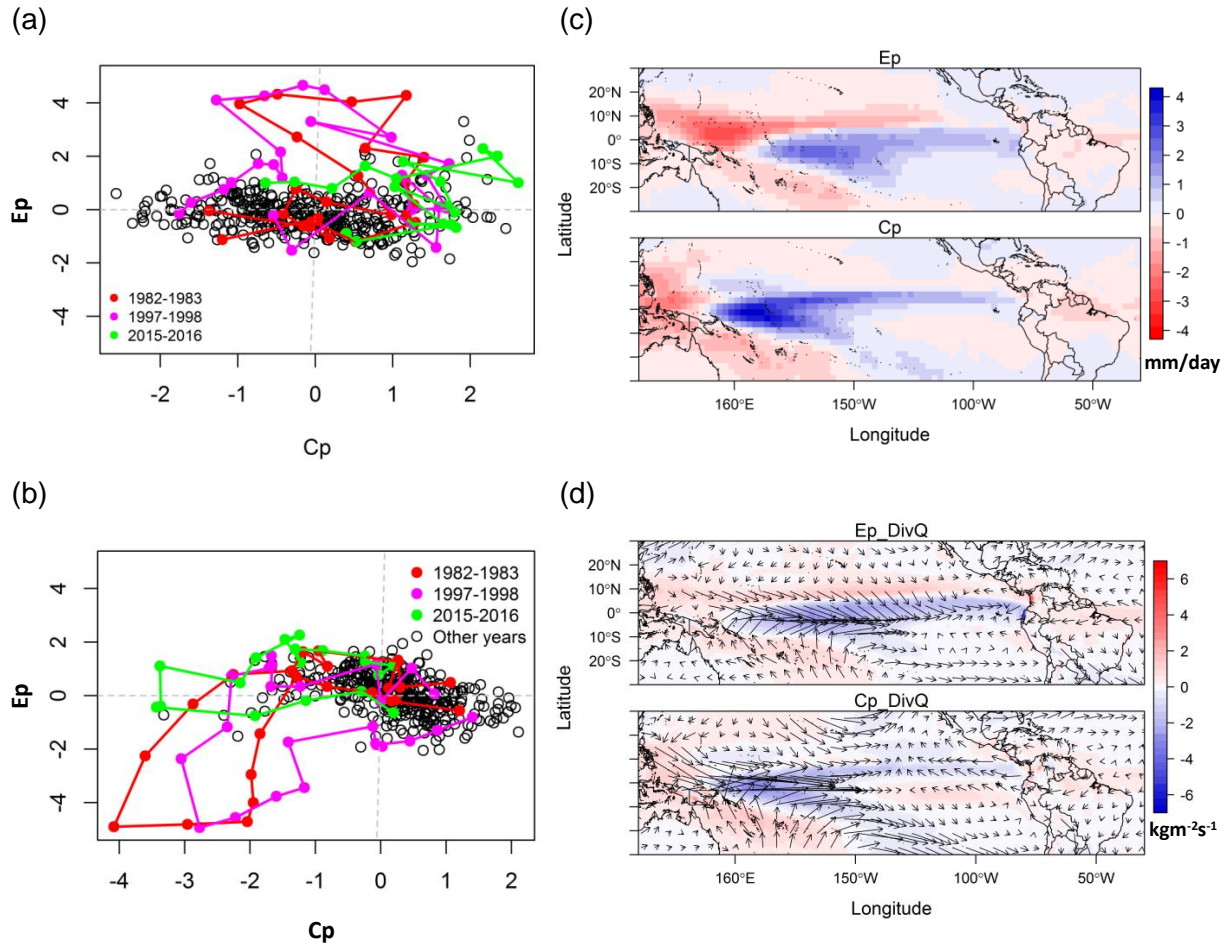


Figure 1. Phase space of the evolution of the Ep and Cp modes: (a) Precipitation (b) vertically integrated water vapor transport convergence ($-\nabla \cdot Q$). The evolution of the 3 strong El Niño events is highlighted with lines connecting the dots for month between January of the first year and December of the second year. Mode patterns associated with Eastern (EP) and Central (CP) Pacific El Niño obtained from EOF regression of period 1979–2016: (c) Precipitation (d) $-\nabla \cdot Q$. Precipitation data used from the Climate Prediction Center (CPC) Merged Analysis of Precipitation (CMAP). $-\nabla \cdot Q$ data used from ERA-Interim reanalysis.

Interestingly, the 2016 event unlike El Niño 1983-1998, exhibits an important Q convergence in the Amazon that expands over the Andes. This pattern seems to be connected to the convergence in the EPB near 4°N (Fig. 2b). Our analysis suggest that this is important to feed the necessary moisture that trigger important convection in the Andes band which come mainly from lower (1000 to 800 hPa) and middle (600 to 400 hPa) levels (Fig. S2). In 2016, over the South Pacific Ocean predominates strong Q divergence linked to strong southerly winds with opposite configuration to the other two events (Fig 2b, upper and middle panel). Therefore, strong south Pacific Ocean semi-permanent anticyclone is not necessary a positive sign that weakening El Niño, but a positive feedback to allow moist air transport in the Amazonia that later will be an important source of moisture to trigger convection in the northern region.

The out-of-phase and marked difference between the Pacific and Amazon basin is observed in the 1983-1998 and 2016 El Niño years. In 1983-1998, the Pacific side observes a strong Q convergence (Fig 2b) linked to strong upward motions noted in upper vertical levels of high specific moisture that reaches 300mb (Fig. 3a). In 2016, a moderate Q divergence in the Pacific Ocean (Fig 2b) is linked to downward motions as suppression of convection with noted dry air in low levels (Fig 3a). In the Amazon basin, this behavior is opposite but follows the same explanation. These results suggest that the two events are similar. The large-scale atmospheric patterns are from the same source. Although there are differences in the Q convergence magnitudes, responses associated with rainfall variability in the EPB is the same. Both 1983-1998 and 2016 have similar large-scale circulation drivers as represented by SST. However, the atmospheric difference in a large-scale is noted with respect to the 2016 event which is opposite to the 1983-1998 events. The analysis implies that opposed vertical movement of large-scale i.e. subsidence or convergence due to changes in the Walker circulation forced by SST anomalies (Ambrizzi *et al.*, 2004; Shimizu *et al.*, 2016) can lead to convergence patterns of preferential position over the Pacific or Amazonian basin, which represent the out-of-phase pattern that primary characterize the moisture source in the EPB. This analysis supports the hypothesis that rainfall in EPB can experience out-of-phase driver patterns in similar El Niño 3.4. In light of these results, in the following step we take a closer look of the mechanism that determines the differences in the meridional extension of Q convergence by EPB between one and other event.

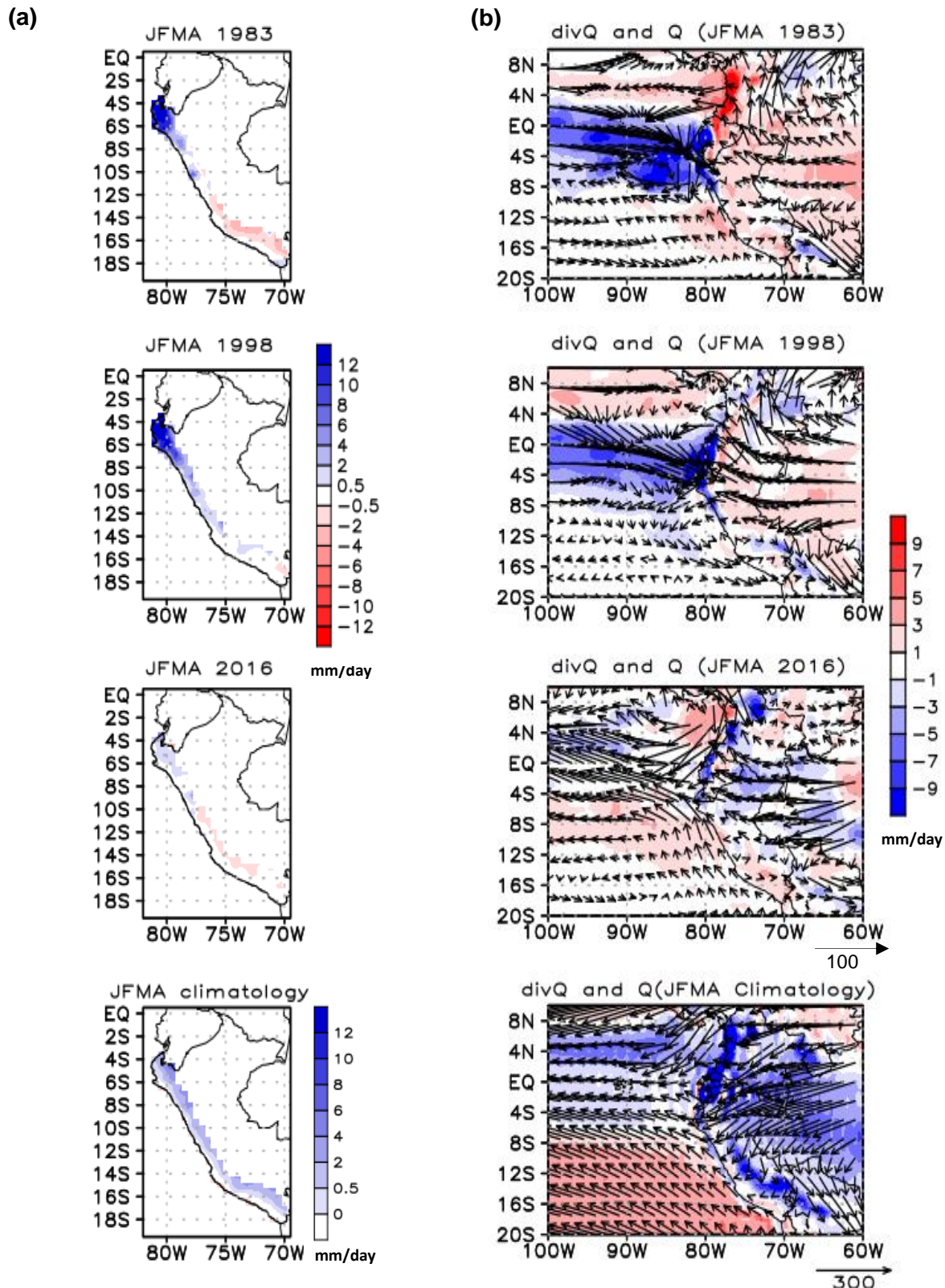


Figure 2. (a) JFMA Composites of observed precipitation anomalies (mm/day) over Peruvian Pacific region (b) JFMA Composites of vertically integrated water vapor transport (Q) anomalies ($\text{kg m}^{-1} \text{s}^{-1}$) (vector) and Q convergence anomalies ($-\nabla \cdot Q$) y/o Q divergence anomalies ($\nabla \cdot Q$) (mm/day). Respective climatology over 1979-2016 period. The continuous shading encompasses positive and negative significant values at the 95% confidence level using the Student's t-test.

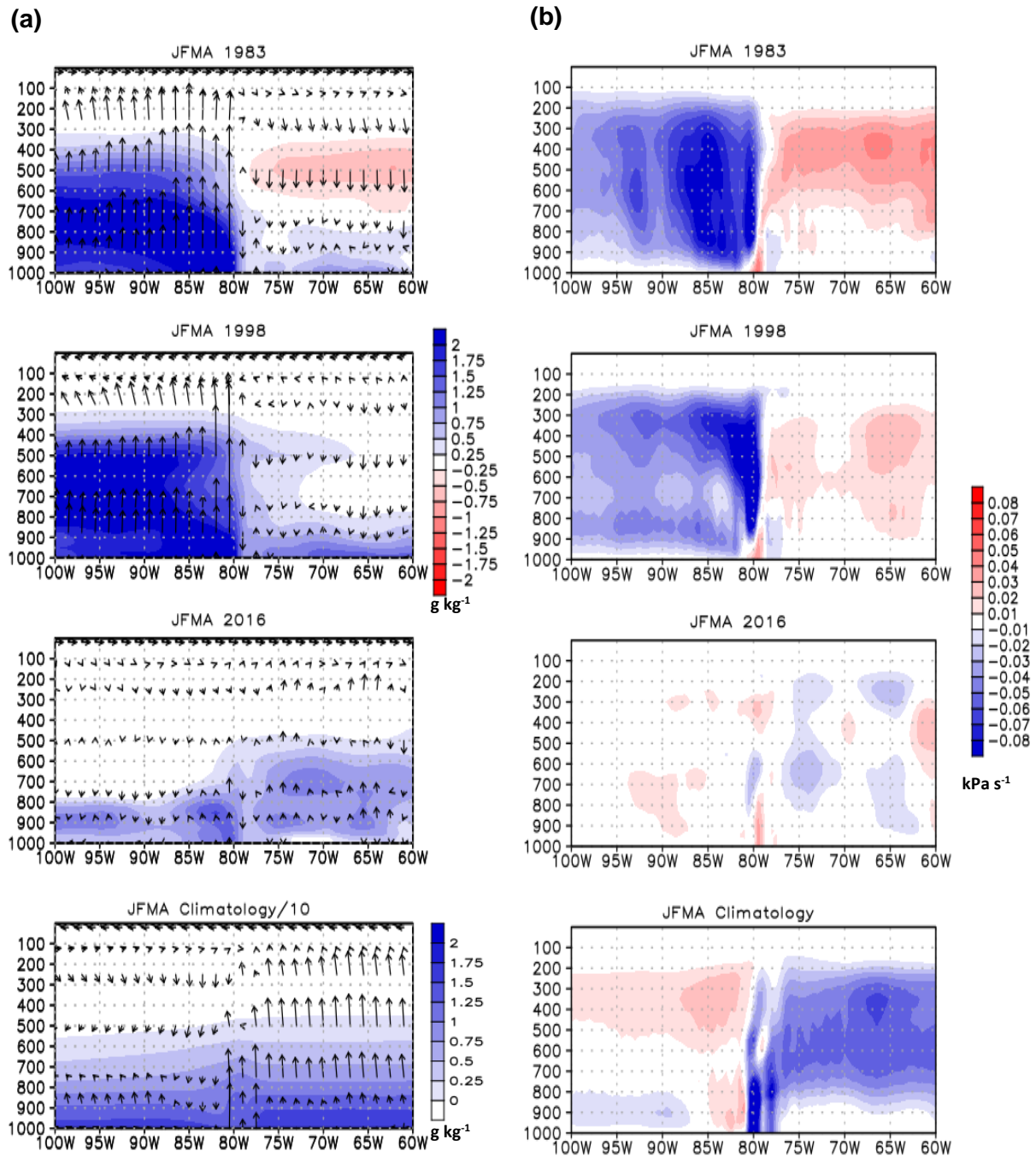


Figure 3. JFMA composites of longitude vertical cross-section of (a) specific moisture anomalies (g kg^{-1}) and (b) vertical motion anomalies ω (kPa s^{-1}), averaged between 2°S and 7.5°S (northern region) for El Niño of 1983, 1998 and 2016. Respective climatology over 1979-2016 period. The continuous shading encompasses positive and negative significant values at the 95% confidence level using the Student's t-test

3.3 Regional and local physical mechanisms

Figure 4 depicts vertical structure of q and wind in the 2016 event and the others two El Niño. In the Pacific Ocean, the 2016 (1998 and 1983) event has predominated southerly (northerly) winds that do not (do) support the moist air transport located north (south) that feeds the EPB region. Also it verified by the weak (strong) q along the vertical column. Over the Amazon, humidity in mid-levels (up to 500 mb.) is significant in the 2016 event. In the first two events the presence (or absence) of depression in the upper level southerly (or northerly) winds induce to a strengthening (or weakening) of subsidence that allows a lower (greater) q influx in the EPB, as in El Niño 1983 (and 1998) (Fig. 4a). Instead, in El Niño 2016 the absence of depression in the upper level southerly winds allowed low and middle level q influx from the Amazon supported by strong easterly winds (Figs. 4a,b). Considering that the q is part of the same atmospheric mass of the convergence band Q (Knippertz et al., 2013) it can inferred that the regional mechanism of 100 to 300 hPa upper winds is a forcing of magnitude and southern extension of Q convergence band by EPB that in the El Niño 2016 (1983 and 1998) reached around 6 ° S (10 ° S and 14 ° S) which founded the extremes (weak) rainfall in the north-Center EPB (Fig 2b).

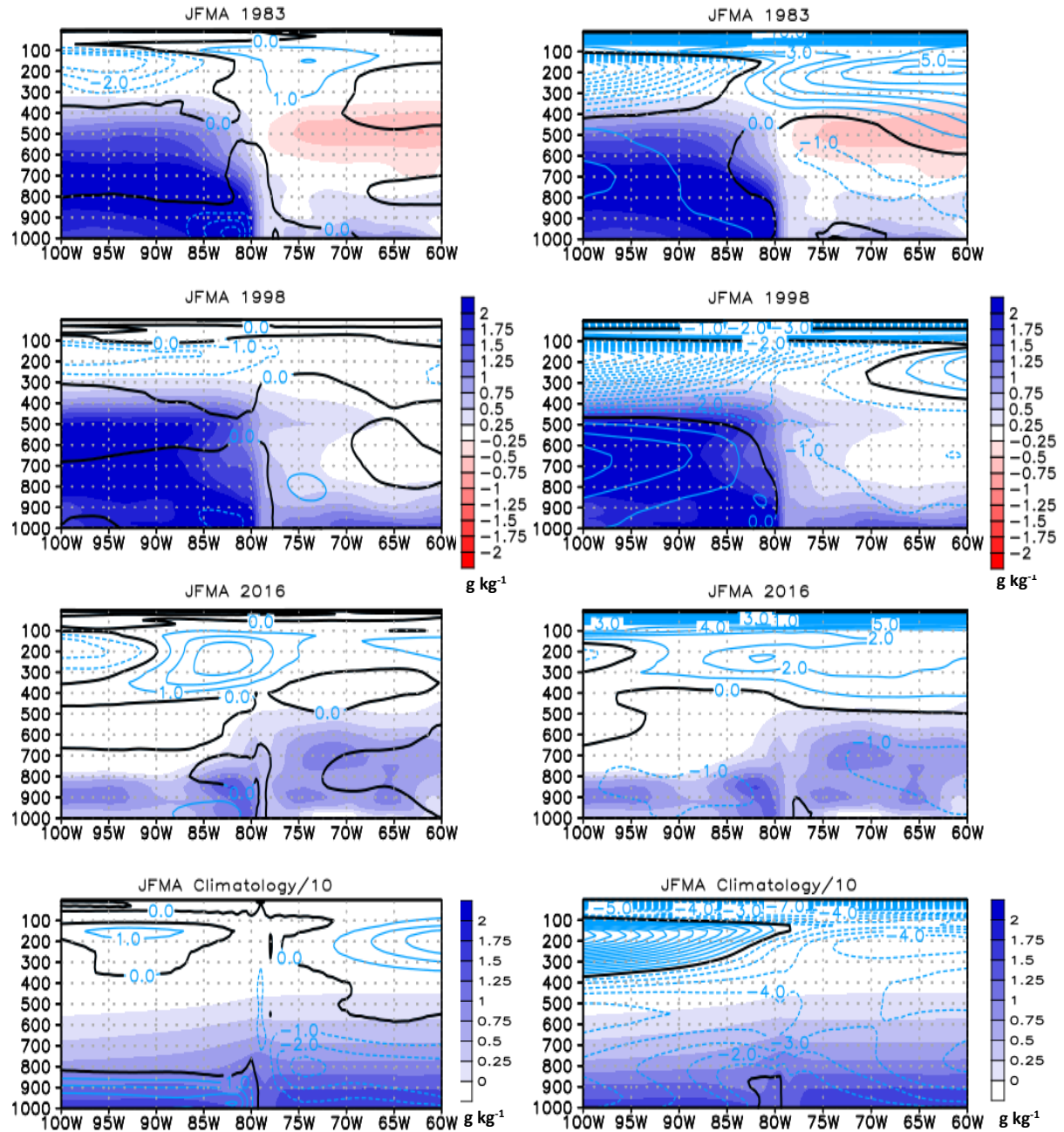


Figure 4. JFMA composites of longitude vertical cross-section of specific moisture anomalies (g kg^{-1}) associated with (a) meridional wind anomalies (m s^{-1}) from the south (north) indicated by the positive (negative) values (b) zonal wind anomalies (m s^{-1}) from the western (eastern) indicated by the negative (positive) values. Average between 2°S and 7.5°S (northern region) for El Niño of 1983, 1998 and 2016. Respective climatology over 1979-2016 period. The continuous shading encompasses positive and negative significant values at the 95% confidence level using the Student's t-test.

4. Conclusions

This study evaluates whether moisture transport and other atmospheric forcing such as moisture transport from the Amazon associated to El Niño can have a preferential response that may be responsible for extremes rainfall variability in the Eastern Pacific basin (EPB). Here we evaluate moisture transport associated with regional and large-scale atmospheric variability. We use reanalysis ERA-Interim during the last three El Niño 1983, 1998 and 2016, to evaluate atmospheric moisture transport (Q) with focus in prevailing paths of water vapor, and moisture convergence ($-\nabla \cdot Q$) as proxy for precipitation. This analysis is evaluated exploring large-scale to continental spatiotemporal variability in $-\nabla \cdot Q$ to the occurrence of extreme rainfall. Our results suggest that EPB can experience out-of-phase patterns in similar El Niño events.

Although the three strongest El Niño 1983 (and 1998) and 2016 in the 1950–2016 period are comparable in Niño 3.4 (similar warming of sea water), they induced different atmospheric moisture convergence responses which primarily characterize the moisture source in the EPB. Fundamentally, the different rainfall pattern at a regional scale in the EPB are defined by the interplay of large-scale (moisture source contributors) and regional (modulate moisture influx in EPB) atmospheric factors. In large-scale atmospheric differences between El Niño 2016 and 1983-1998 involve a coherent out-of-phase pattern associated with dominant subsidence and convergence in EPB and the Amazon basins associated with the Walker circulation forced by SST anomalies (Ambrizzi *et al.*, 2004; Shimizu *et al.*, 2016). Thus, convection during El Niño 2016 (1983 and 1998) migrates North (South) around 4°N (around 4°S) from its climatological position which is sustained by southerly (northerly) winds over the Pacific Ocean along the coast of Peru, coupled a weak (strong) $-\nabla \cdot Q$. Unlike the 1983-1998 El Niño, El Niño 2016 exhibits $-\nabla \cdot Q > 0$ in the Amazon that reaches (Q) highlands of the EPB, which is evidence of the lack of subsidence in the Amazon basin.

While the topography stops the $-\nabla \cdot Q$ concomitantly the amount entering the EPB is influenced by regional atmospheric circulation of upper level southerly or northerly winds (100 to 300 hPa) that can induce strengthening (or weakening) of subsidence allowing lower (greater) income from $-\nabla \cdot Q$ characterizing different enhanced $-\nabla \cdot Q$ transported by the EPB which are reflected in the different rainfall patterns. The extended band of $-\nabla \cdot Q$ by the EPB possibly accounts for the local effects humidity (Knippertz *et al.*, 2013) of circulation land-sea breeze (Horel and Cornejo, 1986; Goldberg *et al.*, 1987; Bendix, 2000) and convection by orographic uplifting (Takahashi, 2004; Douglas *et al.*, 2009) but our results are limited to evaluate their contribution in rainfall. The $-\nabla \cdot Q$ that enters the EPB directly from the Pacific Ocean seems

to be more important than the other processes due to the agreement of the same variations of the extension of $-\nabla \cdot Q$ and observed rainfall exhibited in North-Center EPB. Instead, the orographic convection due to transport moisture seems to be the main mechanism for generating rainfall in the south EPB. Although, we demonstrated strong differences in the moisture transport and its link to the different rain patterns in the EPB.

This study provides guidelines to understand the role of moisture transport and atmospheric circulation of large and regional scales in two different rainfall patterns which have implications in the prediction on EPB rainfall during the strong El Niño events. Determining moisture transport pathways may help inform stakeholders about extreme rainfalls location to manage dam safety and flood prevention. The complexity of El Niño events associated with rainfall in the EPB need to consider and understand other factors such as the interaction of the quasi-biennial oscillation (QBO) and Hadley-like circulation (Salby and Callaghan, 2007), which seems well-described in changes of upper level winds (100 to 300 hPa). The upper EPB exhibits high humidity due to the transportation in medium levels (600 to 400 hPa) from the Pacific Ocean as in El Niño 1998. In a scenario where moisture flows from both the Pacific and Amazonia concur would produce intensified convection similar to Niño 2016, and it could generate serious impacts with rains throughout the EPB leading floods and landslides, causing deaths and diverse damages (Di Liberto, 2017) with serious implications in the productive sectors and economic services of the country (BCRP, 2017).

Rainfall and moisture patterns associated with strong El Niño events in the eastern Pacific region

Supplementary Figures

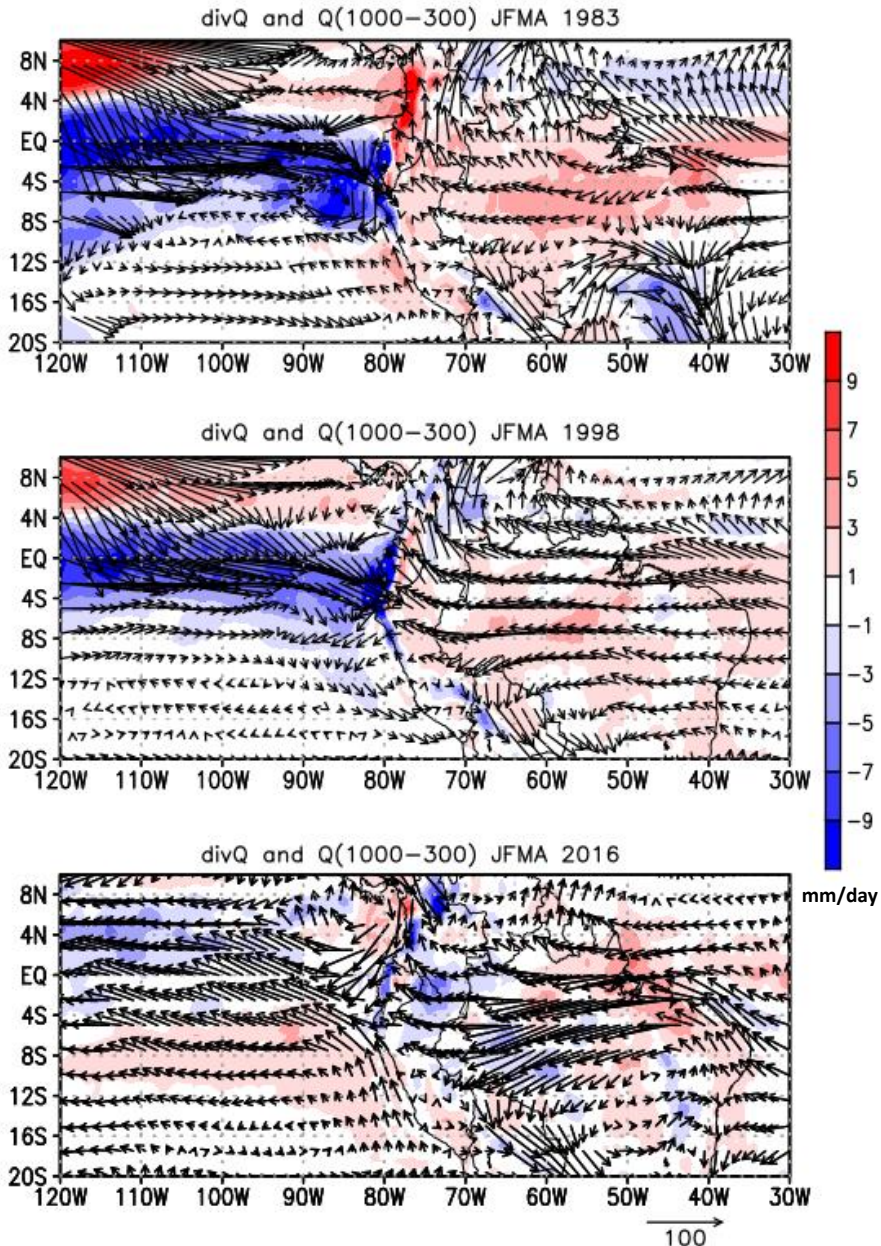


Figure S1. JFMA composites of (a) the vertically integrated water vapor transport(Q) anomalies ($\text{kg m}^{-1} \text{s}^{-1}$) (vector) and Q convergence ($-\nabla \cdot Q$) y/o Q divergence ($-\nabla \cdot Q$) anomalies (mm/day) for El Niño of 1983, 1998 and 2016 along of the zone Lon: 120W – 30W Lat: 20°S to 10°N. The Q and $-\nabla \cdot Q$ integrated between 1000 and 300 hPa. The continuous shading encompasses positive and negative significant values at the 95% confidence level using the Student's t-test.

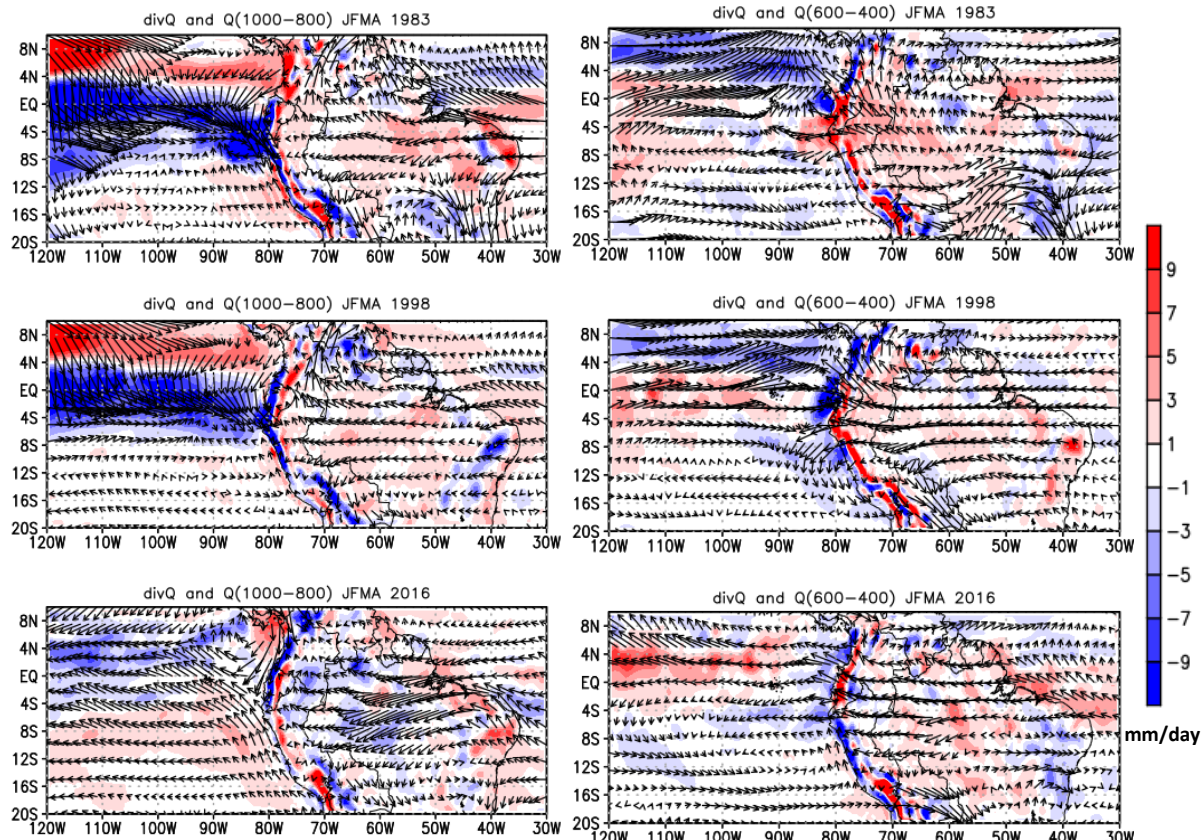


Figure S2. JFMA composites of (a) the vertically integrated water vapor transport (Q) anomalies ($\text{kg m}^{-1} \text{s}^{-1}$) (vector) and Q convergence ($-\nabla \cdot Q$) y/o Q divergence ($-\nabla \cdot Q$) anomalies (mm/day), integrated between 1000 and 800 hPa, for El Niño of 1983, 1998 and 2016 events along of the zone Lon: 120W – 30W Lat: 20°S to 10°N. (b) The same figure but Q and $-\nabla \cdot Q$ integrated between 600 and 400 hPa. The continuous shading encompasses positive and negative significant values at the 95% confidence level using the Student's t-test.

Bibliography

Ambrizzi, T.E., de Souza, B., & Pulwarty, S.R. (2005) The Hadley and Walker regional circulations and associated ENSO impacts on South American seasonal rainfall, in Hadley Circulation: Present, Past and Future. Edited by Diaz HF and Bradley RS. pp 203-235.

Andreoli, R. V., de Oliveira, S. S., Kayano, M. T., Viegas, J., de Souza, R. A. F., & Candido, L. A. (2016). The influence of different El Niño types on the South American rainfall. *International Journal of Climatology*. <https://doi.org/10.1002/joc.4783>.

BCRP. (2017) Actividad Económica (Marzo y Abril). Banco Central de Reserva del Perú (Central Reserve Bank of Peru). Notas Estudio 36: 1–15 45: 1–3. <http://www.bcrp.gob.pe/publicaciones/notas-de-estudios.html>

Bendix, J. (2000). Precipitation dynamics in Ecuador and northern Peru during the 1991/92 El Niño: A remote sensing perspective. *International Journal of Remote Sensing.*, 21 (3), 533–548, doi:10.1080/014311600210731.

Boers, N., Donner, R. V., Bookhagen, B., & Kurths, J. (2014). Complex network analysis helps to identify impacts of the El Niño Southern Oscillation on moisture divergence in South America. *Climate Dynamics*. <https://doi.org/10.1007/s00382-014-2265-7>

Bourrel, L., Rau, P., Dewitte, B., Labat, D., Lavado, W., Coutaud, A., Vera, A., Alvarado, A., & Ordoñez, J. (2015). Low-frequency modulation and trend of the relationship between ENSO and precipitation along the northern to centre Peruvian Pacific coast. *Hydrological Processes*, 29(6), 1252–1266. <https://doi.org/10.1002/hyp.10247>

Capotondi, A., Wittenberg, A.T., Newman, M., Di Lorenzo, E., Yu, J.-Y., Braconnot, P., Cole, J., Dewitte, B., Giese, B., Guilyardi, E., Jin, F-F., Karnauskas, K., Kirtman, B., Lee, T., Schneider, N., Xue, Y., & Yeh, S.-W. (2015). Understanding ENSO diversity. *Bulletin of the American Meteorological Society*, 96(June), 921–938. <https://doi.org/10.1175/BAMS-D-13-00117.1>

Castillo, R., Nieto, R., Drumond, A., & Gimeno, L. (2014). The role of the ENSO cycle in the modulation of moisture transport from major oceanic moisture sources, *Water Resources Research.*, 50, 1046– 1058, doi:10.1002/2013WR013900.

Clem, K.R., Renwick, J.A., & McGregor, J. (2017). Relationship between eastern tropical Pacific cooling and recent trends in the Southern Hemisphere zonal-mean circulation. *Climate dynamics* 49: 113. <https://doi.org/10.1007/s00382-016-3329-7>

Dee, D. P., Uppala, S. M., Simmons, a. J., Berrisford, P., Poli, P., Kobayashi, S., Andrae, U., Balmaseda, M. a., Balsamo, G., Bauer, P., Bechtold, P., Beljaars, a. C. M., van de Berg, L., Bid- lot, J., Bormann, N., Delsol, C., Dragani, R., Fuentes, M., Geer, a. J., Haimberger, L., Healy, S. B., Hersbach, H., Hólm, E. V., Isaksen, L., Kållberg, P., Köhler, M., Matricardi, M., McNally, a. P., Monge-Sanz, B. M., Morcrette, J.-J., Park, B.-K., Peubey, C., de Rosnay, P., Tavolato, C., Thépaut, J.-N., & Vitart, F. (2011) The ERA-Interim reanalysis: configuration and performance of the data assimilation system, *Q. J. Roy. Meteorol. Soc.*, 137, 553– 597, doi:10.1002/qj.828, 2011

Drumond, A., Marengo, J., Ambrizzi, T., Nieto, R., Moreira, L., & Gimeno, L. (2014). The role of the Amazon Basin moisture in the atmospheric branch of the hydrological cycle: A Lagrangian analysis. *Hydrology and Earth System Sciences*, 18(7), 2577–2598. <https://doi.org/10.5194/hess-18-2577-2014>

Eichler, T. P., & Londoño, A. C. (2013). South American climatology and impacts of El Niño in NCEP's CFSR data. *Advances in Meteorology*, 2013. <https://doi.org/10.1155/2013/492630>

Garreaud, R. D. (2009). The Andes climate and weather. *Advances in Geosciences*, 7, 1–9. Retrieved from www.adv-geosci.net/7/1/2009/

Gimeno, L., Dominguez, F., Nieto, R., Trigo, R., Drumond, A., Reason, CJC., Kumar, R., & Marengo, J. (2016). Major Mechanisms of Atmospheric Moisture Transport and their Role in Extreme Precipitation Events Major Mechanisms of Atmospheric Moisture Transport and their Role in Extreme Precipitation Events, (June). <https://doi.org/10.1146/annurev-environ-110615-085558>

Goldberg, R. A., Tisnado, G. M., & Scofield, R. A. (1987). Characteristics of extreme rainfall events in northwestern Peru during the 1982-1983 El Niño period. *Journal of Geophysical Research*, 92(C13), 14225–14241. <https://doi.org/10.1029/JC092iC13p14225>

Gu, G., & Adler, R. F. (2016). Precipitation, temperature, and moisture transport variations associated with two distinct ENSO flavors during 1979–2014. *Climate Dynamics*. <https://doi.org/10.1007/s00382-016-3462-3>

Horel, J.D., & Cornejo-Garrido, A.G. 1986. Convection along the coast of northern Peru during 1983: Special and temporal variation of clouds and rainfall. *Monthly Weather Review*. 114: 2091–2105.

Hu, S., & Fedorov, A. V. (2017). The extreme El Niño of 2015–2016: the role of westerly and easterly wind bursts, and preconditioning by the failed 2014 event. *Climate Dynamics*, (123456789). <https://doi.org/10.1007/s00382-017-3531-2>

Huaman, L., & Takahashi, K. (2016). The vertical structure of the eastern Pacific ITCZs and associated circulation using the TRMM Precipitation Radar and in situ data. *Geophysical Research Letters*, 43(15), 8230–8239. <https://doi.org/10.1002/2016GL068835>

Kao, H. Y., & Yu, J. Y. (2009). Contrasting Eastern-Pacific and Central-Pacific types of ENSO. *Journal of Climate*, 22(3), 615–632. <https://doi.org/10.1175/2008JCLI2309.1>

Knippertz, P., Wernli, H., & Gläser, G. (2013). A global climatology of tropical moisture exports. *Journal of Climate*, 26(10), 3031–3045. <https://doi.org/10.1175/JCLI-D-12-00401.1>

L'Heureux, M. L., Takahashi, K., Watkins, A. B., Barnston, A. G., Becker, E. J., Di Liberto, T. E., ... Wittenberg, A. T. (2017). Observing and Predicting the 2015-16 El Niño. *Bulletin of the American Meteorological Society*, BAMS-D-16-0009.1. <https://doi.org/10.1175/BAMS-D-16-0009.1>

Levine, A. F. Z., & McPhaden, M. J. (2016). How the July 2014 easterly wind burst gave the 2015-2016 El Niño a head start. *Geophysical Research Letters*, 43(12), 6503–6510. <https://doi.org/10.1002/2016GL069204>

Lorenz, C., & Kunstmann, H. (2012). The hydrological cycle in three state-of-the-art reanalyses: Intercomparison and performance analysis. *Journal of Hydrometeorology*, 13(5), 1397–1420. <https://doi.org/10.1175/JHM-D-11-088.1>

Paek, H., Yu, J.-Y., & Qian, C. (2017). Why were the 2015/16 and 1997/98 Extreme El Niños different? *Geophysical Research Letters*, 1–9. <https://doi.org/10.1002/2016GL071515>

Paixao Veiga, J. A., Rao, V. B., & Franchito, S. H. (2005). Heat and moisture budgets of the walker circulation and associated rainfall anomalies during El Niño events. *International Journal of Climatology*, 25(2), 193–213. <https://doi.org/10.1002/joc.1115>

Peixoto, J. P., & Oort, A.H. (1992) Physics of Climate. American Institute of Physics, MIT press: San Diego, CA. 520 pp.

Pineda, L., Ntegeka, V., & Willems, P. (2013). Rainfall variability related to sea surface temperature anomalies in a Pacific-Andean basin into Ecuador and Peru. *Advances in Geosciences*. <https://doi.org/10.5194/adgeo-33-53-2013>

Rau, P., Bourrel, L., Labat, D., Melo, P., Dewitte, B., Frappart, F., Lavado, W., & Felipe, O. (2017). Regionalization of rainfall over the Peruvian Pacific slope and coast. *International Journal of Climatology*, 37(1), 143–158. <https://doi.org/10.1002/joc.4693>

Sanabria, J., Bourrel, L., Dewitte, B., Frappart, F., Rau, P., Solis, O., & Labat, D. (2018). Rainfall along the coast of Peru during strong El Niño events. *Int. J. Climatology* 38 (4): 1737 – 1747. <https://doi.org/10.1002/joc.5292>

Schneider, T., Bischoff, T., & Haug, G. H. (2014). Migrations and dynamics of the intertropical convergence zone. *Nature*, 513(7516), 45–53. <https://doi.org/10.1038/nature13636>.

Seager R, Naik N, Vecchi GA. 2010. Thermodynamic and dynamic mechanisms for large-scale changes in the hydrological cycle in response to global warming. *Journal of Climate* 23(17): 4651–4668. DOI: 10.1175/2010JCLI3655.1.

Shimizu, M. H., Ambrizzi, T., & Liebmann, B. (2016). Extreme precipitation events and their relationship with ENSO and MJO phases over northern South America. *International Journal of Climatology*. <https://doi.org/10.1002/joc.4893>

Simmons, A., S. Uppala, D. Dee, and S. Kobayashi, 2006: ERA- Interim: New ECMWF reanalysis products from 1989 onwards. ECMWF Newsletter, No.110, ECMWF, Reading, United Kingdom, 25–35.

[Available online at http://www.ecmwf.int/publications/newsletters/pdf/110_rev.pdf.]

Sohn, B-J., Smith, EA., Robertson, FR., & Park S-C. (2004) Derived over- ocean water vapor transports from satellite-retrieved E-P data- sets. *Journal of Climate* 17:1352–1365

Solman, S.A., Sanchez, E., Samuelsson, P., da Rocha, R. P., Li, L., Marengo, J., Pessacq, N.L., Remedio, AR.C., Chou, S.C., Berbery, H., Le Treut, H., de Castro, M., & Jacob, D. (2013). Evaluation of an ensemble of regional climate model simulations over South America

driven by the ERA-Interim reanalysis: Model performance and uncertainties. *Climate Dynamics*, 41(5–6), 1139–1157. <https://doi.org/10.1007/s00382-013-1667-2>

Sulca, J., Takahashi, K., Espinoza, J., Vuille, M., & Lavado, W. (2017). Impacts of ENSO flavors and tropical Pacific convection variability (ITCZ, SPCZ) on austral summer rainfall in South America focused on Peru. <https://doi.org/10.1002/joc.5185>

Takahashi, K. (2004). The atmospheric circulation associated with extreme rainfall events in Piura, Peru, during the 1997–1998 and 2002 El Niño events. *Annales Geophysicae*, 22(11), 3917–3926. <https://doi.org/10.5194/angeo-22-3917-2004>

Takahashi, K., & Battisti, D. S. (2007). Processes controlling the mean tropical Pacific precipitation pattern. Part II: The SPCZ and the Southeast Pacific dry zone. *Journal of Climate*. <https://doi.org/10.1175/2007JCLI1656.1>

Takahashi, K., Montecinos, A., Goubanova, K., & Dewitte, B. (2011). ENSO regimes: Reinterpreting the canonical and Modoki El Niño. *Research Letters Geophysical*. <https://doi.org/10.1029/2011GL047364>

Tedeschi, R. G., Cavalcanti, I. F. A., & Grimm, A. M. (2013). Influences of two types of ENSO on South American precipitation. *International Journal of Climatology*, 33(6), 1382–1400. <https://doi.org/10.1002/joc.3519>

Trenberth, K.E., Fasullo, J.T., & Mackaro J. (2011). Atmospheric moisture transports from ocean to land and global energy flows in reanalyses. *J. Climate*, 24, 4907–4924, doi:10.1175/2011JCLI4171.1.

Vecchi, G. A. (2006). The termination of the 1997–98 El Niño. Part II: Mechanisms of atmospheric change. *Journal of Climate*, 19(12), 2647–2664. <https://doi.org/10.1175/JCLI3780.1>

Xie, P., & Arkin, P.A. (1997) Global precipitation: A 17-year monthly analysis based on gauge observations, satellite estimates, and numerical model outputs. *Bull. Amer. Meteor. Soc.*, 78, 2539–2558.

Xu, G., Osborn, T. J., Matthews, A. J., & Joshi, M. M. (2015). Different atmospheric moisture divergence responses to extreme and moderate El Niños. *Climate Dynamics*.

<https://doi.org/10.1007/s00382-015-2844-2>

Yang, G.-Y., & Hoskins, B. (2013). ENSO Impact on Kelvin Waves and Associated Tropical Convection. *Journal of the Atmospheric Sciences*, 70(11), 3513–3532.
<https://doi.org/10.1175/JAS-D-13-081.1>

This page intentionally left blank

Chapter 5: Conclusions and Perspectives

5.1 CONCLUSIONS

Four strong El Niño events took place within the last five decades (1972/1973, 1982/1983, 1997/1998 and 2015/2016) recorded as strong in the Niño 3.4 region. They exhibit significant differences in their evolution associated with a distinct rainfall anomaly evolution along the PPB (Peruvian Pacific Basin), which illustrates the strong nonlinearity of the ENSO teleconnection on the rainfall in this area. The extremes rainfalls have harmful impact on the population and productive sectors because they trigger floods and landslides, and on the other small changes in rainfall over highland areas can affect agriculture, water reservoir storage level and hydroelectric resources (BCRP, 2016, 2017).

The results of the thesis bring to the following principal conclusions:

The interannual rainfall variability in the PPB in the light of the strongest El Niño events of the last five decades present distinct anomalies and evolutions of rainfall which is interpreted as resulting from the contribution of EP and CP El Niño establishing a specific teleconnection pattern. These specific teleconnections are linked with different atmospheric responses that depend of the large-scale moisture transport and interplay between regional and large-scale circulations. Interplay that establish the conditions necessary for heavy precipitation to occur and also shape the different rainfall pattern characterizing the rainfall variability.

The rainfall anomalies variability is interpreted as resulting from the combination of a meridional see-saw mode (North–South) (Ep mode) and a zonal see-saw mode (East–West) (Cp mode) that represent, respectively, 34 and 21% of the explained variance. The extreme 1982/1983 and 1997/1998 El Niño events have a dominant projection on the Ep mode that has a strong loading in the northern region which is linked to strong low-level (1000 to 800 hPa) and upper-level (600 to 400 hPa) moisture transport originated in the Pacific Ocean that reach the Peruvian northern coast. While the moderate 1972/1973 and 2015/2016 El Niño events have a relatively weak projection onto the Ep mode (about ten times less at the peak

of the rainy season than the extreme events) and mostly project onto the Cp mode which are linked to weak low-level moisture transport coming from the Pacific Ocean and also significant low and mid-level moisture transport from Amazon that reach the northern coast and Peruvian Pacific highlands, respectively. All strong El Niño events are associated with positive rainfall anomalies in the northern part of Peru which is accounted by the Ep mode linked to strong (weak) moisture transport from Pacific during the extremes (moderate) El Niño events.

The evolution of rainfall anomalies along the Cp mode exhibits a significant dispersion associated with the presence or absence of moisture in highlands. In the 1983 and 1998 events it is linked to upper level (600 to 400hPa) moisture transport coming from the Pacific Ocean toward highlands which the amount entering the PPB influenced by regional circulation of upper levels (100 to 300 hPa). Whereas in the moderate events, in particular El Niño 2015/2016, unlike the extreme El Niño events, is linked to moisture transport from the Amazon reaching highlands. These behaviors respond to the impact of strong El Niño events on the highlands cannot solely be inferred from the magnitude of the sea surface temperature anomalies in the central equatorial Pacific Ocean, but also to the role of the regional circulation that interplay with large-scale atmospheric mechanisms controlling the moisture and convergence amount entering the PPB which coming from large-scale moisture transport from several sources that have distinct dynamical even when it is started with a similar large-scale circulation driver (Niño 3.4).

Although these rainfalls are linked to the moisture arrival from those sources, the moisture amount entering the PPB can be influenced by regional atmospheric circulation of upper level southerly or northerly winds (100 to 300 hPa) that can induce to a strengthening (or weakening) of Amazon subsidence allowing a lower (greater) moisture and convergence income, characterizing different convergence enhanced by the PPB, and reflected in the different rainfall patterns. This enhanced transport in El Niño 1982/1983, 1997/1998 and 2015/2016 reached about 10°S, 14°S and 6°S, founding the extremes (1982/1983 and 1997/1998) and weak (2016) rainfalls anomalous, in the North-Centre PPB. This illustrates the interplay of large-scale (i.e. subsidence) and regional (i.e. upper level wind) mechanisms on the large-scale moisture transport in determining different rainfall patterns during these El Niño events. This mechanisms and Pacific Ocean moisture transport found the Ep mode behavior associated with rainfall in the North-Centre PPB.

The evaluation of reanalysis (ERA-Interim, JRA-55 and CFSR) indicates that ERA -Interim is more realistic reproducing the rainfall variability modes mainly the Ep mode linked with heavy rainfall. While still there is difficulty to reproduce rainfall in highlands (Cp mode) in JRA-55

and CFSR more than ERA -Interim. In particular, the three reanalysis closely reproduce the differences among the strong El Niño events, such as the intensity of rainfall peak (extreme events about ten times more than moderate events) and the evolution. The evolution of 1982/1983 and 1997/1998 events on the mode Ep show better agree than the evolution of 1972/1973 and 2015/2016 events on Cp mode. Despite these reanalysis well agree with the different projections onto the modes and indicating that the strong El Niño events are the result of two modes still they have deficiencies in the exact reproduction of peak magnitude.

These conclusions indicate that the dynamical origins of the rainfall associated with strong El Niño events can be distinguished and their teleconnection patterns can be reasonably understood (i.e. the opposite atmospheric response experiencing an out-of-phase moisture convergence pattern regarding the 2016 event and 1983 and 1998 events -that are similar- allows us to understand the dynamical origins of the mainly rainfall variability modes).

As well the thesis provides guidelines to understand the role of moisture transport and of large-scale and regional atmospheric circulation in two different rainfall patterns which have implications in the prediction on PPB rainfall during the strong El Niño events. Determining moisture transport pathways may help inform stakeholders about extreme rainfalls location to manage floods and landslides prevention. This thesis presents also a way of looking at extreme rainfall from the atmospheric moisture transport perspective.

In the second chapter of the thesis, apart from determining the rainfall variability and present the different rainfall evolution during the strong El Niño events, we have also modeled the relationship between rainfall and SST taking into account the nonlinear evolution of ENSO through the consideration of the EP and CP ENSO regimes. This has allowed affirm the knowledge about the influences of both El Niño regimes in each mode, and identify how both regimes can set up a specific teleconnection pattern that affects rainfall variability and results in different rainfall patterns. In the third chapter it is demonstrated that ERA-Interim shows better performance for reproducing rainfall variability in the PPB in terms of the spatial pattern (Ep and Cp Mode). As well, it is reaffirmed in the analysis of moisture transport convergence for 37-yr give consistent results with observed rainfall being a useful tool for future hydrological studies in the PPB. In the fourth chapter, the results conclude that the different rainfall patterns are associated with different atmospheric responses experiencing out-of phase moisture convergence patterns that have different dynamics even when it is started with a similar large-scale circulation driver (Niño 3.4). The different rainfall patterns depend mainly on the large-scale moisture transport and interplay between regional and large-scale circulations. All this atmospheric mechanism helps understand the processes governing the variability of each rainfall mode.

5.2 PERSPECTIVES

Studying the complexity of strong El Niño events associated with rainfall in the PPB needs to consider and understand better such as:

- A more detailed temporal variability during the strong El Niño events i.e. explain them, and specifically on the peak periods, not only at monthly scale but also at decadal (10 days) until daily scale if necessary (to take into account of the mainly explicative processes).
- Other factors explaining the differences between events including the distinct processes associated with synoptic variability due either to the Madden–Julian oscillation (Madden and Julian, 1972) and to the extra-tropical storm activity of the mid-latitudes that are influential on the along-shore winds along the coast of Peru (Dewitte et al., 2011) or the South Pacific meridional mode (Zhang et al., 2014). We have analysed the evolution of the MJO during three of the four strong El Niño events (Figure S3). It indicates that these three events have a different evolution. While the 1997/1998 El Niño event was associated to an anomalous positive MJO activity prior to its peak, the 1982/1983 and 2015/2016 El Niño events did not. Regarding the 1982/1983 and 1997/1998 El Niño events, this is consistent with previous studies (Tang and Yu, 2008; Gushchina and Dewitte, 2012).

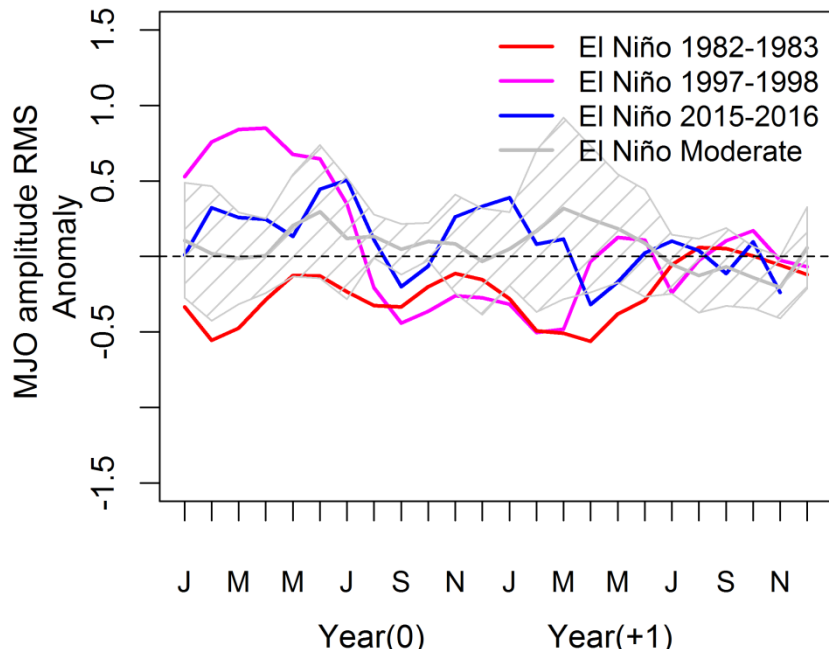


Figure S1. Evolution of the anomalous MJO activity for the 1982/1983, 1997/1998 and 2015/2016 El Niño events. The MJO activity is defined as 3-month running variance of the RMM index (daily) as defined by Wheeler and Hendon (2004). Anomalies of the MJO activity

are relative to the average seasonal cycle over the period 1980-2015. The mean evolution for moderate El Niño events along with the dispersion among events is also shown. Data are from <https://iri.ldeo.columbia.edu/SOURCES/.BoM/.MJO/.RMM/>

The differences in MJO activity between events are consistent with the differences in rainfall over Peru assuming that MJO is influential. However, the processes that link the MJO activity to the rainfall off Peru is not straightforward. MJO activity can impact the oceanic Kelvin wave activity that leads to warming off Peru although a peak MJO does not necessarily imply an anomalous winds stress (Westerly Wind Burst) that forces a Kelvin wave. MJO could also influence the tropospheric circulation over Peru and reduce temperature stratification, which would favour deep convection. It can be also influential on the mid-latitude atmospheric circulation and modulate the South Pacific anticyclone (Dewitte et al., 2011; Rahn, 2012).

- The interaction of the quasi-biennial oscillation (QBO) and Hadley-like circulation (Salby and Callaghan, 2007), which seems well-described in changes of upper level winds (100 to 300 hPa) should will be reserved for future research. References suggest that the wind changes could be related to the differences of latent heat release associated with tropical deep convection (Ho *et al.*, 2009; Liess and Geller, 2012). The tropical deep convection amplitude associated with MJO is modulated by QBO rather than the ENSO (Son *et al.*, 2016). The MJO activity becomes stronger and more organized during the easterly QBO (Son *et al.*, 2017; Hood, 2017) which is influenced by the 11-year solar cycle (Nishimoto and Yoden 2017).
- Local processes of air–sea interactions are also thought to be at work during El Niño events in this region (B. Dewitte, 2017). Processes that include also assessing the contribution of moisture on the rainfall by local effects of sea breeze circulation (Horel and Cornejo, 1986; Goldberg *et al.*, 1987; Bendix, 2000) and convection by orographic uplifting (Takahashi, 2004; Douglas *et al.*, 2009). However, the local SST anomalies are not likely to be the only factor influencing the rainfall conditions during strong El Niño events (Takahashi and Martinez, 2017). Our study calls for investigating the sensitivity of the rainfall distribution and evolution to the regional oceanic conditions, which could be through the use of a regional atmospheric model. In the same way, one aspect that is not currently well accounted for in global coupled models are the regional SST anomalies along the coast of Peru and Ecuador (Takahashi *et al.*, 2014), which calls for investigating regional physical processes explaining such a diverse response of rainfall under strong El Niño conditions, and considering also the likely impact of decadal variability on the relationship between ENSO and rainfall in Peru (Bourrel *et al.*, 2015; Segura *et al.*, 2016).

Chapitre 5 : Conclusions et Perspectives (Version française)

5.1 CONCLUSIONS

Quatre événements El Niño extrêmes ont eu lieu durant les cinq dernières décennies (1972/1973, 1982/1983, 1997/1998 et 2015/2016) et étaient caractérisés comme forts dans la région Niño 3.4. Ils présentent des différences significatives dans leur évolution qui induisent des anomalies distinctes de précipitations le long du versant Pacifique Péruvien illustrant la non-linéarité de la téléconnection ENSO sur les précipitations dans cette région. Les pluies extrêmes ont un impact néfaste sur la population et les secteurs productifs en raison des inondations et des glissements de terrain qui s'ensuivent, et d'autre part, de faibles changements dans les hautes terres peuvent affecter l'agriculture, les réservoirs et les ressources hydroélectriques (BCRP, 2016, 2017).

Les résultats de la thèse amènent aux principales conclusions :

La variabilité interannuelle des précipitations dans le PPB à la lumière des événements El Niño les plus forts des cinq dernières décennies présente des anomalies et des évolutions distinctes des précipitations qui sont interprétées comme résultant de la contribution de EP et CP El Niño établissant un patron de téléconnection spécifique. Ces téléconnexions spécifiques sont liées à différentes réponses atmosphériques qui dépendent du transport d'humidité à grande échelle et de l'interaction entre les circulations régionales et à grande échelle. Les interactions qui établissent les conditions nécessaires pour que de fortes précipitations puissent se produire et configurent également les différents régimes de précipitations caractérisant la variabilité des précipitations.

La variabilité des anomalies de pluie est interprétée comme résultat de la combinaison d'un mode de "see-saw" méridional (Nord-Sud) (mode Ep) et d'un mode de "see-saw" zonal (Est-Ouest) (mode Cp) représentant respectivement 34 et 21% de la variance expliquée. Les événements extrêmes El Niño de 1982/1983 et 1997/1998 ont une projection dominante sur

le mode Ep qui a une forte décharge dans la région du nord qui est liée à de forts transports de l'humidité des niveaux bas (1000 à 800 hPa) et des hauts niveaux (600 à 400 hPa) originaire du Pacifique qui atteint la côte nord péruvienne. Alors que les événements modérés El Niño de 1972/1973 et 2015/2016 ont une projection relativement faible sur le mode Ep (environ dix fois moins au pic de la saison des pluies que les événements extrêmes) et se projettent principalement sur le mode Cp et sont liés à un faible transport de l'humidité provenant du Pacifique et aussi à un important transport de l'humidité de niveau basse et moyen provenant d'Amazonie qui atteint la côte nord et les hautes terres du versant Pacifique péruvien, respectivement. Tous les événements forts El Niño sont associés à des anomalies de pluies positives dans la partie nord du Pérou qui sont expliquées par le mode Ep lié au fort (faible) transport d'humidité du Pacifique pendant les événements extrêmes (modérés) El Niño.

L'évolution des anomalies de pluie le long du mode Cp montre une dispersion significative associée à la présence ou à l'absence d'humidité dans les hautes terres. Dans les événements de 1983 et 1998, elle est liée au transport d'humidité de niveau supérieur (600 à 400 hPa) provenant du Pacifique vers les hautes terres dont la quantité entrant dans le PPB est influencée par la circulation régionale des niveaux supérieurs (100 à 300 hPa). Alors que dans les événements modérés, en particulier El Niño 2015/2016 contrairement aux événements extrêmes El Niño, elle est liée au transport de l'humidité provenant de l'Amazonie et atteignant les hautes terres. Ces comportements qui induisent l'impact d'événements El Niño forts sur les hautes terres et le long de la côte ne peuvent pas être déduits uniquement de la magnitude des anomalies de température de la surface de la mer dans le Pacifique équatorial central. Ils sont aussi liés au rôle de la circulation régionale qui interagit avec les mécanismes atmosphériques à grande échelle qui contrôlent la quantité d'humidité et la convergence qui entre dans le PPB et qui proviennent du transport d'humidité à grande échelle issues de plusieurs sources et qui présentent des dynamiques distinctes bien qu'ils commencent avec une source commune (El Niño 3.4) du vecteur de circulation à grande échelle.

Bien que ces précipitations soient liées à l'humidité provenant de ces sources, la quantité d'humidité pénétrant dans le PPB peut être influencée par la circulation atmosphérique régionale des vents du sud et du nord de hauts niveaux (100 à 300 hPa) qui peuvent induire un renforcement (ou affaiblissement) de la subsidence Amazonienne permettant une entrée et une convergence d'humidité plus faible (plus élevée). Ceci caractérise ainsi différentes extensions de convergence, reflétées ainsi dans les différents patrons de pluies dans le PPB. Cette extension de transport d'humidité durant El Niño 1982/1983, 1997/1998 et 2015/2016

a atteint respectivement environ 10 ° S, 14 ° S et 6 ° S, avec les anomalies des pluies extrêmes (1982/1983 et 1997/1998) et des faibles anomalies (2016), dans le nord-centre du PPB. Ceci illustre l'interaction des mécanismes à grande échelle (c'est-à-dire l'affaissement) et régionaux (vents de niveau supérieur) sur le transport de l'humidité à grande échelle déterminant ainsi les différents patrons de pluie pendant ces événements El Niño. Ces mécanismes et le transport de l'humidité du Pacifique corroborent le comportement du mode Ep qui est associé à la pluie dans le nord-centre du PPB.

L'évaluation des réanalyses (ERA-Interim, JRA-55 et CFSR) indique qu' ERA-Interim est plus réaliste pour reproduire les modes de variabilité des précipitations principalement le mode Ep lié à de fortes précipitations. Il y a encore plus de difficultés pour reproduire les précipitations dans les régions montagneuses (mode Cp) dans JRA-55 et CFSR que dans ERA-Interim. En particulier, les trois réanalyses reproduisent fidèlement les différences entre les événements El Niño forts, tels que l'intensité des pics des précipitations (événements extrêmes environ dix fois plus forts que les événements modérés) et leur évolution. L'évolution des événements de 1982/1983 et de 1997/1998 sur le mode Ep montre un meilleur accord que l'évolution des événements de 1972/1973 et de 2015/2016 sur le mode Cp. Bien que ces réanalyses présentent un bon accord avec les différentes projections sur les deux modes et indiquent bien que les forts événements El Niño sont les résultats des deux modes, ils ont encore des déficiences dans la reproduction exacte de la magnitude des pics.

Ces conclusions indiquent que les origines de la dynamique des précipitations associée aux événements extrêmes El Niño peuvent être distinguées et que leurs patrons de téléconnection peuvent être raisonnablement compris (i.e. la réponse atmosphérique opposée montre différents patrons de convergence d'humidité entre l'événement de 2016 et les événements de 1983 et 1998 (qui sont similaires), ce qui permet de comprendre les origines dynamiques des principaux modes de variabilité de la pluie le long du PPB.

La thèse fournit aussi des lignes directrices pour comprendre le rôle du transport de l'humidité et de la circulation atmosphérique régionale et à grande échelle générant deux patrons de pluie qui ont des implications différentes dans la prédiction des pluies du PPB lors des forts événements El Niño. Ce qui permet également de déterminer des voies de transport de l'humidité qui peuvent ainsi aider à informer les parties intéressées sur la localisation des pluies extrêmes afin de mieux gérer la prévention des inondations et des glissements de terrain. Cette thèse présente également une manière d'observer les précipitations extrêmes du point de vue du transport de l'humidité atmosphérique.

Dans le second chapitre de la thèse, en plus de déterminer la variabilité des pluies et de comprendre l'évolution des celles-ci pendant les forts événements El Niño, nous avons aussi modélisé la relation entre précipitations et SST en tenant compte de l'évolution non linéaire de l'ENSO en considérant les régimes ENSO EP et CP. Cela nous a permis d'améliorer la connaissance sur les influences des deux régime El Niño et d'identifier comment les deux régimes peuvent établir un patron de téléconnection spécifique qui affecte la variabilité des précipitations et produit différents patrons de précipitation.

Dans le troisième chapitre, nous montrons que ERA-Interim est le produit de réanalyses qui donne les meilleures performances pour reproduire la variabilité des précipitations dans le PPB en termes de structure spatiale (mode Ep et Cp). Il est également montré, dans l'analyse de la convergence du transport de l'humidité sur une période de 37 ans qu'il donne aussi des résultats cohérents avec les précipitations observées et qu'il est donc un outil adapté pour les futures études hydrologiques dans le PPB.

Dans le quatrième chapitre, les résultats concluent que les différents patrons pluviométriques sont associés à des réponses atmosphériques différentes dues à des patrons de convergence d'humidité déphasées qui présentent des dynamiques distinctes, bien qu'ils commencent avec une source commune (El Niño 3.4) du vecteur de circulation à grande échelle. Les différents patrons de précipitations dépendent principalement du transport d'humidité à grande échelle et de leur interaction avec les circulations régionales. Tous ces mécanismes atmosphériques aident à comprendre les processus qui contrôlent la variabilité de chaque mode de pluie.

5.2 PERSPECTIVES

Etudier la complexité des événements El Niño forts associés aux précipitations dans le PPB nécessite de considérer et mieux comprendre :

- D'autres facteurs expliquant les différences entre les événements en incluant les processus distincts associés à la variabilité synoptique due aussi bien à l'oscillation de Madden-Julian (Madden et Julian, 1972) qu'à l'activité de tempête extra-tropicale des latitudes moyennes qui influent sur les vents côtiers le long de la côte péruvienne (Dewitte et al., 2011) ou le mode méridional du Pacifique Sud (Zhang et al., 2014). Nous avons analysé l'évolution de la MJO lors de trois des quatre forts événements El Niño (Figure S1). Ces trois événements montrent une évolution différente. Alors que l'épisode El Niño de 1997/98 était associé à une activité MJO positive anormale avant son pic, les événements El Niño de 1982/1983 et 2015/2016 ne l'ont pas été. En ce qui concerne les événements El Niño de

1982/1983 et 1997/1998, ceci est cohérent avec études précédentes (Tang et Yu, 2008, Gushchina et Dewitte, 2012).

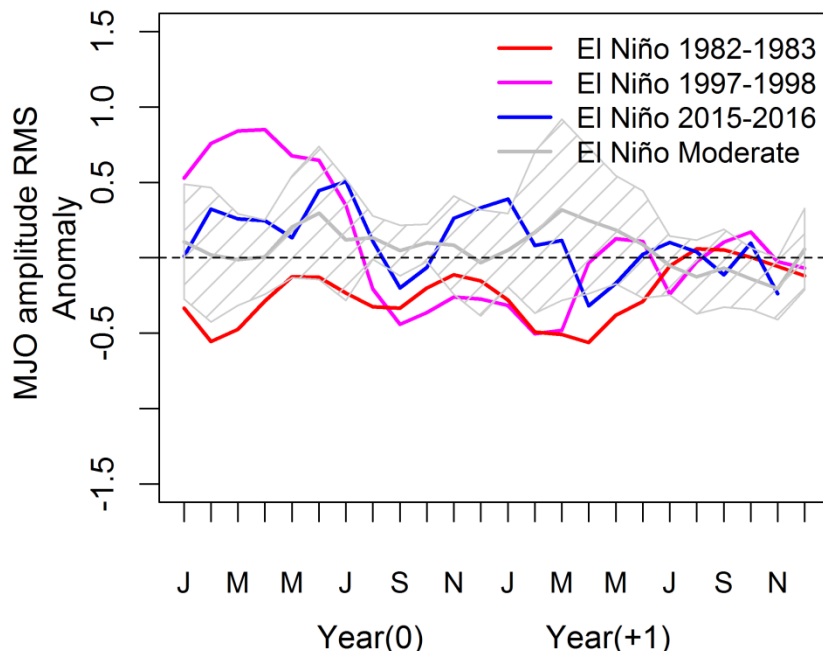


Figure S1. Evolution des anomalies de l'activité MJO pour les événements El Niño forts de 1982/1983, 1997/1998 and 2015/2016. L'activité MJO est définie par variance glissante sur 3 mois de l'indice RMM (journalier) définie par Wheeler and Hendon (2004). Les anomalies de l'activité de la MJO sont relatives au cycle moyen saisonnier sur la période 1980-2015. L'évolution moyenne pour les El Niño modérés est aussi montrée en regard avec la dispersion entre les événements. Les données sont issues de <https://iri.ldeo.columbia.edu/SOURCES/.BoM/.MJO/.RMM/>

Les différences d'activité de la MJO entre les événements sont cohérentes avec les différences de précipitations au Pérou, en supposant que MJO est influent. Cependant, les processus qui relient l'activité MJO aux précipitations au Pérou ne sont pas directs. L'activité MJO peut avoir un impact sur l'activité des ondes Kelvin océaniques qui conduit au réchauffement de la côte du Pérou, bien qu'un pic MJO n'implique pas nécessairement un stress de vent anormal (Rafale de vent d'ouest) qui force une onde de Kelvin. Les MJO pourraient également influencer la circulation troposphérique sur le Pérou et réduire la stratification de la température, ce qui favoriserait la convection profonde. Il peut également influencer la circulation atmosphérique dans les latitudes moyennes et moduler l'anticyclone du Pacifique Sud (Dewitte et al., 2011 ; Rahn, 2012).

- L'interaction de l'oscillation quasi-biennale (QBO) et de la circulation de type Hadley (Salby et Callaghan, 2007), qui semble bien décrite dans les changements de vents de niveau supérieur (100 à 300 hPa) devrait être réservée aux recherches futures. Les références suggèrent que les changements de vent pourraient être liés aux différences de libération de chaleur latente associées à la convection profonde tropicale (Ho et al., 2009, Liess et Geller, 2012). L'amplitude de convection profonde tropicale associée à la MJO est modulée par la QBO plus que par l'ENSO (Son et al., 2016). L'activité MJO devient plus forte et plus organisée pendant la QBO d'Est (Son et al., 2017, Hood, 2017) qui est influencée par le cycle solaire de 11 ans (Nishimoto et Yoden 2017).
- On pense également que des processus locaux d'interactions air-mer doivent être activés lors d'événements El Niño dans cette région (B. Dewitte, 2017). Ces processus comprennent l'évaluation de la contribution de l'humidité par des effets locaux de la circulation vent de mer-mer (Horel et Cornejo, 1986, Goldberg et al., 1987, Bendix, 2000) et la convection par élévation orographique (Takahashi, 2004, Douglas et al., 2009). Cependant, les anomalies SST locales ne sont probablement pas le seul facteur influençant les conditions pluviométriques lors d'événements El Niño forts (Takahashi et Martinez, 2017). Notre étude appelle à étudier la sensibilité de la distribution et de l'évolution des précipitations aux conditions océaniques régionales, ce qui pourrait être fait à travers de l'utilisation d'un modèle atmosphérique régional. De même, un aspect qui n'est actuellement pas bien pris en compte dans les modèles couplés globaux sont les anomalies régionales de la SST le long des côtes du Pérou et de l'Équateur (Takahashi et al., 2014), ce qui appelle à étudier les processus physiques régionaux expliquant une réponse diverse de pluie dans des conditions fortes El Niño, et en considérant aussi l'impact probable de la variabilité décennale sur la relation entre l'ENSO et les précipitations au Pérou (Bourrel et al., 2015 ; Segura et al., 2016).

BIBLIOGRAPHY

Aceituno P. 1988. On the functioning of the Southern Oscillation in the South American sector. Part I: surface climate. *Monthly Weather Review* 116: 505–524.

Ahrens D, Henson R. 2009. Meteorology today. An introduction to weather, climate and the environment. USA. pp 277.

Albuquerque de Almeida V, Marton E, Nunes AMB. 2018. Assessing the ability of three global reanalysis products to reproduce South American monsoon precipitation. *Atmósfera* 31(1): 1–10. DOI: 10.20937/ATM.2018.31.01.01.

Allan RP, Lavers DA, Champion AJ. 2016. Diagnosing links between atmospheric moisture and extreme daily precipitation over the UK. *International Journal of Climatology* 36(9): 3191–3206. DOI: 10.1002/joc.4547.

Ambrizzi TE, de Souza B, Pulwarty SR. 2005. The Hadley and Walker regional circulations and associated ENSO impacts on South American seasonal rainfall, in Hadley Circulation: Present, Past and Future. Edited by Diaz HF and Bradley RS. pp 203-235.

American Meteorological Society (AMS). 2013. Glossary of Meteorology. <http://glossary.ametsoc.org/wiki/El Ni%C3%B1o>

ANA. 2012. Recursos Hídricos en el Perú. 2nd edn. Ministerio de Agricultura. Autoridad Nacional del Agua, Lima; pp 45-189.

Andreoli RV, de Oliveira SS, Kayano MT, Viegas J, de Souza RAF, Candido LA. 2016. The influence of different El Niño types on the South American rainfall. *International Journal of Climatology*. DOI: 10.1002/joc.4783.

Angélil O, Perkins-Kirkpatrick S, Alexander L V., Stone D, Donat MG, Wehner M, Shiogama H, Ciavarella A, Christidis N. 2016. Comparing regional precipitation and temperature extremes in climate model and reanalysis products. *Weather and Climate Extremes*. Elsevier 13: 35–43. DOI: 10.1016/j.wace.2016.07.001.

Ashok KS, Behera K, Rao SA, Weng H, and Yamagata T. 2007. El Niño Modoki and its possible teleconnections. *Journal of Geophysical Research.*, 112, C11007, doi:10.1029/2006JC003798.

Ashok K and Yamagata T. 2009. Climate change: El Niño with a difference. *Nature* 461:481-484. doi:10.1038/461481

Banacos PC, Schultz DM (2005) The use of moisture flux convergence in forecasting convective initiation: historical and operational perspectives. *Weather Forecast* 20:351–366.

Barnston AG, Chelliah M, Goldenberg SB. 1997. Documentation of a highly ENSO-related SST region in the equatorial Pacific. *Atmosphere-Ocean*. 35: 367-383.

Barsugli JJ, Sardeshmukh PD. 2002. Global atmospheric sensitivity to tropical SST anomalies throughout the Indo-Pacific basin. *Journal of Climate*. 15(23): 3427–3442.

Bazo J, Lorenzo MDLN, Porfirio Da Rocha R. 2013. Relationship between monthly rainfall in NW Peru and tropical sea surface temperature. *Advances in Meteorology*. DOI: 10.1155/2013/152875.

BCRP 2016. Actividad Económica (Marzo, abril y setiembre). Banco Central de Reserva del Perú (Central Reserve Bank of Peru). *Notas de Estudio* 35: 2-3,43: 2-3 y 80: 2-4.

Blázquez J, Solman SA. 2017. Interannual variability of the frontal activity in the Southern Hemisphere: relationship with atmospheric circulation and precipitation over southern South America. *Climate Dynamics*. Springer Berlin Heidelberg 48(7–8): 2569–2579. DOI: 10.1007/s00382-016-3223-3.

Bell GD, Halpert MS, Ropelewski CF, Kousky VE, Douglas AV, Schnell RC, Gelman ME. 1999. Climate assessment for 1998. *Bulletin of the American Meteorological Society* 80: S1–S48.

Bendix J and Bendix A. 1998. Climatological aspects of the 1991/1993 El Niño in Ecuador. *Bull. Inst. fr. etudes andines*. 27 (3): 655–666.

Bendix J, Bendix A, Richter M. 2000. El Niño 1997/98 in northern Peru: An indication for a change of the ecosystem. (in German). *Peterm. Geogr. Mit.*, 144, H. 4: 20–31.

Bendix A, Bendix J. 2006. Heavy rainfall episodes in Ecuador during El Niño events and associated regional atmospheric circulation and SST patterns. *Advances in Geosciences*. 6: 43–49.

Bjerknes JA. (1966). Possible response of the atmospheric Hadley Circulation to equatorial anomalies of ocean temperature. *Tellus*, 97: 820–829.

Bjerknes J. 1969. Atmospheric teleconnections from the equatorial Pacific. *Monthly Weather Review* 97:163–172.

Blacutt LA, Herdies DL, de Gonçalves LGG, Vila DA, Andrade M. 2015. Precipitation comparison for the CFSR, MERRA, TRMM3B42 and Combined Scheme datasets in Bolivia. *Atmospheric Research*. The Authors 163: 117–131. DOI: 10.1016/j.atmosres.2015.02.002.

Boers N, Donner R V., Bookhagen B, Kurths J. 2014. Complex network analysis helps to identify impacts of the El Niño Southern Oscillation on moisture divergence in South America. *Climate Dynamics*. DOI: 10.1007/s00382-014-2265-7.

Borlace S, Santoso A, Cai W, & Collins M. 2014. Extreme swings of the South Pacific convergence zone and the different types of el Niño events. *Geophysical Research Letters*, 41, 4695–4703. <https://doi.org/10.1002/2014GL060551>

Bosilovich MG, Chern JD, Mocko D, Robertson FR, Da Silva AM. 2015. Evaluating observation influence on regional water budgets in reanalyses. *Journal of Climate*, 28(9): 3631–3649. doi:10.1175/JCLI-D-14-00623.1.

Bourrel L, Rau P, Dewitte B, Labat D, Lavado W, Coutaud A, Vera A, Alvarado A, Ordoñez J. 2015. Low-frequency modulation and trend of the relationship between ENSO and precipitation along the northern to centre Peruvian Pacific coast. *Hydrological Processes* 29(6): 1252–1266.

Cai W, Borlace S, Lengaigne M, van Renssch P, Collins M, Vecchi G, Timmermann A, Santoso A, McPhaden MJ, Wu L, England MH, Wang G, Guilyardi E, Jin F-F. 2014. Increasing frequency of extreme El Niño events due to greenhouse warming. *Nature Climate Change* 5(2): 1–6. DOI: 10.1038/nclimate2100.

Cane MA. 1983. Oceanographic events during El Niño. *Science* 222(4629):1189–1195

Capotondi A, Wittenberg AT, Newman M, Di Lorenzo E, Yu J-Y, Bra- connot P, Cole J, Dewitte B, Giese B, Guilyardi E, Jin F-F, Kar- nauskas K, Kirtman B, Lee T, Schneider N, Xue Y, Yeh S-W. 2015. Understanding ENSO diversity. *Bulletin of the American Meteorological Society*. 96(June): 921–938.

Carvalho LMV, Jones C, Liebmann B. 2004. The south Atlantic convergence zone: intensity, form, persistence, and relationships with intra-seasonal to inter-annual activity and extreme rainfall. *Journal of Climate*. 17: 88–108. [https://doi.org/10.1175/1520-0442\(2004\)017,0088:TSACZI.2.0.CO;2](https://doi.org/10.1175/1520-0442(2004)017,0088:TSACZI.2.0.CO;2).

Castillo R, Nieto R, Drumond A, Gimeno L. 2014. Transport From Major Oceanic Moisture Sources. 2014. *Water Resources Research*. 50(2): 1–13. DOI: 10.1002/2013WR013900.

Castro LC, McKee TB, Pielke RA (2001) The relationship of the North American monsoon to tropical and North Pacific sea surface temperature as revealed by observational analysis. *Journal of Climate*. 14:4449-4473.

Castro LC, Pielke RA, Adegoke JO, Shubert SD, Pegan PJ (2007) Investigation of the summer climate of the contiguous U.S. and Mexico Using the regional Atmospheric Modeling System (RAMS). Part II: Model Climate variability. *Journal of Climate*. 20:3866-3887.

Cheng H, Sinha A, Cruz FW, Wang X, Edwards RL, d' Horta FM, Ribas CC, Vuille M, Stott LD, Auler AS. 2013. Climate change patterns in Amazonia and biodiversity Nat. Commun. 4: 1411. doi:10.1038/ncomms2415.

Clarke AJ. 1983. The reflection of equatorial waves from oceanic boundaries. *Journal of Physical Oceanography*. 13(7): 1193–1207. Cressman GP. 1959. An operational objective

Compo, G.P. & coauthors, 2011: The Twentieth Century Reanalysis Project. *Quarterly Journal of the Royal Meteorological Society*. 137: 1-28. doi: 10.1002/qj.776.

Cook KH. 2009. South American climate variability and change: Remote and regional forcing processes. In *Past Climate Variability in South America and Surrounding Regions: From the last Glacial Maximum to the Holocene*. F. Vimeux, F. Sylvestre, and M. Khodri, Eds., Springer.

Curtis, S and Hastenrath S. 1995. Forcing of anomalous sea surface temperature evolution in the tropical Atlantic during Pacific warm events. *Journal of Geophysical Research. Oceans*. 100: 15835-15847.

Dai A and Wigley TM L (2000). Global patterns of ENSO-induced precipitation. *Geophysical Research Letters*. 27:1283–1286.

Dacre HF, Clark PA, Martinez-Alvarado O, Stringer MA, Lavers DA. 2014. How do atmospheric rivers form? *Bulletin of the American Meteorological Society* 96: 1243–1255, doi: 10.1175/bams-d-14-00031.1.

Dee D P, Uppala S M, Simmons A J, Berrisford P, Poli P, Kobayashi S, Andrae U, Balmaseda M A, Balsamo G, Bauer P, Bechtold P, Beljaars A C M, van de Berg L, Bidlot J, Bormann N, Delsol C, Dragani R, Fuentes M, Geer A J, Haimberger L, Healy S B, Hersbach H, Hólm E V, Isaksen L, Källberg P, Köhler M, Matricardi M, McNally A P, Monge-Sanz B M, Morcrette J J, Park B K, Peubey C, de Rosnay P, Tavolato C, Thépaut J N, Vitart F. 2011. The ERA-Interim reanalysis: Configuration and performance of the data assimilation system. *Q J R Meteorol Soc*, 137: 553–597.

De Souza EB, Ambrizzi T. 2002: ENSO impacts on the South American rainfall during 1980s: Hadley and Walker circulation. *Atmósfera*, 15, 105-120.

Dewitte B, Illig S, Renault L, Goubanova K, Takahashi K, Gushchina D, Mosquera K, Purca S. 2011. Modes of covariability between sea surface temperature and wind stress intraseasonal anomalies along the coast of Peru from satellite observations (2000-2008). *Journal of Geophysical Research*, 116, C04028, doi:10.1029/2010JC006495.

Dewitte B, Giese B, Guilyardi E, Jin F-F, Kar-nauskas K, Kirtman B, Lee T, Schneider N, Xue Y, Yeh S-W. 2015. Understanding ENSO diversity. *Bulletin of the American Meteorological Society* 96(June): 921–938.

Dewitte B, Takahashi K. 2017. Diversity of moderate El Niño events evolution: role of air-sea interactions in the eastern tropical Pacific. *Climate Dynamics*, 0(0), 1–22. <https://doi.org/10.1007/s00382-017-4051-9>.

Diaz HF, Hoerling MP, Eischeid JK. 2001. ENSO variability, telecon- nections and climate change climate variability; El Niño-Southern Oscillation (ENSO); teleconnections. *International Journal of Climatology*. 21(15): 1845–1862.

Dirmeyer PA, and Brubaker KL. 2007. Characterization of the global hydrologic cycle from a back-trajectory analysis of atmospheric water vapor. *Journal of Hydrometeorology*. 8:20–37. doi:10.1175/JHM557.1

Donat MG, Sillmann J, Wild S, Alexander L, Lippmann T, Zwiers FW. 2014. Consistency of temperature and precipitation extremes across various global gridded in situ and reanalysis datasets. *Journal of Climate*. doi:10.1175/JCLI-D-13-00405.1

Douglas MW, Mejia J, Ordinola N, Boustead J. 2009. Synoptic variability of rainfall and cloudiness along the coasts of Northern Peru and Ecuador during the 1997/98 El Niño event. *Monthly Weather Review*. 137: 116 – 136.

Drumond A, Marengo J, Ambrizzi T, Nieto R, Moreira L, Gimeno L. 2014. The role of the Amazon Basin moisture in the atmospheric branch of the hydrological cycle: A Lagrangian analysis. *Hydrology and Earth System Sciences* 18(7): 2577–2598. DOI: 10.5194/hess-18-2577-2014.

Eichler TP, Londoño AC. 2013. South American climatology and impacts of El Niño in NCEP's CFSR data. *Advances in Meteorology* 2013. DOI: 10.1155/2013/492630.

Edwards PN. 2010. Avast Machine: Computer Models, Climate Data and the Politics of Global Warming. Cambridge, MA: MIT Press.

Falvey M, Garreaud R, 2005. Moisture variability over the South American Altiplano during the SALLJEX observing season. *Journal of Geophysical Research*. 110: D22105. doi:10.1029/2005JD006152.

Ferreira RN, Rickenbach TM, Herdies DL, Carvalho LM V. 2003. Variability of South American Convective Cloud Systems and Tropospheric Circulation during January–March 1998 and 1999. *Monthly Weather Review* 131(5): 961–973. DOI: 10.1175/1520-0493(2003)131<0961:VOSACC>2.0.CO;2.

Flantua SGA, Hooghiemstra H, Vuille M, Behling H, Carson JF, Gosling WD, Hoyos I, Ledru MP, Montoya E, Mayle F, Maldonado A, Rull V, Tonello MS, Whitney BS, González-Arango C. 2016. Climate variability and human impact on the environment in South America during the last 2000 years: synthesis and perspectives. *Climate of the Past Discussions*. 12, 483–523, doi:10.5194/cp-12-483-2016, 2016.

Frauen C, Dommelget D. 2010. El Niño and la Niña amplitude asymmetry caused by

atmospheric feedbacks. *Geophysical Research Letters* 37(18): 1–6. DOI: 10.1029/2010GL044444.

Frauen C, Dommelget D, Tyrrell N, Rezny M, Wales S. 2014. Analysis of the nonlinearity of El Niño-Southern Oscillation teleconnections. *Journal of Climate*. 27(16): 6225–6244.

Garreaud RD. 1999. Multiscale analysis of the summertime precipitation over the central Andes. *Monthly Weather Review*. 127: 901–921. doi:10.1175/1520-0493(1999)127,0901:MAOTSP.2.0.CO;2.

Garreaud RD. 2000. Intraseasonal variability of moisture and rainfall over the South American Altiplano. *Monthly Weather Review*. 128: 3337–3346. doi:10.1175/1520-0493(2000)128,3337:IVOMAR.2.0.CO;2.

Garreaud RD, Vuille M, Clement AC. 2003. The climate of the Altiplano: Observed current conditions and mechanisms of past changes. *Palaeogeogr., Palaeoclimatol., Palaeoecol.*, 194: 5–22. doi:10.1016/S0031-0182(03)00269-4.

Garreaud R, Aceituno P. 2007. Atmospheric circulation and climatic variability. In: Veblen TT, Young KR, Orme AR (eds) *The physical geography of South America*. Oxford University Press, Oxford.

Garreaud R, Vuille M, Compagnucci R, Marengo, J. 2009. Present-day South American climate. *Paleo3*. doi:10.1016/j.paleo.

Giannini A, Chiang JC, Cane H, Kushnir MA, Seager R. 2001. The ENSO teleconnection to the tropical Atlantic Ocean: contributions of the remote and local SSTs to rainfall variability in the tropical Americas. *Journal of Climate*. 14: 4530–4544.

Gill AE. 1980. Some simple solutions for heat-induced tropical circulation. *Quarterly Journal of the Royal Meteorological Society*, 106: 447–462. <https://doi.org/10.1002/qj.49710644905>.

Gimeno L, Dominguez F, Nieto R, Trigo R, Drumond A, Reason CJC, Kumar R, Marengo J. 2016. Major Mechanisms of Atmospheric Moisture Transport and their Role in Extreme Precipitation Events Major Mechanisms of Atmospheric Moisture Transport and their Role in Extreme Precipitation Events. (June). DOI: 10.1146/annurev-environ-110615-085558

Gimeno L, Drumond A, Nieto R, Trigo RM, Stohl A. 2010. On the origin of continental precipitation. *Geophysical Research Letters*, 37: L13804. doi:10.1029/2010GL043712.

Gimeno L, Stohl A, Trigo RM, Dominguez F, Yoshimura K., Yu L., ... Nieto R. 2012. Oceanic and terrestrial sources of continental precipitation. *Reviews of Geophysics*. 50(4): 1–41. <https://doi.org/10.1029/2012RG000389>.

Gimeno L. 2014. Oceanic sources of continental precipitation. *Water Resources Research* 50. doi:10.1002/2014WR015477.

Goddard L, Mason SJ, Zebiak SE, Ropelewski CF, Basher R, Cane MA, Jolla L. 2001. Current Approaches To Seasonal-To-Interannual. 1152: 1111–1152.

Goldberg RA, Tisnado GM, Scofield RA. 1987. Characteristics of extreme rainfall events in northwestern Peru during the 1982-1983 El Niño period. *Journal of Geophysical Research*. 92(C13): 14225–14241.

Grimm AM, Ferraz S, Gomez J. 1998. Precipitation anomalies in southern Brazil associated with El Niño and La Niña events. *Journal of Climate*, 11:2863–2880.

Grimm AM, Barros VR, Doyle ME (2000) Climate variability in Southern South America associated with El Niño and La Niña events. *Journal of Climate* 13: 35–58

Grimm AM. 2003. The El Niño impact on the summer monsoon in Brazil: Regional processes versus remote Influences. *Journal of Climate*. 16: 263-280.

Grimm AM. 2004. How do La Niña events disturb the summer monsoon system in Brazil? *Climate Dynamics* 22(2–3): 123–138. DOI: 10.1007/s00382-003-0368-7.

Grimm AM, Tedeschi RG. 2009. ENSO and extreme rainfall events in South America. *Journal of Climate* 22(7): 1589–1609. DOI: 10.1175/2008JCLI2429.1.

Gu G, Adler RF. 2016. Precipitation, temperature, and moisture transport variations associated with two distinct ENSO flavors during 1979–2014. *Climate Dynamics*. Springer Berlin Heidelberg. DOI: 10.1007/s00382-016-3462-3.

Gushchina D. and B. Dewitte, 2012: Intraseasonal tropical atmospheric variability associated with the two flavors of El Niño. *Monthly Weather Review*. 140(11): 3669-3681.

Harada Y, Kamahori H, Kobayashi C, Endo H, Kobayashi S, Ota Y, Onoda H, Onogi K, Miyaoka K, Takahashi K. 2016. The JRA-55 Reanalysis: Representation of Atmospheric Circulation and Climate Variability. *Journal of the Meteorological Society of Japan. Ser. II* 94(3): 269–302. DOI: 10.2151/jmsj.2016-015.

Hastenrath S. 1978. On modes of tropical circulation and climate anomalies. *Journal of the Atmospheric Sciences*. 35: 222–223.

Ho CH, Kim HS, Jeong JH, Son SW. 2009. Influence of stratospheric quasi-biennial oscillation on tropical cyclone tracks in western north Pacific, *Geophysical Research Letters*. 36: L06702. Doi:10.1029/ 2009GL037163.

Hoerling MP and Kumar A. 2002. Atmospheric response patterns associated with tropical forcing. *Journal of Climate*, 15, 2184–2203.

Holton J, Pyle J, Curry J. 2002. Encyclopedia of Atmospheric Science. Academic Press and Elsevier. London U. K. 1(1):2251-2257

Hood LL. 2017. QBO/solar modulation of the boreal winter Madden-Julian oscillation: A prediction for the coming solar minimum. *Geophysical Research Letters*. 44: 3849–3857. doi:10.1002/2017GL072832.

Horel JD, Wallace JM. 1981. Planetary-scale atmospheric phenomena associated with the Southern Oscillation. *Mon. Weather Rev.* 109: 813–829.

Horel JD, Cornejo Garrido A. 1986. Convection along the coast of northern Peru during 1983: Spatial and temporal variation of clouds and rainfall. *Monthly Weather Review* 114: 2091-2105.

Hoyos I, Dominguez F, Cañon-Barriga J, Martinez JA, Nieto R, Gimeno L, Dirmeyer PA. 2017. Moisture origin and transport processes in Colombia, northern South America. *Climate Dynamics*. Springer Berlin Heidelberg 0(0): 1–20. DOI: 10.1007/s00382-017-3653-6

Hu S, Fedorov AV. 2017. The extreme El Niño of 2015–2016: the role of westerly and easterly wind bursts, and preconditioning by the failed 2014 event. *Climate Dynamics*. Springer Berlin Heidelberg (123456789). DOI: 10.1007/s00382-017-3531-2.

Huang B, Thorne PW, Banzon VF, Boyer T, Chepurin G, Lawrimore JH, Menne MJ, Smith TM, Vose RS, Zhang HM. 2017. Extended reconstructed Sea surface temperature, Version 5 (ERSSTv5): Upgrades, validations, and intercomparisons. *Journal of Climate* **30**(20): 8179–8205. DOI: 10.1175/JCLI-D-16-0836.1.

Isaksen L, Bonavita M, Buizza R, Fisher M, Haseler J, Leutbecher M, Raynaud L. 2010. Ensemble of data assimilations at ECMWF. ECMWF Tech. Memo. 636, 45 pp. [Available online at <http://www.ecmwf.int/sites/default/files/elibrary/2010/10125-ensemble-data-assimilations-ecmwf.pdf>.]

Kalnay E, Kanamitsu M, Kistler R, Collins W, Deaven D, Gandin L, Iredell M, Saha S, White G, Woollen J, Zhu Y, Chelliah M, Ebisuzak W, Higgins W, Janowiak J, Mo KC, Ropelewski C, Wang J, Leetmaa A, Reynolds R, Jenne R, Joseph D. 1996. The NCEP/NCAR 40-year reanalysis project. *Bulletin of the American Meteorological Society* **77**(3): 437–471. doi:10.1175/1520-0477(1996)077<0437:TNYR>2.0.CO;2.

Kao HY, Yu JY. 2009. Contrasting eastern Pacific and central Pacific types of ENSO. *Journal of Climate*. **22**(3): 615–632.

Keshavamurty RN. 1982. Response of the atmosphere to sea surface temperature anomalies over the equatorial Pacific and the teleconnections of the Southern Oscillation. *Journal of the Atmospheric Sciences*. **39**: 1241–1259.

Knippertz P and Wernli H. 2010. A Lagrangian climatology of tropical moisture exports to the Northern Hemispheric extratropics. *Journal of Climate*, **23**, 987–1003.doi: 10.1175/2009JCLI3333.1.

Knippertz P, Wernli H, Glaser G. 2013. A global climatology of tropical moisture. *Journal of Climate*. **26**: 3031–3045. doi:10.1175/JCLI-D-12-00401.1.

Kobayashi S, Ota Y, Harada Y, Ebita A, Moriya M, Onoda H, Onogi K, Kamahori H, Kobayashi C, Endo H, Miyaoka K, Takahashi K. 2015. The JRA-55 Reanalysis:General specifications and basic characteristics. *Journal of the Meteorological Society of Japan*. **93**:5-48. doi:10.2151/jmsj.2015-001.

Kodoma Y. 1992. Large-scale common features of subtropical precipitation zones (the Baiu frontal zone, the SPCZ and the SACZ). Part I: characteristic of subtropical frontal zones. *Journal of the Meteorological Society of Japan*. **70**: 813–836.

Kousky VE, Kayano MT, Cavalcanti IFA. 1984. A review of the Southern Oscillation: oceanic–atmospheric circulation changes and related rain- fall anomalies. *Tellus* **36A**, 490–504.

Krishnamurthy V, Misra V. 2010. Observed ENSO teleconnections with the South American monsoon system. *Atmospheric Science Letters*. DOI: 10.1002/asl.245.

Kug JS, Jin FF, An SI. 2009. Two types of El Niño events: cold tongue El Niño and warm pool El Niño. *Journal of Climate*. **22**(6): 1499–1515.

Larkin NK and Harrison DE. 2005. On the definition of El Niño and associated seasonal average U.S. weather anomalies. *Geophysical Research Letters*, **32**, L13705, doi:10.1029/2005GL022738.

Lau KM, Zhou J. 2003. Anomalies of the South American summer monsoon associated with the 1997-99 El Niño -southern oscillation. *International Journal of Climatology* **23**(5): 529–539. DOI: 10.1002/joc.900.

Lavado WS, Ronchail J, Labat D, Espinoza JC, Guyot JL. 2012. Basin-scale analysis of rainfall and runoff in Peru (1969–2004): Pacific, Titicaca and Amazonas drainages. *Hydrological Sciences Journal* 57(4): 1–18.

Lavado W, Silvestre E, Felipe O, Bourrel L. 2013. ENSO impact on hydrology in Peru. *Advances in Geosciences* 11: 1–7, 2013.

Lavado W, Espinoza JC. 2014. Impactos de El Niño y La Niña en las lluvias del Perú. *Rev. Bras. Med.* 29: 171–182.

Lavers DA, Allan RP, Wood EF, Villarini G, Brayshaw DJ, Wade AJ. 2011. Winter floods in Britain are connected to atmospheric rivers. *Geophysical Research Letters*. 38, L23803. doi: 10.1029/2011GL049783.

Lavers DA, Villarini G. 2014. The relationship between daily European precipitation and measures of atmospheric water vapor transport. *International Journal of Climatology*. 35: 2187–2192, doi: 10.1002/joc.4119.

Lavers DA, Waliser DE, Ralph FM, Dettinger MD. 2016. Predictability of horizontal water vapor transport relative to precipitation: Enhancing situational awareness for forecasting western U.S. extreme precipitation and flooding. *Geophysical Research Letters*. 43(5):2275–2282. doi:10.1002/2016GL067765.Received.

L'Heureux. 2014. What is the El Niño–Southern Oscillation (ENSO) in a nutshell?. NOAA (Centre Prediction Climate). <https://www.climate.gov/news-features/blogs/enso/what-el-ni%C3%BCo%E2%80%93southern-oscillation-enso-nutshell>.

L'Heureux ML, Takahashi K, Watkins AB, Barnston AG, Becker EJ, Di Liberto TE, Gamble F, Gottschalck J, Halpert MS, Huang B, Mosquera-Vásquez K, Wittenberg AT. 2017. Observing and predicting the 2015–16 El Niño. *Bulletin of the American Meteorological Society* 98: 1363–1382. <https://doi.org/10.1175/BAMS-D-16-0009.1>

Lenters JD and Cook KH. 1997. On the origin of the Bolivian High and related circulation features of the South American climate. *Journal of the Atmospheric Sciences*. 54: 656–678.

Liebmann B, Kiladis G, Marengo J, Ambrizzi T, Glick J.D. 1999. Submonthly convective variability over South America and the South Atlantic Convergence Zone. *Journal of Climate* 11: 2898–2909.

Liebmann B, Marengo J. 2001. Interannual variability of the rainy season and rainfall in the Brazilian Amazon Basin. *Journal of Climate*. 14: 4308–4318.

Liebmann B, Mechoso CR. 2011. The South American Monsoon System. *The Global Monsoon System: Research and Forecast (2nd Edition)* 137–157.

Liess S, Geller MA. 2012. On the relationship between QBO and distribution of tropical deep convection. *Journal of Geophysical Research Atmospheres* 117(3): 1–12. DOI: 10.1029/2011JD016317,

Lin Y, Colle B, Yuter SE. 2013. Impact of moisture flux and freezing level on simulated orographic precipitation errors over the Pacific Northwest. *Journal of Hydrometeorology*. 14(1): 140–152. doi:10.1175/JHM-D-12-019.1.

Lorenz C, Kunstmann H. 2012. The hydrological cycle in three state-of-the-art reanalyses: Intercomparison and performance analysis. *Journal of Hydrometeorology* 13(5): 1397–1420. DOI: 10.1175/JHM-D-11-088.1

Marengo JA, Soares WR, Saulo C, Nicolini M. 2004. Climatology of the low-level east of the Andes as derived from the NCEP-NCAR reanalyses: characteristics and temporal variability. *Journal of Climate*. 17(12): 2261–2280. [https://doi.org/10.1175/1520-0442\(2004\)017<2261:COTLJE>2.0.CO;2](https://doi.org/10.1175/1520-0442(2004)017<2261:COTLJE>2.0.CO;2).

Marengo JA, Alves LM, Soares WR, Rodriguez DA, Camargo H, Riveros MP, Pablo AD. 2013., Two Contrasting Severe Seasonal Extremes in Tropical South America in 2012: Flood in Amazonia and Drought in Northeast Brazil, *Journal of Climate*, 26(22), 9137–9154.

Mason SJ, Goddard L. 2001. Probabilistic precipitation anomalies associated with ENSO. *Bulletin of the American Meteorological Society*. Soc. 82: 619–638

Mayer M, Trenberth KE, Haimberger L, Fasullo JT. 2013. The response of tropical atmospheric energy budgets to ENSO. *Journal of Climate* 26(13): 4710–4724. DOI: 10.1175/JCLI-D-12-00681.1.

McPhaden MJ, Zebiak SE, Glantz MH. 2006. ENSO as an intriguing concept in Earth Science, *Science*, 314, 1740–1745.

McPhaden MJ and Zhang XB. 2009. Asymmetry in zonal phase propagation of ENSO sea surface temperature anomalies. *Geophysical Research Letters*, 36, L13703. <https://doi.org/10.1029/2009GL038774>.

Moura AD, Shukla EJ. 1981. On the dynamics of the droughts in northeast Brazil: Observations, theory and numerical experiments with a general circulation model. *Journal of Atmospheric Science*. 38: 2653–2673.

Murphy RC. 1926. Oceanic and climatic phenomena along the west coast of South America during 1925. *Geographical Review*, 16, 26–64.

Navarra A, Ward MN, Miyakoda K. 1999. Tropical-wide teleconnections and oscillation. I: teleconnection indices and type I/II states. *Quarterly Journal of the Royal Meteorological Society* 125:2909–2935

Neiman PJ, Schick LJ, Ralph FM, Hughes M., and Wick, G. A. (2011). Flooding in western washington: the connection to atmospheric rivers. *Journal of Hydrometeorology*. 12, 1337–1358. doi: 10.1175/2011JHM1358.1

Nishimoto E and Yoden S.2017. Influence of the stratospheric Quasi-Biennial Oscillation on the Madden-Julian Oscillation during austral summer. *Journal of the Atmospheric Sciences*. doi:10.1175/JAS-D-16-0205.1, in press.

Onogi K, Tsutsui J, Koide H, Sakamoto M, Kobayashi S, Hatsushika H, Matsumoto T, Yamazaki N, Kamahori H, Takahashi K, Kadokura K, Wada K, Kato K, Oyama R, Ose T, Mannoji, Taira R. 2007. The JRA-25 Reanalysis. *Journal of the Meteorological Society of Japan*: 85: 369–432.

Paixao Veiga JA, Rao VB, Franchito SH. 2005. Heat and moisture budgets of the walker circulation and associated rainfall anomalies during El Niño events. *International Journal of Climatology* 25(2): 193–213. DOI: 10.1002/joc.1115.

Paek H, Yu J-Y, Qian C. 2017. Why were the 2015/16 and 1997/98 Extreme El Niños different? *Geophysical Research Letters* 1–9. DOI: 10.1002/2016GL071515.

Peixoto, J P and Oort AH. 1992. Physics of Climate. American Institute of Physics, MIT press:

San Diego, CA. 520 pp.

Philander SGH. 1983. El Niño Southern Oscillation phenomena. *Nature*, 302(5906), 295–301. <https://doi.org/10.1038/302295a0>

Philander SGH. 1985. El Niño and La Niña. *Journal of the Atmospheric Sciences*. Sci. 42: 2652–2662.

Pineda L, Ntegeka V, Willems P. 2013. Rainfall variability related to sea surface temperature anomalies in a Pacific-Andean basin into Ecuador and Peru. *Advances in Geosciences*. DOI: 10.5194/adgeo-33-53-2013.

Poli P, Poli P, Hersbach H, Tan DGH, Dee DP, Thepaut J-J, Simmons A, Peubey C, Laloyaux P, Komori T, Berrisford P, Dragani R, Trémolet Y, Hólm EV, Bonavita M, Isaksen L, Fisher M. 2013. The data assimilation system and initial performance evaluation of the ECMWF pilot reanalysis of the 20th-century assimilating surface observations only (ERA-20C). ECMWF ERA Rep. 14, 59 pp. [Available online at <http://www.ecmwf.int/en/elibrary/11699-data-assimilation-system-and-initial-performance-evaluation-ecmwf-pilot-reanalysis>.]

Poli P, Hersbach H, Berrisford P, Dee D, Simmons A, Laloyaux P. 2015. ERA-20C deterministic. ECMWF ERA Rep. 20, 48 pp. [Available online at <http://www.ecmwf.int/en/elibrary/11700-era-20c-deterministic>.]

Poli P, Hersbach H, Dee DP, Berrisford P, Simmons AJ, Vitart F, Laloyaux P, Tan DGH, Peubey C, Thépaut JN, Trémolet Y, Hólm E V., Bonavita M, Isaksen L, Fisher M. 2016. ERA-20C: An atmospheric reanalysis of the twentieth century. *Journal of Climate* 29(11): 4083–4097. DOI: 10.1175/JCLI-D-15-0556.1

Rahn DA. 2012. Influence of large scale oscillations on upwelling-favorable coastal wind off central Chile. 117(October): 1–11. DOI: 10.1029/2012JD018016.

Ralph FM, Neiman PJ and Wick G A. 2004. Satellite and CALJET aircraft observations of atmospheric rivers over the eastern North Pacific ocean during the winter of 1997/98. *Monthly Weather Review*. 132, 1721–1745. doi: 10.1175/1520-493(2004)132<1721:SACAOO>2.0.CO;2.

Rasmusson EM, Carpenter TH. 1982. Variations in tropical sea surface temperature and surface wind fields associated with the Southern Oscillation/El Niño. *Monthly Weather Review* 110: 354–384.

Rau P, Bourrel L, Labat D, Melo P, Dewitte B, Frappart F, Lavado W, Felipe O. 2017. Regionalization of rainfall over the Peruvian Pacific slope and coast. *International Journal of Climatology*. 37(1): 143–158.

Rienecker MM, Suarez MJ, Gelaro R, Todling R, Bacmeister J, Liu E, Bosilovich MG, Schubert SD, Takacs L, Kim GK, Bloom S, Chen J, Collins D, Conaty A, Da Silva A, Gu W, Joiner J, Koster RD, Lucchesi R, Molod A, Owens T, Pawson S, Pégion P, Redder CR, Reichle R, Robertson FR, Ruddick AG, Sienkiewicz M, Woollen J. 2011. MERRA: NASA's Modern-Era Retrospective Analysis for Research and Applications. *Journal of Climate*, 24, 3624–3648, doi:10.1175/JCLI-D-11-00015.1.

Robertson A, Mechoso C. 2000. Interannual and interdecadal variability of the South Atlantic convergence zone. *Monthly Weather Review*. 128: 2947–2957, doi: 10.1175/1520-0493(2000)128<2947:IAIVOT>2.0.CO;2.

Rome S, Ronchail J. 1998. La pluviométrie au Pérou pendant les phases ENSO et LNSO. *Bulletin de l'Institut Francaise d'Etudes Andines* 27: 675–685.

Ronchail J, Cochonneau G, Molinier M, Guyot J.-L, De Miranda Chaves AG, Guimarães V, de Oliveira E. 2002. Interannual rainfall variability in the Amazon basin and sea-surface temperatures in the equatorial Pacific and the tropical Atlantic oceans. *International Journal of Climatology*. 22: 1663–1686.

Ropelewski CF, Halpert MS. 1987. Global and regional scale precipitation patterns associated with El Niño/Southern Oscillation. *Monthly Weather Review*. 115: 1606–1626

Ropelewski CH, Halpert MS . 1989. Precipitation patterns associated with the high index phase of the Southern Oscillation. *Journal of Climate* 2: 268–284.

Ruiz-Barradas A, Kalnay E, Peña M, BozorgMagham AE, Motesharrei S. 2017. Finding the driver of local ocean–atmosphere coupling in reanalyses and CMIP5 climate models. *Climate Dynamics*. Springer Berlin Heidelberg 48(7–8): 2153–2172. DOI: 10.1007/s00382-016-3197-1.

Rundel PW, Dillon MO, Palma B, Mooney HA, Gulmon SL, Ehleringer JR. 1991. The phytogeography and ecology of the coastal Atacama and Peruvian deserts. *Alico*, 13, 1–50

Saha S, Moorthi S, Pan H L, Wu X, Wang J, Nadiga S, Tripp P, Kistler R, Woollen J, Behringer D, Liu H, Stokes D, Grumbine R, Gayno G, Wang J, Hou Y T, Chuang H Y, Juang H M, Sela J, Iredell M, Treadon R, Kleist D, Van Delst P, Keyser D, Derber J, Ek M, Meng J, Wei H, Yang R, Lord S, Van den Dool H, Kumar A, Wang W, Long C, Chel- liah M, Xue Y, Huang B, Schemm J K, Ebisuzaki W, Lin R, Xie P, Chen M, Zhou S, Higgins W, Zou C Z, Liu Q, Chen Y, Han Y, Cucu- rull L, Reynolds R W, Rutledge G, Goldberg M. 2010. The NCEP climate forecast system reanalysis. *Bulletin of the American Meteorological Society*, 91: 1015–1057.

Saha S, Moorthi S, Wu X, Wang J, Nadiga S, Tripp P, Behringer D, Hou YT, Chuang HY, Iredell M, Ek M, Meng J, Yang R, Mendez MP, Van Den Dool H, Zhang Q, Wang W, Chen M, Becker E. 2014. The NCEP climate forecast system version 2. *Journal of Climate*, 27(6): 2185–2208. doi:10.1175/JCLI-D-12-00823.1.

Salby ML, Callaghan PF. 2007. Interaction between the QBO and the Hadley circulation: Evidence of solar influence? *Journal of Climate* 20(8): 1583–1592. DOI: 10.1175/JCLI4076.1.

Sanabria J, Bourrel L, Dewitte B, Frappart F, Rau P, Solis O, Labat D. 2018. Rainfall along the coast of Peru during strong El Niño events. *International Journal of Climatology*. 38: 1737–1747.

Santoso A, McPhaden MJ, Cai W. 2017. The Defining Characteristics of ENSO Extremes and the Strong 2015/2016 El Niño. *Reviews of Geophysics* 55(4): 1079–1129. DOI: 10.1002/2017RG000560.

Saulo AC, Nicolini M, Chou SC. 2000. Model characterization of the South American low-level flow during the 1997–98 spring–summer season. *Climate Dynamics*. 16: 867–881.

Saurral RI, Camilloni IA, Ambrizzi T. 2014. Links between topography, moisture fluxes pathways and precipitation over South America. *Climate Dynamics*. Springer Berlin Heidelberg 777–789. DOI: 10.1007/s00382-014-2309-z.

Seager R, Naik N, Vecchi GA. 2010. Thermodynamic and dynamic mechanisms for large-scale changes in the hydrological cycle in response to global warming. *Journal of Climate* 23(17): 4651–4668. DOI: 10.1175/2010JCLI3655.1

Segura H, Espinoza JC, Junquas C, Takahashi K. 2016. Evidencing decadal and interdecadal hydroclimatic variability over the Central Andes. *Environmental Research Letters*. IOP Publishing 11(9): 1–8. DOI: 10.1088/1748-9326/11/9/094016.

Shimizu, M. H., Ambrizzi, T., & Liebmann, B. (2016). Extreme precipitation events and their relationship with ENSO and MJO phases over northern South America. *International Journal of Climatology*. <https://doi.org/10.1002/joc.4893>

Schneider T, Bischoff T, Haug GH. 2014. Migrations and dynamics of the intertropical convergence zone. *Nature*. Nature Publishing Group 513(7516): 45–53. DOI: 10.1038/nature13636.

Silva Dias PL, Schubert WH, DeMaria M. 1983. Large-scale response of the tropical atmosphere to transient convection. *Journal of the Atmospheric Sciences* 40: 2689–2707.

Silva GAM, Ambrizzi T. 2006. Inter-El Niño variability and its impact on the South American low-level jet east of the Andes during austral summer – two case studies. *Advances in Geosciences*. 6: 283–287. <https://doi.org/10.1680/adgeo.20006.6-283>.

Silva GAM, Ambrizzi T, Marengo JA. 2009. Observational evidences on the modulation of the South American low level jet east of the Andes according the ENSO variability. *Annals of Geophysics*. 27: 645–657.

Silva VBS, Kousky VE, Higgins RW. 2011. Daily precipitation statistics for South America: an intercomparison between NCEP reanalyses and observations. *Journal of Hydrometeorology*. 12: 101–117. <http://dx.doi.org/10.1175/2010JHM1303.1>.

Solman SA, Sanchez E, Samuelsson P, da Rocha RP, Li L, Marengo J, Pessacq NL, Remedio ARC, Chou SC, Berbery H, Le Treut H, de Castro M, Jacob D. 2013. Evaluation of an ensemble of regional climate model simulations over South America driven by the ERA-Interim reanalysis: Model performance and uncertainties. *Climate Dynamics* 41(5-6): 1139–1157. DOI: 10.1007/s00382-013-1667-2.

Son S, Lim Y, Yoo C, Hendon H, Kim J. 2016: Stratospheric control of Madden Julian Oscillation. *J. Climate*. doi:10.1175/JCLI-D-16-0620.1, in press.

Stephens DJ, Meuleners MJ, van Loon H, Lamond MH, Telcik NP. 2007. Differences in atmospheric circulation between the development of weak and strong warm events in the Southern Oscillation. *Journal of Climate* 20(10): 2191–2209. DOI: 10.1175/JCLI4131.1.

Sulca J, Takahashi K, Espinoza J, Vuille M, Lavado W. 2017. Impacts of ENSO flavors and tropical Pacific convection variability (ITCZ, SPCZ) on austral summer rainfall in South America focused on Peru. . DOI: 10.1002/joc.5185

Swales D, Alexander M., Hughes M.. 2016. Examining moisture pathways and extreme precipitation in the U.S. Intermountain West using self-organizing maps. *Geophysical Research Letters*. 43(4): 1727–1735. doi:10.1002/2015GL067478.

Takahashi K. 2004. The atmospheric circulation associated with extreme rainfall events in Piura, Peru, during the 1997–1998 and 2002 El Niño events. *Annales Geophysicae*, 22(11), 3917–3926. <https://doi.org/10.5194/angeo-22-3917-2004>

Takahashi K, Battisti DS. 2007. Processes controlling the mean tropical Pacific precipitation pattern. Part II: The SPCZ and the Southeast Pacific dry zone. *Journal of Climate*. <https://doi.org/10.1175/2007JCLI1656.1>

Takahashi K, Montecinos A, Goubanova K, Dewitte B. 2011. ENSO regimes: Reinterpreting

the canonical and Modoki El Niño. *Research Letters Geophysical*. <https://doi.org/10.1029/2011GL047364>

Takahashi K, Dewitte B. 2016. Strong and moderate nonlinear El Niño regimes. *Climate dynamics* <https://doi.org/10.1007/s00382-015-2665-3>.

Takahashi K, Martinez AG. 2017. The very strong El Niño in 1925 in the far-eastern Pacific. *Climate Dynamics*. <https://doi.org/10.1007/s00382-017-3702-1>.

Tang Y, Yu B. 2008. MJO and its relationship to ENSO. *Journal of Geophysical Research Atmospheres* 113(14): 1–18. DOI: 10.1029/2007JD009230.

Tapley TD, Waylen PR. 1990. Spatial variability of annual precipitation and ENSO events in western Peru. *Hydrological Sciences Journal*. 35(4): 429–446.

Tedeschi RG, Cavalcanti IFA, Grimm AM. 2013. Influences of two types of ENSO on South American precipitation. *International Journal of Climatology* 33(6): 1382–1400. DOI: 10.1002/joc.3519.

Torralba V, Rodríguez-Fonseca B, Mohino E, Losada T. 2015. The non-stationary influence of the Atlantic and Pacific Niños on North Eastern South American rainfall. *Frontiers in Earth Science* 3(September): 1–10. DOI: 10.3389/feart.2015.00055.

Trenberth KE, Branstator GW, Karoly D, Kumar A, Lau N-C, Ropelewski C. 1997. Progress during TOGA in understanding and modeling global teleconnections associated with tropical sea surface temperatures. *Journal of Geophysical Research*. 103:14291–14324.

Trenberth KE, Branstator GW, Karoly D, Kumar A, Lau N, Ropelewski C. 1998. Progress during TOGA in understanding and modelling global teleconnections associated with tropical sea surface temperatures. *Journal of Geophysical Research*. 103(C7): 14291–14324.

Trenberth KE, Stepaniak DP. 2001. Indices of El Niño evolution. *Journal of Climate*, 14, 1697–1701, doi:10.1175/1520-0442(2001)014,1697:LIOENO.2.0.CO;2.

Trenberth KE, Smith L. 2009. Variations in the three-dimensional structure of the atmospheric circulation with different flavors of El Niño. *Journal of Climate* 22:2978–2991. doi:10.1175/2008JCLI2691.1.

Trenberth K E, Fasullo J T, Mackaro J. 2011. Atmospheric moisture transports from ocean to land and global energy flows in reanalyses. *Journal of Climate*, 24: 4907–4924. DOI: 10.1175/2011JCLI4171.1.

Uppala SM, Källberg PW, Simmons AJ, Andrae U, Bechtold V, Fiorino M, Woollen J. 2005. The ERA-40 Re-Analysis. *Quart. J. Roy. Meteor. Soc.*, 131:2961–3012.

Van der Wiel K, Matthews AJ, Joshi MM, Stevens DP. 2016. Why the south Pacific convergence zone is diagonal. *Climate Dynamics*. 46: 1683–1698. <https://doi.org/10.1007/s00382-015-2668-0>.

Vecchi GA. 2006. The termination of the 1997–98 El Niño. Part II: Mechanisms of atmospheric change. *Journal of Climate*, 19(12): 2647–2664. <https://doi.org/10.1175/JCLI3780.1>.

Vera C, Higgins W, Amador J, Ambrizzi T, Garreaud R, Gochis D, Gutzler D, Lettenmaier D, Marengo J, Mechoso CR, Nogues-Paegle J, Silva Dias PL, Zhang C. 2006. Toward a unified view of the American monsoon systems. *Journal of Climate* 19(20): 4977–5000. DOI: 10.1175/JCLI3896.1.

- Vincent EM, Lengaigne M, Menkes CE, Jourdain NC, Marchesiello P, Madec G. 2011. Interannual variability of the south Pacific convergence zone and implications for tropical cyclone genesis. *Clim. Dyn.* 36(9): 1881–1896. <https://doi.org/10.1007/s00382-009-0716-3>.
- Virji H. 1981. A preliminary study of summertime tropo-spheric circulation patterns over South America estimated from cloud winds. *Monthly Weather Review*. 109, 599–610.
- Vuille M. 1999. Atmospheric circulation over the Bolivian Altiplano during dry and wet periods and extreme phases of the Southern Oscillation. *International Journal of Climatology*. 19: 1579–1600. doi:10.1002/(SICI)1097-0088(19991130)19:14,1579::AID-JOC441.3.0.CO;2-N.
- Vuille M, Bradley RS, Keimig F. 2000. Interannual climate variability in the central Andes and its relation to tropical Pacific and Atlantic forcing. *Journal of Geophysical Research*. 105: 12 447– 12 460. doi:10.1029/2000JD900134.
- Vuille M, Keimig F. 2004. Interannual variability of sum-mertime convective cloudiness and precipitation in the central Andes derived from ISCCP-B3 data. *Journal of Climate*. 17: 3334–3348, doi:10.1175/1520-0442(2004)017,3334: IVOSCC.2.0.CO;2.
- Vuille M, Burns SJ, Taylor BL, Cruz FW, Bird BW, Abbott MB, Kanner LC, Cheng H, Novello VF. 2012a. A review of the South American monsoon history as recorded in stable isotopic proxies over the past two millennia. *Climate of the Past* 8(4): 1309–1321. DOI: 10.5194/cp-8-1309-2012
- Vuille M, Garreaud RD. 2012b. Ocean-atmosphere interactions on interannual to decadal timescales, in *Handbook of Environmental Change*, vol. 1, edited by: J. A. Matthews, P. J. Bartlein, K. R. Briffa, A. Dawson, A. de Vernal, T. Denham, S. C. Fritz, and F. Oldfield, Sage Publications, London, Los Angeles, New Delhi, Singapore., 2012:471–496.
- Walker GT, Bliss EW. 1932. World Weather V. Members of the Royal Meteorological Society 4:53–84.
- Wang J, Wang W, Fu X, Seo KH. 2012. Tropical intraseasonal rainfall variability in the CFSR. *Climate Dynamics* 38(11-12): 2191–2207. DOI: 10.1007/s00382-011-1087-0.
- Waylen P, Caviedes C. 1986. El Niño and annual floods on the north Peruvian littoral. *Journal of Hydrology* 89: 141–156. doi:10.1016/0022-1694(86)90148-4.
- Wei J, Su H, Yang ZL. 2016. Impact of moisture flux convergence and soil moisture on precipitation: a case study for the southern United States with implications for the globe. *Climate Dynamics*. Springer Berlin Heidelberg 46(1–2): 467–481. DOI: 10.1007/s00382-015-2593-2.
- Weng H, Ashok K, Behera S, Rao SA, Yamagata T (2007) Impacts of recent El Niño Modoki on dry/wet conditions in the Pacific rim during boreal summer. *Climate dynamics* 29:113–129. doi:10.1007/s00382-007-0234-0
- Widlansky MJ, Webster PJ, Hoyos CD. 2011. On the location and orientation of the south Pacific convergence zone. *Climate Dynamics*. 36(3): 561–578. <https://doi.org/10.1007/s00382-010-0871-6>.
- Wyrtki K. 1975. El Niño—the dynamic response of the equatorial Pacific Ocean to atmospheric forcing. *Journal of Physical Oceanography* 5: 572–584.
- Wyrtki K. 1985. Water displacements in the Pacific and the genesis of El Niño cycles. *Journal of Geophysical Research.*, 90: 7129-7132.

Xu G, Osborn TJ, Matthews AJ, Joshi MM. 2015. Different atmospheric moisture divergence responses to extreme and moderate El Niños. *Climate Dynamics*. Springer Berlin Heidelberg. DOI: 10.1007/s00382-015-2844-2

Yeh SW, Kug JS, Dewitte B, Kwon MH, Kirtman B, Jin FF. 2009. El Niño in a changing climate. *Nature*, 461, doi:10.1038/nature08316.

Young KR, León B, Jorgensen PM, Ulloa Ulloa C. 2007. Tropical and Subtropical Landscapes of the Andes. The physical geography of South America. Oxford University Press, Oxford.

Yu JY, Kao H-Y. 2007. Decadal changes of ENSO persistence barrier in SST and ocean heat content indices: 1958–2001. *Journal of Geophysical Research.*, 112, D13106, doi:10.1029/2006JD007715.

Yu JY, Kim ST. 2013. Identifying the types of major El Niño events since 1870. *International Journal of Climatology*. 33(8): 2105–2112.

Zhang H, Clement AC, DiNezio P. 2014. The South Pacific Meridional Mode: A mechanism for ENSO-like variability. *Journal of Climate*, 27: 769–783, doi: 10.1175/JCLI-D-13-00082.1.

Zheleznova I V., Gushchina DY. 2015. The response of global atmospheric circulation to two types of El Niño. *Russian Meteorology and Hydrology* 40(3): 170–179. DOI: 10.3103/S1068373915030036.

Zhou J, Lau K. 2001. Principal modes of interannual and decadal variability of summer rainfall over South America. *International Journal of Climatology*. 21: 1623–1644.

Zveryaev II, Wibig J, Allan RP. 2008. Contrasting interannual variability of atmospheric moisture over Europe during cold and warm seasons. *Tellus A* 60(1): 32–41, doi: 10.1111/j.1600-0870.2007.00283.x.

ANNEX 1

Location and available rainfall dataset periods of the 145 meteorological stations provided by the National Service of Meteorology and Hydrology of Peru (SENAMHI)

	Station	Latitude	Longitude	Altitude (m)	Start Data	Final Data
1	AMBAR	-10,8	-77,3	2100	01/01/1980	31/03/2018
2	ANDAHUA	-15,5	-72,3	3587	01/01/1964	31/12/2011
3	ANDAJES	-10,8	-76,9	3950	01/09/1963	28/02/2018
4	ANTIOQUIA	-12,1	-76,5	1839	01/09/1963	28/02/2018
5	APLAO	-16,1	-72,5	645	01/12/1963	28/02/2018
6	AYABACA	-4,6	-79,7	2740	01/01/1963	30/09/2017
7	AYO	-15,7	-72,3	1956	01/12/1950	28/02/2018
8	BERNAL	-5,5	-80,8	20	01/11/1963	30/09/2017
9	BUENA VISTA	-9,4	-78,2	419	01/08/1964	28/02/2018
10	CABANA CONDE	-15,6	-72	3379	01/08/1964	31/12/2011
11	CABANILLAS	-15,6	-70,3	3890	01/12/1963	31/01/2018
12	CACHACHI	-7,5	-78,3	3200	01/01/1963	30/11/2017
13	CACHICA	-8,1	-78,2	2890	01/01/1964	31/12/2011
14	CAJAMARQUILLA	-9,6	-77,7	3028	01/11/1963	28/02/2018
15	CALACOA	-16,7	-70,7	3260	01/03/1964	28/02/2018
16	CALANA	-17,9	-70,2	900	01/11/1963	28/02/2018
17	CANDARAVE	-17,3	-70,3	3750	01/11/1963	31/12/2017
18	CAÑETE	-13,1	-76,3	158	01/07/1936	31/07/2010
19	CARANIA	-12,3	-75,9	3875	01/09/1963	28/02/2018
20	CARAVELI	-15,8	-73,4	1779	01/10/1963	28/02/2018
21	CARIAMA	-4,3	-79,6	1880	01/01/1964	31/12/2011
22	CASA GRANDE	-7,8	-79,2	240	01/01/1934	30/09/1989
23	CASCAS	-7,5	-78,8	1330	01/02/1964	30/06/1983
24	CATACOC	-4,1	-79,6	1183	01/02/1964	31/12/1964
25	CAYALTI	-6,9	-79,6	75	01/01/1935	31/01/2018
26	CELICA	-4,1	-80	1970	01/01/1964	31/12/2011
27	CHACCHAN	-9,5	-77,8	2285	01/09/1963	28/02/2018
28	CHACHAS	-15,5	-72,3	3130	01/12/1963	28/02/2018
29	CHALACO	-5	-79,8	1640	01/11/1963	30/09/2017
30	CHALLAPALCA	-17,2	-69,8	4280	01/01/1964	31/01/2017
31	CHAMANA	-10,2	-77,6	2000	01/09/1980	28/02/2018
32	CHAVIN	-9,6	-77,2	3210	01/01/1986	28/02/2018
33	CHICHAS	-15,5	-72,9	2120	01/12/1963	28/02/2018
34	CHILCAYOC	-13,9	-73,7	3410	01/08/1963	31/01/2018
35	CHINCHAYLLAPA	-14,9	-72,7	4100	01/12/1963	30/04/2010
36	CHIQUIAN	-10,2	-77,2	3350	01/02/1964	28/02/2018
37	CHIVAY	-15,6	-71,6	3633	01/10/1964	28/02/2018
38	CHOCLOCOCHA	-13,1	-75	4406	01/06/1958	28/02/2018
39	CHOCO	-15,6	-72,1	2473	01/12/1963	28/02/2018
40	CHOSICA	-11,9	-76,7	850	01/03/1989	28/02/2018

Continues annex 1

	Station	Latitude	Longitude	Altitude (m)	Start Data	Final Data
41	CHUGUR	-6,7	-78,7	2744	01/09/1963	31/10/2017
42	COCHABAMBA	-6,5	-78,9	1650	01/10/1963	31/01/2018
43	COLAISA	-4,3	-79,7	6476	01/10/1964	31/12/2011
44	CONDORAMA	-15,4	-71,3	4160	01/09/1977	31/03/2000
45	CONTUMAZA	-7,4	-78,8	2520	01/02/1964	31/12/2017
46	COPARA	-15	-74,9	620	01/04/1957	28/02/2018
47	CORACORA	-15	-73,8	3172	01/10/1963	28/02/2018
48	CORDOVA	-14	-75,2	3170	01/01/1964	28/02/2018
49	COTAPARACO	-10	-77,6	3008	01/11/1963	01/12/2010
50	CRUCERO ALTO	-15,8	-70,9	4470	01/11/1963	28/02/2018
51	CUEVA BLANCA	-6,1	-79,4	3300	01/09/1964	28/02/2018
52	CUSICANCHA	-13,5	-75,3	3550	01/11/1963	28/02/2018
53	EL ALTO	-4,3	-81,2	295	01/09/1977	31/03/2000
54	EL FRAYLE	-16,1	-71,2	4060	01/09/1963	28/02/2018
55	EL TIGRE	-3,8	-80,5	40	01/09/1963	30/09/2017
56	HACIENDA BERNALES	-13,8	-76	250	01/10/1963	28/02/2018
57	HACIENDA BIGOTE	-5,3	-79,8	480	01/04/1957	28/02/2018
58	HACIENDA SHUMAYA	-5,4	-79,4	2220	01/02/1964	31/12/2017
59	HUAMACHUCO	-7,8	-78,1	3150	01/11/1963	01/12/2010
60	HUAMANTANGA	-11,5	-76,8	3392	01/11/1963	28/02/2018
61	HUAMBO	-15,7	-72,1	3332	01/09/1964	28/02/2018
62	HUAÑEC	-12,3	-76,1	3205	01/01/1964	28/02/2018
63	HUANGASCAR	-12,9	-75,8	2533	01/11/1963	28/02/2018
64	HUARMACA	-5,6	-79,5	2240	01/10/1963	30/09/2017
65	HUARMEY	-10,1	-78,2	20	01/11/1965	28/02/2018
66	HUAROS	-11,4	-76,6	3585	01/09/1963	31/03/2018
67	HUASACACHE	-16,5	-71,6	2242	01/11/1992	28/02/2018
68	HUAYAN	-11,5	-77,1	350	01/08/1963	28/02/2018
69	ICHUNA	-16,1	-70,6	3800	01/01/1964	31/12/2011
70	IMATA	-15,8	-71,1	4519	01/07/1935	28/02/2018
71	INCAHUASI	-6,2	-79,3	2740	01/10/1963	31/01/2018
72	JAYANCA (LA VIÑA)	-6,3	-79,8	75	01/03/1964	31/01/2018
73	JULCAN	-8,1	-78,5	3460	01/09/1963	30/11/2017
74	LA CAPILLA 2	-12,5	-76,5	442	01/02/1964	28/02/2018
75	LACHAQUI	-11,6	-76,6	3668	01/09/1963	28/02/2018
76	LA ESPERANZA	-4,9	-81,1	12	01/07/1966	30/09/2017
77	LA JOYA	-16,6	-71,9	1292	01/11/1965	28/02/2018
78	LAMBAYEQUE	-6,7	-79,9	18	01/11/1928	28/02/2018
79	LAMPA	-15,2	-73,4	3900	01/01/1964	28/02/2018
80	LANCONES	-4,6	-80,5	135	01/09/1963	30/09/2017
81	LA PAMPILLA	-16,4	-71,5	2400	01/02/1931	28/02/2018
82	LAREDO	-8,1	-78,9	100	01/08/1964	30/09/2003
83	LAS SALINAS	-16,3	-71,1	4378	01/11/1963	28/02/2018
84	LIRCAY	-13	-74,7	3300	01/06/1949	31/01/2018

Continues annex 1

	Station	Latitude	Longitude	Altitude (m)	Start Data	Final Data
85	LIVES	-7,1	-79	1850	01/09/1963	31/12/2017
86	LLAPA	-7	-78,8	3030	01/09/1963	30/11/2017
87	LOCUMBA	-17,6	-70,8	591	01/11/1963	30/11/2016
88	LUCANAS	-14,6	-74,2	3340	01/03/1963	28/02/2018
89	MACHAGUAY	-15,6	-72,5	3150	01/01/1963	31/12/1998
90	MADRIGAL	-15,6	-71,8	3262	01/11/1963	28/02/2018
91	MAGDALENA	-7,3	-78,7	1260	01/09/1963	31/12/2017
92	MARCAPOMACOCHA	-11,4	-76,3	4479	01/09/1964	28/02/2018
93	MATUCANA	-11,8	-76,4	2479	01/02/1964	28/02/2018
94	MAZOCRUZ	-16,7	-69,7	3970	01/11/1963	31/12/2017
95	MIRAFLORES	-5,2	-80,6	30	01/04/1971	31/12/2017
96	MOLLEPATA	-8,2	-78	2580	01/09/1963	30/11/2017
97	MOQUEGUA	-17,2	-70,9	1450	01/04/1931	28/02/2018
98	MORROPON	-5,2	-80	140	01/10/1963	30/09/2017
99	NAMORA	-7,2	-78,3	2760	01/01/1964	31/12/2011
100	NIEPOS	-6,9	-79,1	2420	01/08/1963	31/12/2017
101	OCROS	-10,4	-77,4	3230	01/01/1965	31/03/2018
102	OCUCAJE	-14,4	-75,7	330	01/01/1966	28/02/2018
103	OLMOS	-6	-79,7	225,9	01/06/1964	01/05/2006
104	ORCOPAMPA	-15,3	-72,3	3779	01/12/1949	28/02/2018
105	OYON	-10,7	-76,8	3641	01/09/1963	28/02/2018
106	PALLAC	-11,4	-76,8	2333	01/08/1963	28/02/2018
107	PAMPA BLANCA	-17,1	-71,7	100	01/09/1963	28/02/2018
108	PAMPA BLANCA 2	-14,2	-75,1	1009	01/10/1966	31/03/2018
109	PAMPA DE ARRIEROS	-16,1	-71,6	3715	01/11/1963	28/02/2018
110	PAMPA DE MAJES	-16,3	-72,2	1434	01/10/1949	28/02/2018
111	PAMPAHUTA	-15,5	-70,7	4320	01/11/1961	31/12/2017
112	PAMPA UMALZO (TITIJONES)	-16,9	-70,4	4609	01/12/1963	31/01/2018
113	PAÑALA	-6,2	-79,9	80	01/10/1963	31/03/1984
114	PANANGA	-4,6	-80,9	440	01/11/1963	30/09/2017
115	PARAMONGA	-10,7	-77,8	60	01/03/1938	28/02/2018
116	PAUZA	-15,3	-73,4	2560	01/12/1963	28/02/2018
117	PILLONES	-16	-71,2	4455	01/11/1963	28/02/2018
118	PIRA	-9,6	-77,7	3570	01/11/1963	28/02/2018
119	PUENTE CHILETE	-7,2	-78,8	850	01/09/1963	31/01/2018
120	PUERTO PIZARRO	-3,5	-80,5	1	01/09/1963	30/09/2017
121	PUCHACA	-6,4	-79,5	500	01/06/1999	31/12/2017
122	PUQUIO	-14,7	-74,1	3219	01/11/1962	28/02/2018
123	QUEROCOTILLO	-6,3	-79	1960	01/11/1963	28/02/2018
124	QUINISTAQUILLAS	-16,8	-70,9	1590	01/01/1964	28/02/2018
125	RECUAY	-9,7	-77,5	3394	01/02/1964	28/02/2018
126	REQUE	-6,9	-79,8	21	01/04/1964	31/01/2018
127	RICA PLAYA	-3,8	-80,5	98	01/11/1963	30/09/2017

Continues annex 1

	Station	Latitude	Longitude	Altitude (m)	Start Data	Final Data
128	SALAMANCA	-15,5	-72,8	3203	01/01/1964	28/02/2018
129	SALPO	-8	-78,6	3400	01/09/1963	31/12/2017
130	SAMA GRANDE	-17,8	-70,5	534	01/01/1964	28/02/2018
131	SANBENI	-7,4	-78,9	1620	01/01/1964	31/12/2011
132	SAN JUAN	-7,3	-78,5	2460	01/01/1964	30/11/2017
134	SAPILLICA	-4,8	-80	1456	01/08/1963	30/09/2017
135	SAN JUAN DE YANAC	-13,2	-75,8	2400	01/12/1963	28/02/2018
136	SAN CAMILO	-14,1	-75,7	398	01/06/1954	28/02/2018
137	TALLA	-7,3	-79,4	150	01/02/1937	28/02/2018
138	TINAJONES	-6,6	-79,4	226	01/01/1963	28/02/2018
139	TISCO	-15,4	-71,5	4175	01/11/1963	28/02/2018
140	VIRU	-8,4	-78,8	64	01/08/1966	31/08/1985
141	WEBERBAUER	-7,2	-78,5	2660	01/10/1933	31/12/2017
142	YANGANA	-4,4	-79,2	1800	01/01/1964	31/12/2011
143	YAUCA	-15,7	-74,5	48	01/09/1963	31/07/1992
144	YUNGAY	-9,1	-77,8	2537	01/09/1966	28/02/2018
145	ZAPOTIL	-4,4	-80,2	325	01/01/1964	31/12/2011